ISTANBUL TECHNICAL UNIVERSITY ★ GRADUATE SCHOOL

ADVANCED ENERGY AND EXERGY ANALYSIS ON AIRCRAFT JET ENGINES

PhD. THESIS

Sara FAWAL

Department of Aeronautics and Astronautics

Aeronautics and Astronautics Engineering Programme

DECEMBER 2023

ISTANBUL TECHNICAL UNIVERSITY ★ GRADUATE SCHOOL

ADVANCED ENERGY AND EXERGY ANALYSIS ON AIRCRAFT JET ENGINES

PhD. THESIS

Sara FAWAL
(511212113)

Department of Aeronautics and Astronautics

Aeronautics and Astronautics Engineering Programme

Thesis Advisor: Prof. Dr. Ali KODAL

DECEMBER 2023

ISTANBUL TEKNİK ÜNİVERSİTESİ ★ LİSANSÜSTÜ EĞİTİM ENSTİTÜSÜ

HAVACILIK JET MOTORLARINDA İLERİ ENERJİ VE EKSERJİ ANALİZİ

DOKTORA TEZİ

Sara FAWAL
(511212113)

Uçak ve Uzay Mühendisliği Anabilim Dalı

Uçak ve Uzay Mühendisliği Programı

Tez Danışmanı: Prof. Dr. Ali KODAL

ARALIK 2023

Sara FAWAL, a Ph.D. student of İTU Graduate School student ID 511212113, successfully defended the thesis/dissertation entitled "ADVANCED ENERGY AND EXERGY ANALYSIS ON AIRCRAFT JET ENGINES", which she prepared after fulfilling the requirements specified in the associated legislations, before the jury whose signatures are below.

Thesis Advisor :	**Prof. Dr. Ali KODAL** Istanbul Technical University	.....
Jury Members :	**Prof. Dr. Bahri ŞAHİN** Istanbul Gelişim University	.....
	Prof. Dr. İbrahim ÖZKOL Istanbul Technical University	.....
	Assis. Prof. Dr. Hayri ACAR Istanbul Technical University	.....
	Prof. Dr. Muammer KALYON Istanbul Ticaret University	.....

Date of Submission : 15 Ekim 2023
Date of Defense : 8 December 2023

Elhamdüllilah.

My thesis is dedicated to all pursuers of knowledge, truth and justice.

FOREWORD

The chapters in this text are organized essentially along an advanced energy and exergy performance analysis for the folowing types of aircraft engines: Turbojet without an Afterburner, Turbojet with an Afterburner, Ramjet and finally the Turboramjet. Starting with the most simplest application of the Brayton cycle this text provides a comprehensive study and design approach towards more intellignet engines; the text concludes on the discussion of Turbie Based Combined Cycles (TBCC).

I express my sincere appreciation to all my profesors who have contributed to my academic progress and professional development. I would especilly like to thank Dr. Marius PARASCHIVOIU and Dr. Hoi Dick NG for all their support and due diligence, without them I would not have become a PhD. Student and Istanbul Technical University. I would also like to thank my professor and mentor Dr. Ali KODAL at İTÜ for guiding and supporting me every step of the way thoughout my whole PhD. experience. In addition I would like to thank İTÜ for being a home away from home and all its wonderful staff memebers who are always supprotive and helpful and great you with a smile and warm heart.

Finally, I thank both my Mom and Dad for being there for me all my life.

In closing I would like to share a passage by an anonymus writer:

What is Truth?

A question that is sometimes cynical, sometimes sincere, but always important. Truth is real; it is honesty with what is. Truth is learned, it is not something to create, but something to discover. Truth is omniscient; it is above, beyond, around and in us all. Truth is elusive; it can be denied, covered, rejected, ignored and even hated. Truth is noble; it is worth guarding from misguided attempts to wrap truth into half truth. Truth is powerful; it is a friend if embraced, an enemy if denied. Truth is unswerving; it is the straight path to lasting success.

December 2023

Sara FAWAL
(Aerospace Engineering)

TABLE OF CONTENTS

Page

ABBREVIATIONS

AB : Afterburner
ALT : Altitude
CBSF : Carnot Brayton Shape Factor
ECOL : Ecological Function
ECOP : Ecological Coefficient of Performance
$\overline{\textbf{ECOP}}$: Normalized ECOP
EFECPOD : Effective Ecological Power Density
EP : Effective Power
EPD : Effective Power Density
EPLOS : Effective Power Loss Parameter
EXED : Exergy Destruction
EXEF : Exergy Efficiency
ft : Feet
GB : Great Britain
hPa : Hectopascals
km : Kilometer
LHV : Lower Heating Value
MP : Maximum Power
MPD : Maximum Power Density
PLOS : Power Loss Parameter
RAF : Royal Air Force
RF : Radiative Forcing
SFC : Specific Fuel Consumption
TBCC : Turbine Based Combined Cycles
TSFC : Thrust Specific Fuel Consumption
UK : United Kingdom

SYMBOLS

A_5	Cross-sectional Area at Station 5 (m^2)
C_a	Velocity of Air (m/s)
C_4	Velocity at Station 4 (m/s)
C_5	Velocity at Nozzle Exit (m/s)
F_s	Specific Thrust (N-s/kg)
F_{shaft}	Shaft Force (kN)
g	Acceleration due to Gravity (m/s^2)
h	Height from Sea Level (m)
I_a	Air Specific Impulse (s)
LHV	Lower Heating Value (kJ/kg)
$\dot{m}_0$	Mass flow rate (kg/s)
$\dot{m}_a$	Mass flow of air (kg/s)
$\dot{m}_f$	Mass flow of fuel (kg/s)
N	Engine Speed (RPM)
$\acute{P}$	Non-Dimensional Pressure Difference at Inlet and Exit States
p_a	Inlet Air Pressure (kPa)
p_5	Pressure at Station 5 (kPa)
Q_R	Fuel Heating Value (kJ/kg)
$\dot{Q}_{fuel}$	Fuel Heat Release Rate (kJ/s)
$\dot{Q}_{HT}$	Total Heat Transfer (kJ/s)
$\dot{Q}_{LT}$	Total Heat Rejection (kJ/s)
$\dot{Q}_{LK}$	Rate of Heat Leak (kJ/s)
R	Gas Constant (J/kg-K)
$\dot{S}_g$	Rate of Entropy Generation (kJ/K-s)
TSFC	Thrust Specific Fuel Consumption (kg/N-s)
$\breve{T}$	Non-Dimensional Temperature Difference at Inlet and Exit States
T_0	Environment Temperature (K)
T_H	Temperature of Hot Reservoir (K)
T_L	Temperature of Cold Reservoir (K)
v_5	Specific Volume at Station 5 (m^3/kg)

v_{Nozzle}	Nozzle Specific Volume (m^3/kg)
$\dot{W}$	Power produced by Real Brayton Cycle (kJ/s)
$\dot{W}_{Bray}$	Power produced by Ideal Brayton Cycle (kJ/s)
$\dot{W}_d$	Power Density (kJ/s)
$\dot{W}_{lk}$	Power Leaked from the System (kJ/s)
$\dot{W}_{rev}$	Reversible Power (kJ/s)
$\dot{W}_{turbine}$	Turbine Work (kJ/s)
$\dot{W}_{useful}$	Useful Power (kJ/s)
$\dot{X}_{DES}$	Rate of Exergy Destruction (kJ/s)
γ	Specific Heat Ratio
$\sqrt{\theta} = \sqrt{T_{ref}/T_a}$	Temperature Correctıon Factor
η_b	Burner Efficiency
η_c	Compressor Efficiency
η_i	Intake/Diffuser Efficiency
η_j	Jet/Nozzle Efficiency
η_m	Mechanical Efficiency
η_p	Propulsive Efficiency
η_t	Turbine Efficiency
η_{th}	Thermal Efficiency
f	Fuel to Air Ratio
θ_c	Compressor Pressure Ratio Parameter
M_∞	Flight Mach Number
ξ	Percentage of Internal Conductance for Heat Leak
$TSFC^*, {I_a}^*, f^*$	Optimum TSFC, I_a and f
α	Cycle temperature ratio

LIST OF TABLES

Page

LIST OF FIGURES

Page

ADVANCED ENERGY AND EXERGY ANALYSIS ON AIRCRAFT JET ENGINES

SUMMARY

A comparative performance analysis for various optimization criterion functions is to be carried out for an irreversible Brayton cycle applicable to aircraft jet engines: Ramjet, Turbojet (No Afterburner), Turbojet (With Afterburner), Turbo-Ramjet. Newly defined parameters are introduced as power loss parameter (PLOS), effective power loss parameter (EPLOS) and Carnot-Brayton shape factor (CBSF) for a better assessment of the performance and power losses throughout the operation of the engine cycle. In addition, optimization functions, such as maximum power (MP), maximum power density (MPD), ecological coefficient of performance (ECOP) and ecological function (ECOL) are considered and their optimal operation conditions are compared with respect to each other.

This research studied the effects on the prescribed optimization criterions targeted towards the aviation industry under variations of compressor pressure ratio θ_c, compressor and turbine efficiencies (η_c and η_t respectively), cycle temperature ratio / maximum cycle temperature, altitude and flight Mach number M_∞ where applicable with respect to the jet engine being considered. Therefore, the classical irreversible Brayton cycle is extended and applied to airbreathing engines; which included effects of all the engine components (from free stream to inlet to outlet) as part of the thermodynamic cycle model.

While many researchers have carried out performance analysis for internal combustion engines including gas turbine engine, this study is an extension of the available optimization functions such as MP, MPD, ECOP and ECOL for aircraft jet engines. As mentioned, power density is defined as the ratio of power to the maximum specific volume in the cycle. Whereas ECOP is defined as the ratio of power output to the loss rate of availability and ECOL as the power output minus the loss rate of availability. In order to extend the classical irreversible Brayton cycle to airbreathing engines applicable for aircrafts, further development studies must be carried out to obtain: higher propulsion efficiency and higher ratios of power output with respect to engine weight, volume, and frontal area. The objective is to obtain a larger power output to engine size (weight) in a more thermodynamically efficient manner for a real turbojet cycle where maximum ECOP, ECOL, power density and power conditions can be used as a basis for the determination of optimal operating conditions and preliminary design constraints for real turbojet engines at flight conditions.

The comparative performance analysis for various optimization criterion functions used for the aircraft engine cycle will be applied to ramjet, turbojet without afterburner and tubojet with afterburner to reach the final intended application of turboramjet engine. The turboramjet engine cycle is identified as Turbine Based Combined Cycle Engines (TBCC). Such hybrid cycle engines can be applied to UAV's, UCAV's and powering future hypersonic flight vehichles.

The software to be used for the comparative performance analysis for the irreversible Brayton cycle applicable to aircraft jet engine cycles is the academic version of MATLAB 2018b provided by the MathWorks group.

The emissions and radiative forcing (RF) from the aviation industry and its effects on air pollution and the ecology are an important concern, where aviation ranks as one of the top ten emitters. The major greenhouse gas emitters that contribute to RF are: carbon dioxide CO_2, carbon monoxide CO, water H_2O, nitrous oxide NO_X, sulphur oxides SO_X and volatile organic compounds VOCs.

Thus, performance evaluation of aircraft propulsion systems must be assessed with respect to environmental and ecological conditions as well as power and fuel consumption considerations. Therefore, various optimization criterion functions which can be used as tools by the aviation industry to design 'new generation engines' which are economically and ecologically favourable.

It is anticipated that this research would provide valuable insight in the preliminary design of airbreathing engines (Ramjet, Turbojet: No Afterburner, Turbojet: With Afterburner and Turbo-Ramjet) and set a stage for exploration towards adaptive engine components and cycles for the conception of truly intelligent engines; an engine that can assess its current operating state and work under the most efficient power regime (ECOL or ECOP or MP or MPD) to achieve the designers and engine's intended performance potential.

HAVACILIK JET MOTORLARINDA İLERİ ENERJİ VE EKSERJİ ANALİZİ

ÖZET

Uçak jet motorlarına uygulanabilen tersinmez bir Brayton çevrimi için çeşitli optimizasyon kriter fonksiyonları için karşılaştırmalı bir performans analizi yapılacaktır: Turbojet (art yakıcısız), Turbojet (art yakıcılı), Ramjet ve Turbo-Ramjet. Motor çevriminin çalışması boyunca performansın ve güç kayıplarının daha iyi değerlendirilmesi için yeni tanımlanan parametreler güç kaybı parametresi (PLOS), etkin güç kaybı parametresi (EPLOS) ve Carnot-Brayton şekil faktörü (CBSF) olarak tanıtıldı. Ayrıca maksimum güç (MP), maksimum güç yoğunluğu (MPD), ekolojik performans katsayısı (ECOP) ve ekolojik fonksiyon (ECOL) gibi optimizasyon fonksiyonları dikkate alınmakta ve optimum çalışma koşulları birbirleriyle karşılaştırılmaktadır.

Bu araştırma, söz konusu jet motoruna göre, kompresör basınç oranı θ_c, kompresör ve türbin verimlilikleri (η_c and η_t sırasıyla), çevrim sıcaklığı oranı / maksimum çevrim sıcaklığı, yükseklik/irtifa ve uçuş Mach sayısı M_∞ varyasyonları altında havacılık endüstrisine yönelik öngörülen optimizasyon kriterleri üzerindeki etkileri inceledi. Bu nedenle, klasik tersinmez Brayton çevrimi uzatılır ve hava soluyan motorlara uygulanır; termodinamik çevrim modelinin bir parçası olarak tüm motor bileşenlerinin (serbest akıştan girişe ve çıkışa) etkilerini içeriyordu.

Birçok araştırmacı, gaz türbinli motor dahil içten yanmalı motorlar için performans analizi yapmış olsa da, bu çalışma, uçak jet motorları için MP, MPD, ECOP ve ECOL gibi mevcut optimizasyon fonksiyonlarının bir uzantısıdır. Belirtildiği gibi, güç yoğunluğu, gücün çevrimdeki maksimum spesifik hacme oranı olarak tanımlanır. ECOP, güç çıkışının kullanılabilirlik kayıp oranına oranı ve ECOL ise güç çıkışı eksi kullanılabilirlik kayıp oranı olarak tanımlanır. Klasik tersinmez Brayton çevrimini uçaklar için geçerli olan hava soluyan motorlara genişletmek için, motor ağırlığı, hacmi ve ön alana göre daha yüksek tahrik verimliliği ve daha yüksek güç çıkışı oranları elde etmek için daha fazla geliştirme çalışması yapılmalıdır. Amaç, maksimum ECOP, ECOL, güç yoğunluğu ve güç koşullarının optimal çalışma koşullarının belirlenmesi için bir temel olarak kullanılabileceği gerçek bir turbojet çevrimi için termodinamik olarak daha verimli bir şekilde motor boyutuna (ağırlığına) daha büyük bir güç çıkışı elde etmektir. ve uçuş koşullarında gerçek turbojet motorları için ön tasarım kısıtlamaları.

Uçak motoru çevrimi için kullanılan çeşitli optimizasyon kriteri fonksiyonları için karşılaştırmalı performans analizi, turboramjet motorunun nihai amaçlanan uygulamasına ulaşmak için ramjet, art yakıcısız turbojet ve art yakıcılı tubojet'e uygulanacaktır. Turboramjet motor çevrimi, Türbin Tabanlı Kombine Çevrim

Motorları (TBCC) olarak tanımlanır. Bu tür hibrit çevrimli motorlar, İHA'lara, UCAV'lere ve geleceğin hipersonik uçuş araçlarına güç sağlamak için uygulanabilir.

Uçak jet motoru çevrimlerine uygulanan tersinmez Brayton çevrimi için karşılaştırmalı performans analizi için kullanılacak yazılım, MathWorks grubu tarafından sağlanan MATLAB 2018b'nin akademik versiyonudur.

Havacılık endüstrisinden kaynaklanan emisyonlar ve ışınımsal zorlama (RF), hava kirliliği ve ekoloji üzerindeki etkileri, havacılığın ilk on yayıcıdan biri olarak yer aldığı önemli bir endişe kaynağıdır. RF'ye katkıda bulunan başlıca sera gazı emisyonları şunlardır: karbondioksit CO2, karbon monoksit CO, su H2O, azot oksit NOX, kükürt oksitler SOX ve uçucu organik bileşikler VOC'ler.

Bu nedenle, hava taşıtı tahrik sistemlerinin performans değerlendirmesi, güç ve yakıt tüketiminin yanı sıra çevresel ve ekolojik koşullar açısından da değerlendirilmelidir. Bu nedenle, havacılık endüstrisi tarafından ekonomik ve ekolojik olarak uygun 'yeni nesil motorlar' tasarlamak için araç olarak kullanılabilecek çeşitli optimizasyon kriter fonksiyonları.

Art yakıcısız turbojet, yeni tanımlanmış performans parametreleri (PLOS, EPLOS ve CBSF) kullanılarak incelendi ve maksimum güç, maksimum güç yoğunluğu, ECOP ve ECOL gibi mevcut amaç fonksiyonları ile birleştirildi. Ayrıca bu parametreler için MP, MPD, MECOP ve MECOL'ün optimal çalışma koşulları üzerindeki değişken etkileri ve bunların motor performansı üzerindeki etkisi gösterilmiştir.

Art yakıcılı turbojet, maksimum güç (MP), PLOS ve EPLOS bazında değerlendirildi ve art yakıcısız turbojet ile karşılaştırıldı. Çalışan bir art yakıcıya sahip bir turbojet motor düşünüldüğünde, performans analizi ve karşılaştırması, öncelikle Mach sayısı ve irtifa olan daha kısıtlayıcı parametrelere doğru bir kayma alır. Ek olarak, art yakıcısız ve art yakıcılı motor bileşenleri olmayan turbojetin özgül hacmi MP bazında değerlendirilmiş ve karşılaştırılmıştır.

Ramjet sadece maksimum güç (MP) bazında araştırılmış ve brülörsüz ve brülörlü ve brülörlü turbojet ile karşılaştırılmıştır. Ramjet, iki farklı yöntem kullanılarak değerlendirildi: Tek Eğik ve Normal Şok (SOSN) çözümü ile Çoklu Eğik Şok ve Tek Normal Şok çözümü. SOSN varsayımı, giriş için çok daha yüksek bir durgunluk basınç düşüşü sağlar ve gerçek gaz türbini giriş basıncı geri kazanımı (ram geri kazanımı) tasarım özelliklerinin bir temsili değildir. Bu nedenle, MIL-E-5007D spesifikasyonu artık difüzör durgunluk basınç oranının tanımı için kullanılmaktadır ve 1-5 arasındaki Mach sayıları için geçerlidir.

Ramjet'e benzer şekilde, turboramjet motorunun performansı, Mach sayısının bir fonksiyonu olarak irtifa ve giriş hava kütle akışındaki değişiklikler için çift modlu çalışmada maksimum güç (MP) amaç fonksiyonu kullanılarak değerlendirildi. Çift modlu çalışma altında, turbojet motor art yakıcı çalışır durumda kabul edildi.

Motor konfigürasyonları, termodinamik tahrik çevrimlerine ve denklemlerine göre kesinlikle değerlendirildi. Ne yazık ki, bu tür bir değerlendirme kullanıldığında, motor bileşenleri arasındaki bağlantı ve karşılıklı bağımlılık kaybolur. Herhangi bir motorun itici faktörü, yakıt akışındaki değişikliktir. Yakıttaki bir artış basınçları, sıcaklıkları,

NG ve hava akışını yükseltir; bunun tersi de doğrudur. Bu nedenle, gerçek bir motor performansı değerlendirmesi için aşağıdakilerin karşılıklı bağımlılığı: ortam koşulları (serbest akış basıncı, sıcaklık ve Mach sayısı); giriş hava kütle akışı; kompresör, yanma odası, türbin ve çıkış nozulu giriş ve çıkış basınçları ve sıcaklıkları; yakıt akışı; ve gaz jeneratörü hızı birbirini etkilemelidir. Ancak, sevk denklemlerinin sınırlaması nedeniyle, bu ara bağlantı şekli görülemez; güncellenmedikçe.

Bununla birlikte, sevk denklemleri ve amaç fonksiyonları, havacılık endüstrisi tarafından ön tasarım amaçları için bir rehber olarak kullanılabilecek araçlardır.Bu araştırmanın, hava soluyan motorların (Ramjet, Turbojet: No Afterburner, Turbojet: With Afterburner ve Turbo-Ramjet) ön tasarımında değerli bilgiler sağlayacağı ve adaptif motor bileşenlerine ve gerçekten akıllı motorlar; tasarımcıların ve motorun amaçlanan performans potansiyeline ulaşmak için mevcut çalışma durumunu değerlendirebilen ve en verimli güç rejiminde (ECOL veya ECOP veya MP veya MPD) çalışabilen bir motor.

1. INTRODUCTION

It was the inception of the Brayton cycle that gave way to the inevitable invention of internal combustion engine and its use in the power generation, automative, aeronautical and marine industry. The Brayton cycle is defined as a four step process begining by an adiabatic compression, followed by an isobaric heat addition, which is succeeded by an adiabatic expansion and finally ending with an isobaric heat rejection.

It was not long after that the Brayton cycle's full adavantage was realized in the aviation industry through the development of gas turbine / jet engines; where now air is being used as the primary working fluid. For a jet engine the Brayton process corresponds to the compressor, combustion chamber, turbine and surrounding atmosphere respectively [1].

Jet propulsion is based on Sir Isaac Newton's third law of motion: the principle of action and reaction,where the flow of air gets compressed and the addition of fuel converts mechanical and thermal energy into thrust. The thrust is then defined using Newton's second law of motion: $Force = Mass\ x\ Acceleration$, where the force has a large enough acceleration to overcome the mass of the object itself [2][3].

In 1928, as an Air Commodore at the Royal Air Force in Cranwell Sir Frank Whittle wrote his thesis on "Future Developments in Aircraft Design ". In his thesis Whittle writes:

> "There are three ways of speculating on the future. There is the immediate future, the further future, and the far future. The object of the work is to discuss the "middle" future, with a certain amount of speculation which probably overlap the immediate future.
>
> Development will take place along the following lines.
>
> 1. Increase of range,
> 2. Increase of speed,
> 3. Increase of reliability,
> 4. Decrease of structural weight,
> 5. More economical flight,
> 6. Increase of ceiling,
> 7. Increase of load carrying capacity,

8. Greater ability to withstand the elements.

Many of these will be interdependent, for instance, a decrease in structural weight will result in increased range, etc (p. 2,3)."

Whittle explains in his thesis that an increase in rage can be attainable through enhancement of an aircaft's stramline, airfoil section and reduction in structural weight. Where as an increase in speed can be reached from an overall decrease in L/D (due to the increase of passive drag) and flying at higher altitudes. In adition, relability and decrease in structural weight can be sought via multi-powerplant usage and distributing engine weight over the span of the aircraft wings rather than being clustered near the fuselage. Moreover, flying at altitudes above the tropopause (33 000 ft) where occurences such as depressions and convection currents do not exist, ensures that winds will be absolutely steady. However, limitations in structural weight depends on blade velocity and temperature of gases, this is especially true for the turbine. An increase in efficiency and ceiling can be obtained if an air driven turbine is used as the prime mover rather than a steam turbine; where an air turbine has the capability of giving back energy through supercharging, greater efficiency at higher altitudes and more flexibility in rate of rotation than current engines. Also, future power units would utilize the method of drive: forcing gases at high velocity through a nozzle where the reaction obtained being opposite in direction to the flow of the escaping gas [4][5].

It is only but two years after Sir Frank Whittle (accredited as the father of jet engines) had written his thesis that the combination of the Brayton cylce and Jet propulsion materialized into the first jet aircraft engine and patented on the 16th of January 1930, GB347206A "Improvements Relating to the Propulsion of Aircraft and other Vehicles". The single shaft jet engine consisted of a centrifugal compressor, comustion chamber, a multi-stage axial turbine and a propelling nozzle. Air is used as the working fluid where a portion of the expanded air from the turbine is used to drive the compressor and the remaining portion passes throught the propelling nozzle further expanding to the atmosphere providing fluid reaction. The pressure drop during expansion takes place in two stages: the first pressure drop takes place through the nozzles of the turbine and the second occurs in the propelling nozzles. The controling means of the engine include: fuel control, gas flow/path control, mechanical control of the speed of the blower and final emission of the gas may be directionally controlled

for manoeuvering purposes. In additon, an auxiliary unit would be needed for starting, fuel injection, lubrication and the like. In his patenet Whittle claims that his invention will provide larger thrust in proportion to its weight, perform better at higher altitudes, attain higher velocities, operate using existing heavy oils or fuels and have a relatively low fuel consumption. In addition, the efficiency of the device as a propulsive engine is not to be reduced by the reduction of density of the atmosphere, rather, owing to the reduction of temperature of the upper atmosphere may be enhanced [6].

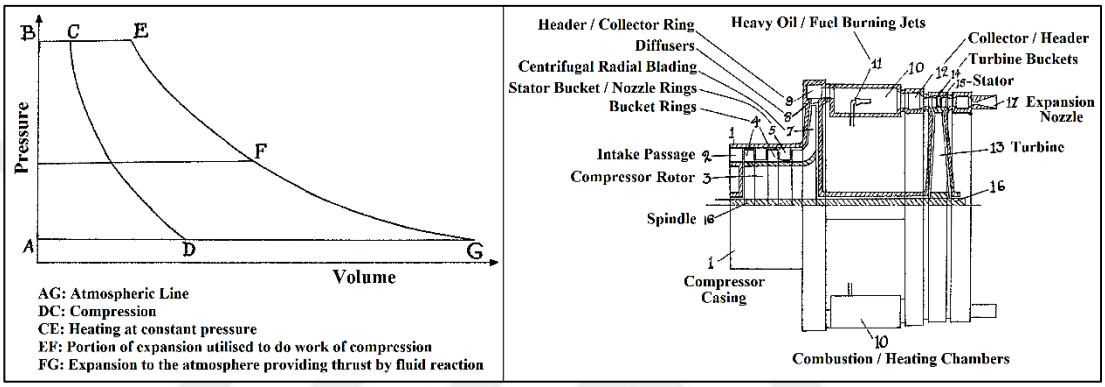

Figure 1.1: *P-v* diagram (left) and Part-section (right) of the Whittle jet engine.

Almost a century later the thermal / energy cycle of preference utilized by the aerospace industry has not deviated away from that of the Brayton cycle and its essential engine components and control systems as described above. In addition, the objectives of the aeronautical industry as described by Sir Frank Whittle, to this day, are still being pursued: longer range; lower weight and fuel consumption; higher speed (Mach number), altitude, thrust and powerplant efficiency.

The focuse of this thesis will be realated to the objectives of: fuel consumption reduction; and higher Mach number, altitude, thrust and powerplant efficiencies. Therefore, the performance of the irreversible Brayton cycle will be assessed by defining new and currently available optimization functions and applied specifically to aircraft gas turbine / jet engines.

1.1 Purpose of Thesis

The increased awareness that energy is a limited resource has triggered researchers to develop new techniques to enhance the utilization of energy conversion devices. In

addition, discharges and radiative forcing (RF) associated to the aeronautical sector along with their impacts upon atmospheric and environmental pollution are a significant concern; with aviation ranking amongst the ten largest emitters. The primary emitters of greenhouse gases that supports radiative forcing include: carbon dioxide CO_2, carbon monoxide CO, water H_2O, nitrous oxide NO_X, sulphur oxides SO_X and volatile organic compounds VOCs.

Therefore, performance assessment pertaining to aeronautical thrust generating power plants must be investigated with regards to ecological and sustainable conditions also taking into account fuel and power consumption. Thus, various optimization criterion functions can be utilized as tools by the aeronautical sector to create 'next generation power plants' that are advantageous from both an economic and environmental standpoint.

The first law of thermodynamics deals with the quantity of energy where energy cannot be created or destroyed but can only be converted from one form to another. The second law deals with the quality of energy and its degradation during a process, entropy generation and the lost opportunities to do work. In compliance with the second law of thermodynamics performance optimization functions are defined in terms of: exergy (availability); reversible work (maximum useful work that can be obtained as a system undergoes a process between two specified states) and irreversible work (wasted work potential during a process as a result of irreversibilities known as exergy destruction or lost work) [7-10].

While numerous scientists have examined the performance of internal combustion engines and industrial based air breathing engines, this work is an addendum of the currently defined optimization functions such as maximum power (MP), maximum power density (MPD), ecological coefficient of performance (ECOP) and ecological function (ECOL) for aeroplane jet engines. Power density abides to the designated proportion concerning power to maximum specific volume of a powerplant configuration. Whilst, ECOP represents a proportion of power generated to loss rate of availability and ECOL as power generated less the loss rate of opportunity. In addition, newly defined parameters are introduced as power loss parameter (PLOS), effective power loss parameter (EPLOS) and Carnot-Brayton shape factor (CBSF) for a better assessment of the performance and power losses throughout the operation of

the engine cycle. Further more, the optimization functions, of MP, MPD, ECOP and ECOL are compared with respect to each other at their optimal operation conditions.

In pursuance of expanding the traditional irreversible Brayton configuration ecompasing aeronatical powerplants implementable for aeroplanes, more advanced investigations must be conducted to achieve: augmented propulsion efficiency and proportions of power generation directed towards engine mass, volume, and inlet area. The purpose is to attain a increased power generation to powerplant dimension (mass) via a much required thermodynamically efficient demeanor considering actual gas turbine powerplants where maximum ECOP, ECOL, power density and power operations are utilized for the foundation and resolution with regards to optimum working circumstances and precursory design limitations for actual air breathing powerplants at flight conditions.

This research will study the impact of the prescribed optimization criterions targeted towards the aviation industry as a function of changes in compressor pressure ratio θ_c, compressor and turbine efficiencies (η_c and η_t respectively), cycle temperature ratio / maximum cycle temperature, altitude along with flight Mach number M_∞ where applicable with respect to the jet engine being considered. Consequently, the classical irreversible Brayton configuration applicable to airbreathing powerplants is extended and includes the impacts of all the engine components (from free straem to inlet to outlet) as members of the thermodynamic cycle representation.

1.2 Literature Review

Angulo-Brown [11] proposed an ecological (ECOL) optimization criterion for finite-time Carnot heat engines as, $ECOL = \dot{W} - T_0\dot{S_g}$, where $\dot{W}$ is the power output, $T_0\dot{S_g}$ is the loss rate of availability. However, the ecological coefficient of performance (ECOP) became a performance criterion for diverse energy transformation power plants for the environment [12] and defined by proportions of power generated to the loss rate of attainability $ECOP = \dot{W}/T_0\dot{S_g}$.

Further researchers made explorations utilizing ECOP and ECOL for the investigation of both Carnot and Brayton thermodynamic configurations to enhance performance along with reducing green house gases. Cheng and Chen [13] utilized ECOL applicable to Carnot heat engines, and augmented regarding to the cycle temperature

and heat conductance fraction. Furthermore, Cheng and Chen [14] performed an analogous examination for an irreversible Brayton heat engine while perfecting for thermal conductance along with adiabatic temperature fraction. Whereas Blank [15] studied a rerciprocal sink outlet temperature to attain the most optimal power of an openended irreversible Brayton and Joule-Brayton heat engine configuration. Üst et al. [16] utilized ECOP for an irreversible Carnot heat engine with losses as a consequence of the heat exchange over finite temperature variations, heat leak and internal irreversibilities. Likewise, Üst et al. [17] directed an investigation for an irreversible Bryton heat engine and extrapolated correlative assessments for thermal efficiencies and power outputs. Furthermore, Üst et al. [18] employed the irreversible regenerative Brayton heat engine configuration and demonstrated benefits of entropy generation rate, thermal efficiency and investment expenditure. Olivera et al. [19] created a representation of an irreversible Brayton configuration to explored optimal quantities of temperature and pressure ratios of the cycle for the initial stages of compression and expansion. In contrast, Haseli [20] carried out an investigation for a trilogy of arrangements and correlated operational conditions at maximum thermal efficiency and work generated and minimum entropy output for the openended power Brayton configurations. Contrarily, Gonca [21] conducted a review for a three-shaft aeroderivative powerplant with a focus on energetic, exergetic and ecological abstracts such as power, power density, second-law efficiency (exergy efficiency), exergy destruction, ecological coefficient of performance (ECOP) and effective ecological power density (EFECPOD). The impact of engine design criterions (namely: gas generator speed, air mass flow rate, equivalence ratio, pressure ratio, etc.) on the performance attributes were evaluated by engaging temperature-reliant specific heats and heat transformation deficits. Although Balli [22] investigated a two-shaft high bypass fraction turbofan engine and expressed approximated results for exergy efficiency, waste exergy fraction, eco-friendly and economical impact element. Durmusoglu and Üst, on the other hand, [23] conducted a thermo-ecological augmentation of an irreversible regenerative close-ended Brayton configuration using a design function derives as the fraction of net power generated to total value change (F); where the price change incorporates variables of fuel, expenditure, eco-friendly and functioning and preservation financial estimates. Furthermorer, Sadatsakkak et al. [24] evaluated an irreversible regenerative close-ended Brayton configuration imparting three design theorems: power generation, thermo-ecological requirements

and an economical equality. Moreover, Açıkkalp [25] examined ecological thermo-environmental formulations for the evaluation of performance for an irreversible solid-oxide fuel cell Brayton heat engine in addition to power, exergy destruction, energy and exergy efficiencies. Finally, Gonca [26] investigates the impact of engine design criterions employing performance parameteres including effective power (EP), effective power density (EPD), ecological coefficient of performance (ECOP), exergy destruction (EXED) along with exergy efficiency (EXEF) of a regenerative aero-derivative engine.

Najjar and Balawneh [34] examined the changes of compressor pressure ratio and turbine inlet temperature and its impact pertaining to specific thrust and specific fuel consumption (SFC). Najjar and AbuEisheh [35] adapted an exergy assessment towards the evaluation of specific thrust and SFC. Also, Najjar and el-Sharif [36] utilized thermodynamic parameters and optimization gradient process based methods for reductions on SFC of a turbofan engine. In addition, Najjar and Balawneh [37] examined compressor and optimum compressor ratio as well as the turbine inlet temperature (TIT) to evaluate the impact on SFC and specific thrust. De Sa and Al Zubaidy [38] evaluated the impact of atmospheric temperature on engine performance. Badami et al. [39] conducted an empirical and algebraic investigation for a miniature model turbojet engine and evaluated its true performance. Salpingidou et al 0 investigaed the thermodynamic configuration of a taditional restorative aero-derivative powrplant, by positioning a heat exchanger downstream of the power turbine, along with drawing comparisons between two nonconventional recuperative aero-derivative powerplant configurations. Wang et al. [41] carried out performance evaluations on a three spool engine. Guha [42][43] studied diverse variables and applied augmentation methods for the ascertion of highest thermal efficiency and specific thrust pertaining to turbofan powerplants. Patel et al. [44] considered efficiency, thrust and fuel consumption augmentation pertaining to turbojet powerplants. Kodal [45] implemented the maximum power density technique for irreversible amalgamated Carnot configurations. Chen et al. [46][47] conducted maximum power density assessments for Brayton configurations, where the intercooling pressure ratio is augmented for normalized power density; inaddition to an Atkinson powerplant configuration whilst the impact of temperature ratio was analyzed. Gonca et al. [48][49] evaluated the power density of a Miller configuration

and then conducted an analogous investigation for a Dual-Atkinson configuration beneficial towards optimization of internal combustion powerplant performances. In addition, Al-Sharki et al. [50] investigated the Miller configuration efficiency utilizing the maximum power density approach. Cheng et al. 0 have also inquiered into Brayton configurations intended for high power producing hypersonic 'next generation type' aircraft/spacecraft vehicle.

Contrastingly, researchers have utilized evaluations via ECOP and ECOL for both Carnot and Brayton thermodynamic configurations aiming at enhanced performance and reduced green house gases. Notwithstanding, ECOP and ECOL are techniques that can be applied by the aeronautical sector for the conceptualization of 'new generation engines' that are ecologically and environmentally advantageous [31-46]. Moreover [52], investigators have studied performance preconditions and their effect on gas turbine cycle performance and module conception. Zenkner et al. [68] examined the maximum fuel expenditure and accessible installation area towards powerplant inlet augmentation. J. J. Otter et al. [69] evaluated aerodynamic installation consequences as well as effects on central nozzle dimension. Chen et al. [70] studied divergences of engine modules and their consequence on the performance of an adaptive engine cycle.

In terms of the ramjet, tubojet with afterburner and turbine based combined cycle (TBCC) engines, researchers have used the application of exergy exploration on various aspects in accordance to task requirements. Şöhret et al. [73] applied an exergy efficiency analysis for a ramjet engine using hydrogen fuel on a component (inlet, combustion zone and nozzle) and overall engine level. Latypov [76] conducted an exergy investigation based on various energy supplies to the air flow of the ramjet duct. Latypov [77] also assessed the specific impulse and thrust-economic characteristics of the ramjet using exergy analysis. Ayaz et al. [78] used exergy analysis on a generic ramjet engine under three different Mach regiems. Moorhouse [79] expanded the exergy method to the design of a complete aircraft vehicle based on mission requirements including component level evaluation. Moorhouse et al. [80] further expands his study to the applicaion of hypersonic vehicle design as an energy problem. Moorhouse et al. [81] also applied the exergy consept to the hypersonic inlet flow problem to determine the optimal shock-on-lip position for off-nominal flight conditon. Marlet et al. [82] also made use of exergy evaluation for a combined ramjet and turbojet engine during transient maneuvers as well as the wake region of the

turbojet engine. Ispir et al. [83] used an exergy simulation based platform for the thermodynamic cycle and performance optimization of the STRATOFLY MR3 aircraft vehicle in DMR mode, ATR combustor, regenerator, nozzle, turbomachinery components and air turbo rocket bypass line. Ehtaei et al. [84] utilized an exergy approach for a turbojet engine with an afterburner (J85-GE-21) on a component level where the highest exergy efficiency was observed for the compressor and nozzle. Roth et al. [85] considered the loss management method for the analysis and quntification of technology impact of the F-5E/J85-GE-21 engine/airframe combintions and its relation to vehicle mass properties (weight). Camberos et al. [86] have published a book specifically describing the advantage of exergy analysis in the field of astronautics and aeronautics for various types of propulsion systems and even applying the concepts of exergy to airfoil drag evaluation. Hayes et al. [87] showed that exergy can be adopted to various aspects in aerospace including design, performance and thermodynamic analysis of commercial aerospace systems, propulsion systems, aerodynamic and structural optimization, multi-disciplinary optimization based on the Breguet equation and mapping exergy over a variable flight envelope. Riggins et al. [88] also makes use of the laws of thermodynamics for the evaluation of a hyperspace vehicle applicble to both ramjets or scramjets using individual stream tubes as components within the overall fluid control volume. Balli 0 conducted a study of exergy destruction rates within engine components which were split into endogenous/exogenous and avoidable/unavoidable parts on a military turbojet engine with afterburner. Balli [90] then used the J85 turbojet engine with afterburner to assess the performance, exergetic, exergoeconomic, sustainability and environmental damage cost at Idle (ID), Intermediate (INT), Military (MIL) and Afterburner (AB) operation modes. Balli [91] further considered the afterburning effect on energetic and exergetic performance of an experimental Turbojet Engine (TJE) and to determine thermodynamic inefficiencies at military (MIL) and afterburner (AB) operation modes. Akkaya et al. [92] defined an exergetic performance coefficient (EPC) to assess a fuel cell power generation system (fuel cell stack, afterburner, fuel and air compressors, and heat exchangers) fed by hydrogen. Yüksel et al. [93] evaluated the exergetic analyses at Military (MIL) and Afterburner (AB) process modes of the (J85-GE-5H) military turbojet engine using kerosene (JP-8) and hydrogen (H2) fuels. Balli et al. [94] conducted a performance assessment for both MIL and AB operation modes; and while under afterburner operation, examined energetic and exergetic performances

and the effects on the environmental, ecological and sustainability metrics of the engine. Akkaya et al. [95] utilize an exergetic performance coefficient (EPC) for a gas turbine to investigate design parameters including fuel utilization, current density, recuperator effectiveness, compressor pressure ratio and pinch point temperature, to achieving higher exergy output with lower exergy loss in the system. Bastani et al. [96] applied exergy analysis and showed that the greatest exergy loss is in the afterburner due to its high irreversibility; therefore, the optimization of afterburner has an important role in reducing the exergy loss of total turbojet engine cycle. Yüksel et al. [97] conducted an exergy-based economic and sustainability analysis for a (J85-GE-5H) military turbojet engine (TJE) using kerosene and H2 fuel under MIL and AB regeims where higher exergy destruction occurred in the afterburner exhaust duct (ABED) and combustion chamber (CC) which led to higher exergy destruction costs. Niknamian [98] exergy analysis on J85-GE-21 turbojet engine and system optimization based on PSO (Particle Swarm Optimization) methods which showed that highest and lowest exergy efficiency of the engine components corresponded to the diffuser and compressor respectively. Sürer et al. [99] performd a critical mini review exergy analyses of jet engines which concluded that if there is no afterburner, the combustion chamber has the greatest exergy destruction and thus minimum exergy efficiency due to its highly thermodynamically irreversible process; whereas the presence of an afterburner constitutes the biggest exergy destruction and smallest exergy efficiency. Dong et al. [100] revealed that the exergy analysis method can be used as a direct indicationof the weaknesses of an entire energy system, reveal the interactions among system components and estimate the realistic work potential of different subsystems; it also provides a significant guidance for the improvement of engine performance, reduction of fuel consumption and optimization of engine combustion. Noori et al. [101] made use of four objective functions (F_s, TSFC, η_{th} and η_p) for the optimization of an ideal turbojet engine with afterburner. Nasab et al. [102] conducted an exergy analysis for the J85-GE-21 turbojet engine with afterburner where the highest exergy efficiency was demonstrated by the diffuser and the lowest belonged to the compressor.

It is clear that the use of exergy as an analysis tool provides an advantage in the evaluation and optimization of aircraft gas turbine propulsion systems. Identification of the level of exergy destruction can be made on a component level and subsequently

exploit optimization functions for the improvement of TSFC, ST, η_{th} and η_p thus reducing the ecological impact of aircraft based engines on the environment.

1.3 Conjecture

A comparative performance analysis for various optimization criterion functions is to be carried out for an irreversible Brayton cycle applicable to aircraft jet engines: Turbojet (Without an Afterburner), Turbojet (With an Afterburner), Ramjet and Turboramjet. Where the turboramjet engine cycle is identified as Turbine Based Combined Cycle Engines (TBCC). Such hybrid cycle engines can be applied to UAV's, UCAV's and powering future hypersonic flight vehichles.

The main focus of the comparative performance analysis for the various optimization criterion functions will be applied to the aircrat turbojet cycle without an afterburner; whereas the tubojet with an afterburner, ramjet and turboramjet engines will be assessed on the basic principle of maximum power generation capability.

It is aspired that this investigation would bestow beneficial comprehension in the precursory configuration of airborn based gas turbibe engines (Turbojet: No Afterburner, Turbojet: With Afterburner, Ramjet and Turbo-Ramjet) and construct a platform towards a journey in promoting adaptive powerplant modules and configurations for the inception of truly intelligent powerplants; a gas turbine with the capability of evaluating its present operating condition and work towards a logical appreciable and favorable power interim (ECOL or ECOP or MP or MPD) such that the developer's and engine's expected performance capability is realized.

The program utilized to investigate the correlative performances of an irreversible Brayton configuration relevant for aircraft jet engine cycles is the scholistic platform of MATLAB 2018b supplied by the MathWorks corporation (See APPENDIX D).

2. THEORETICAL MODEL OF TURBOJET: NO AFTERBURNER

2.1 Objective Formulations and Established Variables

The irreversible Brayton cycle and T-s diagram characterization of the turbojet cycle configuration are shown in Figure 2.1. The elementary states of the Brayton cycle are: air compression accomplished via a multistage compressor; squeezed fluid is further combined with fuel to be ignited at static pressure constraints inside a combustion chamber; lastly, high temperature gases leaving the combustor are dialated across a turbine and nozzle to generate work. The representation of the turbojet engine applied for investigation operates between a high temperature heat source, T_H, and low temperature heat sink, T_L. The rate of heat transmitted from the heat source to the jet engine and rate of heat casted to the heat sink from the jet engine are $\dot{Q}_H$ and $\dot{Q}_L$ respectively.

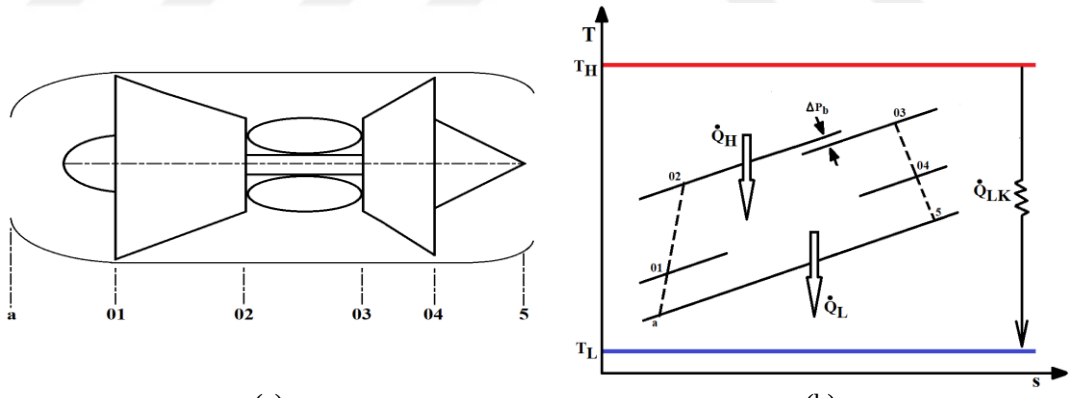

(a) (b)

Figure 2.1: Engine arrangement (a) and T-s schematic representation of a turbojet cycle (b).

The rate of total heat trasmitted $\dot{Q}_{HT}$ and rejection $\dot{Q}_{LT}$ are defined as:

$$\dot{Q}_{HT} = \dot{Q}_H + \dot{Q}_{LK} \tag{2.1}$$

$$\dot{Q}_{LT} = \dot{Q}_L + \dot{Q}_{LK} \tag{2.2}$$

where $\dot{Q}_{LK}$ is the rate of heat seepage coming out of a high and flowing towards a low heat reservoir and can be asserted as:

$$\dot{Q}_{LK} = \dot{m}_a \xi C_{pa}(T_H - T_L) \quad (2.3)$$

where ξ is a percent of internal conductance and $\dot{m}_a$ as air mass flow rate to the powerplant. In agreement with the first law of thermodynamics, the power extracted from the turbojet powerplant configuration is:

$$\dot{W} = \dot{Q}_{HT} - \dot{Q}_{LT} = \dot{Q}_H - \dot{Q}_L \, . \quad (2.4)$$

The total heat trasmission rates coming out of the high temperature source is expressed as:

$$\dot{Q}_{HT} = \dot{m}_f Q_R \eta_b \quad (2.5)$$

where Q_R is the amount of heat discharged from the fuel per unit mass, the mass flow rate of fuel is $\dot{m}_f$ and the combustion efficiency is η_b.

A compression ratio parameter, θ_c is delineated as: $\theta_c = (P_{02}/P_{01})^{(\gamma-1)/\gamma}$; as well as a cycle temperature ratio (α) designation of: $\alpha = T_{03}/T_a$.

Implementing an energy balance between the inlet and outlet of the combustor the fuel to air ratio, f resolves as:

$$f = \frac{C_{pt}T_{03} - C_{pa}T_{02}}{Q_R\eta_b - C_{pt}T_{03}} \quad (2.6)$$

The expression of the turbojet variables including: thrust (F), specific thrust (F_S), thrust specific fuel consumption (TSFC), air specific impulse (I_a), thermal (η_{th}), and propulsive (η_p) efficiencies, power density ($\dot{W}_d$), rate of entropy generation ($\dot{S}_G$), ECOL and ECOP have been prescribed in accordance to the engine configuration imparted in Figure 2.1. Furthermore, variations of altitude were evaluated utilizing the methodology provided by Airbus [30].

Moreover, the dimensional deviation of respective powerplant constituents and their collaboration to the overall performance was analyzed subject to maximum power, power density, ECOP and ECOL constraints. Dimensional deviations were expressed with reference to variations of specific volume (Δv) and dimensionless pressure ($\acute{P}$) and temperature ($\check{T}$). Furthermore, the span of the combustion chamber was assessed for optimum working constraints utilizing the equations imparted by Mattingly [73].

$$L = cP_{t2}^{-r}/\sqrt{T_{t3}} \quad (2.7)$$

Equation 2.7 above was calibrated using a $P_{t2} = 2.5$ and $T_{t3} = 6$ and $L = 0.526\,m$ provided by Farokhi [74] such that the constant c was resolved.

The thermal efficiency for the turbojet powerplant cycle is written as:

$$\eta_{th} = \frac{\dot{W}}{\dot{Q}_{HT}} = \frac{\dot{W}}{\dot{m}_f Q_R \eta_b}\,. \tag{2.8}$$

The thrust formula is acquired by implementing the integral form of the momentum equality by properly designating a control volume across the engine [23].

$$\mathrm{F} = \dot{\mathrm{m}}_a[(1+\mathrm{f})\mathrm{C}_5 - \mathrm{C}_\mathrm{a}] + A_5(p_5 - p_a) \tag{2.9}$$

where C_5 = exit speed, C_a = free stream speed, A_5 = nozzle exit cross sectional area and f = proportion of fuel to air mass flow rate. Accepting that perfect expansion occurs acorss the nozzle and utilizing a per unit weight foundation, specific thrust may be defined in the form below:

$$\mathrm{F}_S = (1+\mathrm{f})\mathrm{C}_5 - \mathrm{C}_\mathrm{a}. \tag{2.10}$$

The thrust specific fuel consumption is directly enumrated as:

$$\mathrm{TSFC} = \frac{f}{F_S} \tag{2.11}$$

and the air specific impulse becomes:

$$\mathrm{I}_\mathrm{a} = \frac{F_S}{g}. \tag{2.12}$$

The power density equals frations of power to the maximum specific volumes of the engine configuration and designated as:

$$\dot{W}_d = \frac{\dot{W}}{v_5}. \tag{2.13}$$

The propulsive efficiency is delineated as:

$$\eta_p = \frac{F\,C_a}{\dot{W}}\,. \tag{2.14}$$

The destruction of exergy for a powerplant equals the reversible power less the actual power generated and formulated such that:

$$\dot{X}_{DES} = \dot{W}_{rev} - \dot{W}\,. \tag{2.15}$$

The power manifested from a Carnot heat powerplant is known as the reversible power:

$$\dot{W}_{rev} = \dot{m}_f Q_R \eta_{Carnot} \quad (2.16)$$

where η_{Carnot} equals a Carnot efficiency. The formulation of a traditional Brayton configuration can be obtained from thermodynamic textbooks such as [28]. The fraction of destroyed exergy to the reversible power is considered as the power loss (PLOS) parameter and given as:

$$PLOS = \frac{\dot{X}_{DES}}{\dot{W}_{rev}}. \quad (2.17)$$

The fraction of ideal minus real power from the Brayton configuration to the reversible power is designated as the effective power loss (EPLOS) and written as:

$$EPLOS = \frac{\dot{W}_{Bray} - \dot{W}}{\dot{W}_{rev}}. \quad (2.18)$$

The rate of entropy generation of the turbojet powerplant configuration is prescribed in the form of:

$$\dot{S}_G = \frac{\dot{Q}_{LT}}{T_L} - \frac{\dot{Q}_{HT}}{T_H} \quad (2.19)$$

The ratio of power output to the loss rate of availability is known as the ECOP objective function and written as:

$$ECOP = \frac{\dot{W}}{T_0 \dot{S}_G} \quad (2.20)$$

The ecological equality is delineated as:

$$ECOL = \dot{W} - T_0 \dot{S}_G \, . \quad (2.21)$$

A portion of the total energy released from fuel combustion is inaccessible energy while the residual energy is considered to be transformable reversible power; that is, the power produced fron the ideal Carnot cycle. However, Brayton cycles are he basis of turbojet engine operation. As a consequence of the powerplant configuration and operational variations amongst the representations of the Brayton and Carnot configurations, performance assessments regarding ideal Carnot configurations cannot be an exemplary evaluation. Furthermore, the Carnot and Brayton cycles are not interchangeable and cannot expect that the power generated by either cycle to be interchangeable with one other; each cycle is unique from the other and must be assessed with their own respective operational states and cycle classification(s). Therefore, the performance of a real physical airbreathing engines must be investigated

and compared to its ideal case: i.e. an ideal Brayton cycle vs. aircraft engine Brayton cycle with losses. In addition, discussions of performance enhancement investigations with rgards to the Carnot cycle are profoundly misleading. The distinctions amongst PLOS and EPLOS depict the power that cannot be produced due to the representative configuration of the powerplant: Carnot vs. Brayton. Thus, the variable, Carnot Brayton Shape Factor (CBSF), which identifies non-reproducible power between the cycle configurations of Carnot and Brayton and specified as:

$$CBSF = PLOS - EPLOS = \frac{\dot{W}_{rev} - \dot{W}_{Bray}}{\dot{W}_{rev}}. \quad (2.22)$$

Based on the second law of thermodynamics, EPLOS is a performance analytical parameter which may be utilized in depicting impacts of internal irreversibilities on power production deficits from an ideal to an actual Brayton configuration. Whereas, PLOS indicates the overall power reduction from the Carnot cycle's reversible power output. Therefore, in terms of power output, PLOS and EPLOS can be used as a means of correlations between two discretionary operational (design) constraints on a hundred percent scale, in addition to assessing the significant objective theorems collectively. Moreover, CBSF shows nor-reproducible power as a consequence of the preference of thermodynamic powerplant (the extent of how mcuh the power generated y the Brayton or any other cycle configuration - Otto, Rankine, Diesel, Stirling, Ericsson, etc.- approaches that of the ideal Carnot cycle). Therefore, the cooperative utilization of the prescribed objective functions of PLOS, EPLOS and CBSF, endows the performance evaluation of the irreversible Brayton configuration utilizing numerous working conditions.

2.2 Mass Flow, Engine Speed and Shaft Force Models and Altitude

The mass flow rate of air for the turbojet engine cycle is defined utilizing free stream standard atmospheric static criteria and given as:

$$\dot{m}_0 = \frac{P_0 A_0 M_0}{\sqrt{T_0}} \sqrt{\frac{\gamma}{R}} \quad (2.23)$$

Where A_0 is the upstream capture area from the engine inlet at altitude along with free stream flight Mach number and written as:

$$\left(\frac{A_0}{A_1}\right)_{MAX} = \frac{1}{M_0}\left[\frac{2}{\gamma+1}\left(1 + \frac{\gamma-1}{2} M_0^2\right)\right]^{\frac{\gamma+1}{2(\gamma-1)}} \quad (2.24)$$

For supersonic conditions the presumtion is that $A_0 \approx A_1$. The corrected gas generator speed (RPM) for the compressor or turbine depends on the tip speed Mach number of the rotor and written as:

$$\frac{N}{\sqrt{\theta}} = \frac{60}{\pi d} M_{tip} \sqrt{\frac{\gamma R T_{ref}}{1+\frac{\gamma-1}{2}M^2}} \quad (2.25)$$

Where the compressor or turbine diameter is d and the temperature normalization parameter θ is defined as T_t/T_{ref}. Stagnation conditions for the turbine inlet are presumed, therfore the Mach number of the flow entering the turbine can be considered as negligible; therefore, the Mach number at the tip of the turbine rotor is assumed to be sonic and under these constraints the preceding formula is truncated to:

$$N = \frac{60}{\pi d} M_{tip} \sqrt{\gamma R T_4} \quad (2.26)$$

The proportion of the turbine work to the exit velocity of the turbine is defined as the shaft force of the turbojet powerplant and written as:

$$F_{shaft} = \dot{W}_{turbine}/C_4. \quad (2.27)$$

Reference [29] can be consulted for the complete comprehensive formulations.

Alterations in altitude (ISA conditions) were examined for the turbojet cycle utilizing the temperature and pressure formulations provided by Airbus [30]. Beneath the tropopause (i.e. ≤ 11000 meters) the temperature and pressure equations are defined as:

$$T = T_0 - 6.5\,\frac{h(m)}{1000} \quad (2.28)$$

$$where\ T_0 = 15^0 C\ for\ h \leq 11000\ m$$

$$P = P_0 \left(1 - 0.0065\,\frac{h}{T_0}\right)^{5.2561} \quad (2.29)$$

$$where\ T_0\ (K), h(m)\ and\ P(hPa)$$

Beyond the tropopause the temperature and pressure formulations provided in the form of:

$$T = -56.5^0 C\ for\ h > 11000\ m$$

$$P = P_{11} e^{-\frac{g}{RT_{11}}(h-h_{11})} \quad (2.30)$$

$where\ P_{11} = 226.32\ hPa, T_{11} = 216.65\ K\ and\ h_{11} = 11000\ m$

2.3 Algebraic Optimization Methodology

The correlative performance assessments implemented for irreversible Brayton turbojet powerplant configuration utilizes the scholastic rendition of MATLAB 2018b software dispensed by the MathWorks corporation.

Various algorithm approaches are created to accomodate the requisites of numerous types of augmentation chalenges. The primary classification of design perspectives are: classical optimization techniques, linear programming, nonlinear programming, geometric programming, dynamic programming, integer programming, stochastic programming, evolutionary algorithms, etc. The methodology of obtaining the criterions that provide the minimum or maximum value of an equation, where the functions constitute the endevour needed or the sought after interest is known as optimization. This research utilizes model optimization to augment (maximize or minimize) an objective equality without breaching capital restrictions; this is known as arithmetic data processing [31][32]. Thus, the compressor pressure ratio parameter (θ_c) being varied in order to resolve the maximum ECOP, ECOL, MP and MPD and minimum PLOS for changes of elevation and free stream flight Mach number M_∞; taking the equivalent mathematical process as the differential of θ_c. Moreover, the optimum operating conditions of maximum TSFC, I_a, f, EPLOS, thrust, and η_{th}. was resolved algebraically (Figure 2.15 to Figure 2.23). Assessments and correlations were subsequently conducted.

2.4 Outcomes and Considerations

The evaluation of the environmental and cost effective consequences of the irreversible Brayton turbojet engine cycle at flight conditions, requiers a sequence of algebraic computations carried out consturcted upon numerical conceptualizations prescribed in the preceding subdivision. The maximums of power and power density, ECOP and ECOL principle expressions were examined and investigated based on optimal circumstances. The operational criterias (altitude and M_∞) at each optimum circumstance, were corelated to one another subject to PLOS, EPLOS and CBSF specifications (Figure 2.15 to Figure 2.25). Performance assessmnets of fundamental turbojet engine variables along with their diversification with regards to constituent efficiencies, altitude and heat leakage were also examined. Table 2.1 constitutes the delegated variable inputs applied throughout this study; any deviation from the prescribed values are disclosed in the individual graphs. Normally, T_L may be distinct from T_a, however, in this work $T_L \cong T_a$. Essential formulae for the turbojet engine configuration state point computation may be obtained in Saravanamutto et al [27].

Table 2.1: Delegated variable inputs.

Inputs		
T_L = 200 K	η_j = 0.95	γ_g = 1.333
T_H = 2200 K	η_m = 0.99	R = 287 J/kg K
T_a = 223.3 K P_a = 26.5 kPa	η_b = 0.98	Di = 0.8 m
ALT = 10000 m	C_{pa} = 1.005 kJ/kg K	Q_R = 43000 kJ/kg
ξ = 0.01	C_{pg} = 1. 148 kJ/kg K	η_c = 0.87
η_i = 0.93	γ_a = 1.4	η_t = 0.9
M = 0.5	ΔP_b = 0.96	T_{03} = 1200 K

Changes of the optimization functions, including PLOS and the thermal efficiency, with regards to power are depicted in Figure 2.2. For a compressor efficiency (η_c) of 95%, the maximum thermal efficiency gives the maximum ECOP and minimum PLOS at a turojet power generation marginally higher than 12000 kW. Conversely, at maximum power density, the power discharge from a given turbojet configuration

approaches 14000 kW for a comparmize on moderate reductions of thermal efficiency, ECOP and PLOS.

Given Figure 2.3, the changes in the normalized construct of power, power density, ECOP, specific volume difference, $\nu_d = (\nu_5 - \nu_a)/\nu_a$) and ECOL collectively with the cycle thermal efficiency are given apropos the compression ratio parameter (θ_c). An increase in the compression ratio parameter results in an overall specific volume difference reduction, therefore, stipulating a reduction in engine size. Figure 2.3 shows distinctively that the optimal compressor ratio parameter at maximum ECOP is higher than that at maximum power density; in addition, the optimal θ_c at maximum power density is greater than that at maximum power conditions. Therefore, the overall outcome is that: $\theta_{c\,ECOP} > \theta_{c\,MPD} > \theta_{c\,MP}$. It is observed from Figure 2.3, that maximum ECOP operating conditions indemnifies favorable thermal efficiency and reduced powerplant dimensions at higher compression ratios. Correlations amongst the maximums of ECOP, power density and power circumstances were interpolated using Figure 2.3. The engine size in terms of normalized specific volume, power and thermal efficiency variations with regards to the maximums of ECOP power density and power conditions may be interpreted by sketching relevant contours that deliberately intersect the admissible lines on the graph. Bear in mind, that ECOL lies is on the secondary y-axis (right) and negative in quantity. While, the designated operating conditions are still physically applicable to the case(s) in question, it is important to address that ECOL can carry both positive or negative values owing to the intrinsic characteristic of its formulation.

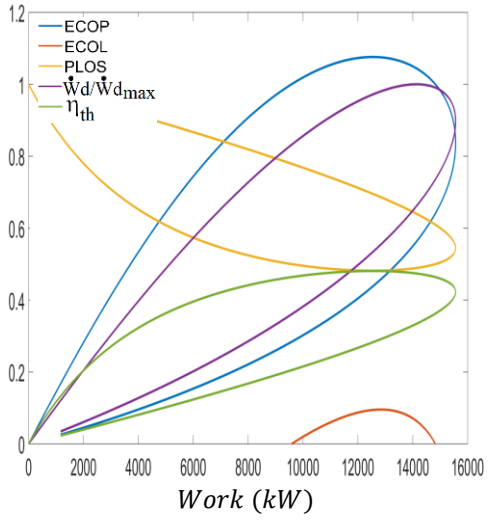

Figure 2.2: Various optimization functions vs. power at $\boldsymbol{\eta_t = \eta_c = 0.95}$.

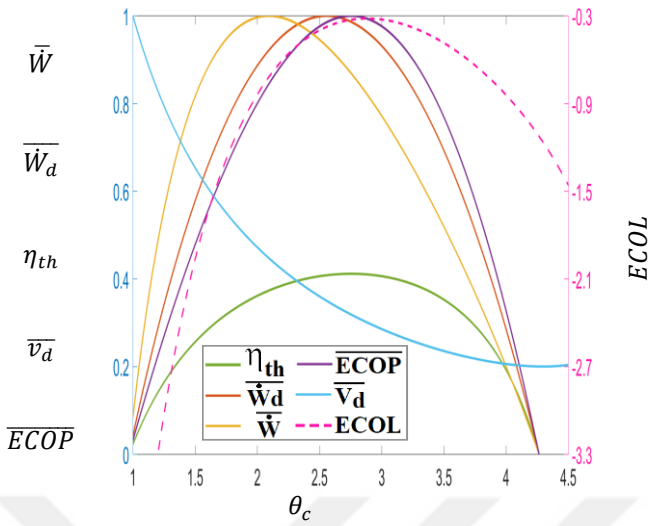

Figure 2.3: Non-dimentionalized power, power density, specific volume variance, ECOP, ECOL and $\boldsymbol{\eta_{th}}$ for variations of compressor pressure ratio parameter, $\boldsymbol{\theta_c}$.

The irreversible Brayton turbojet engine cycle was analyzed and compared with regards to the Carnot configuration utilizing the second law of thermodynamics. In order to provide a set graphical rendition of the different types of power generations or deficits with regards to the assessment equalities, Figure 2.4 is given. The solutions in Figure 2.4b were reconstructed to a 100% scale with regards to $\dot{W}_{rev}$ to be recognized and correlated with the Carnot configuration. The greatest achievable fuel heat discharge rate is denoted by $\dot{Q}_{fuel}$. If $\dot{Q}_{fuel}$ could be wholely translated into power, the topmost curve in Figure 2.4b is attained. Notwithsatnding, the second law of thermodynamics restricts that the most comprehensible reversible power that can be attained from the Carnot configuration (maximum power) can only be $\dot{W}_{rev}$. The heat leak rate, $\dot{W}_{lk}$, for the specified Brayton configuration will inflict additional power deficits. The achievable power from an ideal Brayton configuration is given as $\dot{W}_{Bray}$; in addition the power decrease from $\dot{W}_{rev}$ to $\dot{W}_{Bray}$ is a direct cause of the thermodynamic cycle configuration preference. Commensing with the ideal to the real Brayton configuration, even more power vanishes from cumulative irreversibilities of the respective engine modules (diffuser, compressor, burner, turbine and nozzle) that contribute to the powerplant configuration. Thus, the power generated from the actual Brayton configuration is prescribed by $\dot{W}$. Moreover, the derivable effective power for

a real Brayton configuration is assessed with regards to the attainable specific thrust (thrust force multiplied by the flight speed). Therefore, ultimately attaining the effective applicable power of a real Brayton configuration which is prescribed as $\dot{W}_{useful}$. Therefore, out-of the initial starting position of pure carburent heat discharge rate the culmination of power deficits are a consequence of powerplant differences and inevitably irreversibilities corresponding to physical life powerplants. Even at minimum PLOS, approximately 60 percent power reduction is observed; which indeed is an elevated quantity of power deficit. Notwithstanding, PLOS may be utilized as an approximated performance criterion amonst the ideal Carnot and real Brayton configuration, EPLOS, on the other hand, provides an improved functional correlation amongst the ideal and real Brayton configuration. For minimum PLOS operation, EPLOS is approximately 25 percent, which is precisely associated to intrinsic irreversibilities. The contrasts amongst PLOS and EPLOS is CBSF, this is roughly 35 percent of the total obtainable power and is forfeited due to the thermodynamic powerplant configuration of Brayton vs. Carnot. Thus, an effectively advocation for a collection of suitable projected powerplant performances and evaluate the effect amongst similar powerplant configurations classification via applying the newly asscribed optimization functions.

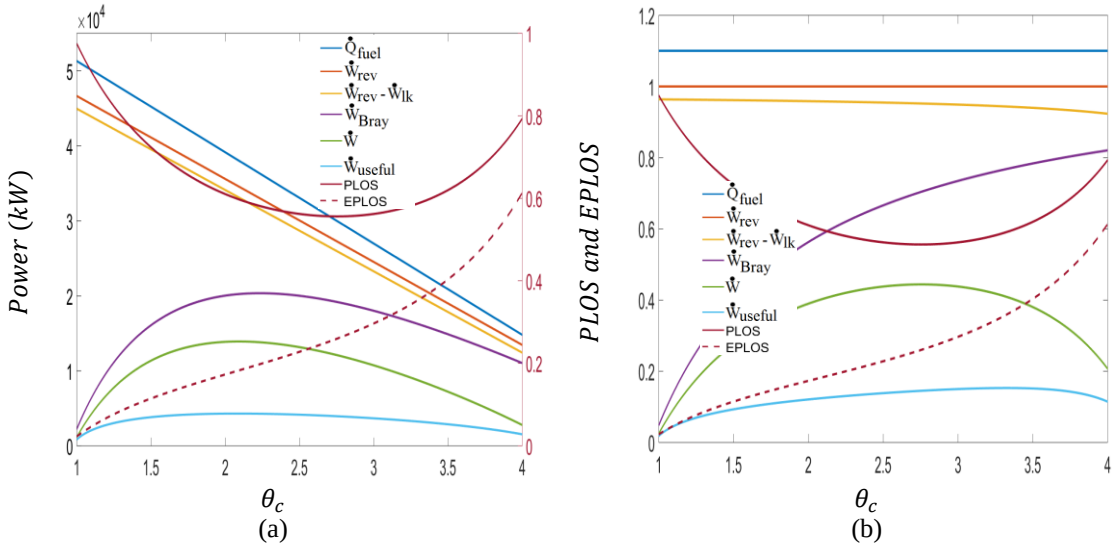

Figure 2.4: Manifestations of power losses (a) and their non-dimentionalized forms (b) for variations of $\boldsymbol{\theta_c}$

Furthermore, evaluating PLOS for variations of NG and shaft force (Figure 2.5a and Figure 2.5b), at reduced NG speeds increased shaft force outputs may be obtained as the compressor and turbine efficiency of the powerplant increases. Changes of power with regards to PLOS and EPLOS are given in Figure 2.6a and Figure 2.6b for different quantities of η_c. Where for maximum power conditions the practical operation range for the compression parameter is $\theta_c = 2 \pm 0.4$ with an exergy destruction range of 60 to 90 percent seen from PLOS values. This portrays the amount of destruction against the environment, even when improved performance is obtained from a power perspective. Moreover, as η_c nears unity, values of EPLOS at MP conditions decreases on the order of 15 percent. Also, EPLOS increases as θ_c increases, in the absence of an extrema circumstance. Therefore, it bcomes discernible that regardless if minimum PLOS or maximum power generation is targeted, there is an invariable limitation of rquired quantity desired.

Maximum power generated by the cycle transpires at quantities of $\theta_c = 2.0 \pm 0.4$ (Figure 2.7) for varying M_∞ and with a reasonable accomodation on PLOS and EPLOS. Minimum PLOS developed for quantities of θ_c in the range of 2.5 and 3, which demands increased compression ratios and therefore substantially larger compressors. Nonetheless, for ecofriendly deliberation, a minimum PLOS criteria is recommended. On the other hand, examining Figure 2.7b, EPLOS quantities are reduced at maximum power than at minimum PLOS constraints; suggesting engine constituent efficiencies are a source of higher power deficits at minimum PLOS operations.

A consolidation with regards to minimum TSFC and maximum I_a can be attained at minimum PLOS quantities (Figure 2.8). Maximum I_a quantities traspire when θ_c is lower than 2.5; on the other hand, minimum TSFC quantities are obtained when θ_c is larger from 3. Where $\theta_c = 2.5 \; and \; 3$ grants a compressor pressure ratios (P_{02}/P_{01}) of 25 and 47 respectively. Although, for $\theta_c \geq 3$ a designer must contemplate material impediments in terms of temperature particularly for combustion chambers and the turbine blades.

When the compressor ratio parameter is $\theta_c \leq 1.75$ (Figure 2.9), and M_∞ is ~1.4 and above, PLOS increases, η_p is still favourable and thrust generated increases. However, for $\theta_c > 1.75$ and M_∞ is ~1.4 and below, the reduction in PLOS and increase in thrust

output arrives for a compromise on η_p. For both thrust and η_p, at M_∞ above 1.4, the quantities of PLOS experience a rapid increase; although η_p is still advantageous, the θ_c of the cycle must be reduced to attain favourable thrust outputs. Given a prescribed compressor and a targeted θ_c design point, the Mach number transforms to an operational condition of preference; however, flight operation is favoured within the minimum PLOS range where the destruction of exergy is reduced and thus less detrimental to the ecology. Consequently, an operational zone chosen in the region of $1.4 < M_\infty < 1.6$ then ecological liabilities (lower PLOS) as well as having the capability for higher thrust generation can be fulfilled. The steep increase in PLOS is ascribed to the sharp reduction of power generated at increased values of θ_c, which subsequently truncates the mathematical statement of PLOS to the ratio of $\dot{W}_{rev}$ to $\dot{W}_{rev}$; thus, under these conditions PLOS nears unity. In addition, EPLOS encounters this similar situation, where a decrease in $\dot{W}$ the mathematical definition reduces to the proportion of ideal Brayton to ideal Carnot power generation; thus, EPLOS also nears unity.

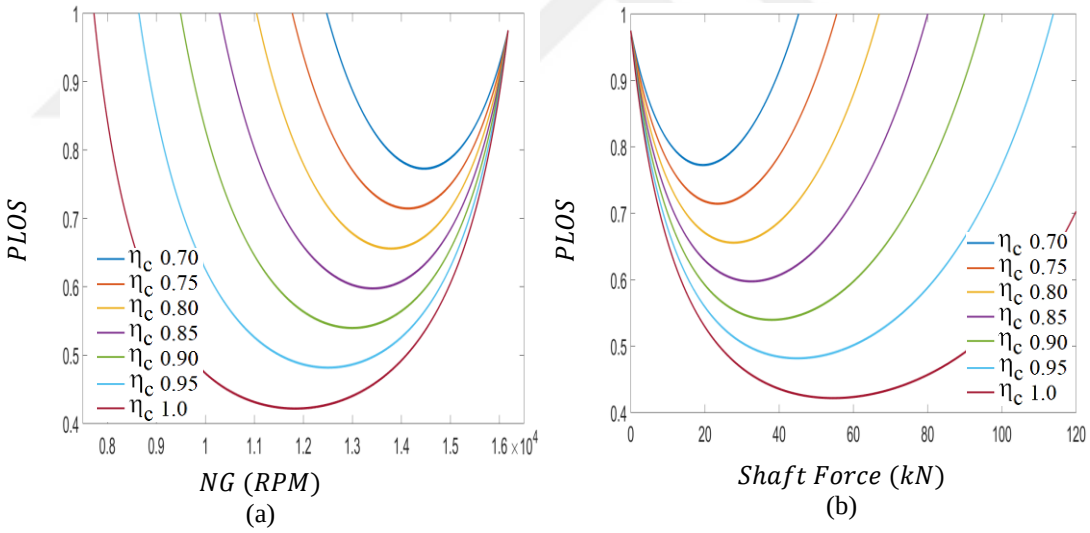

Figure 2.5: Contours of PLOS for variations of (a) NG and (b) Shaft Force for distinct quantities of $\boldsymbol{\eta_c = \eta_t}$

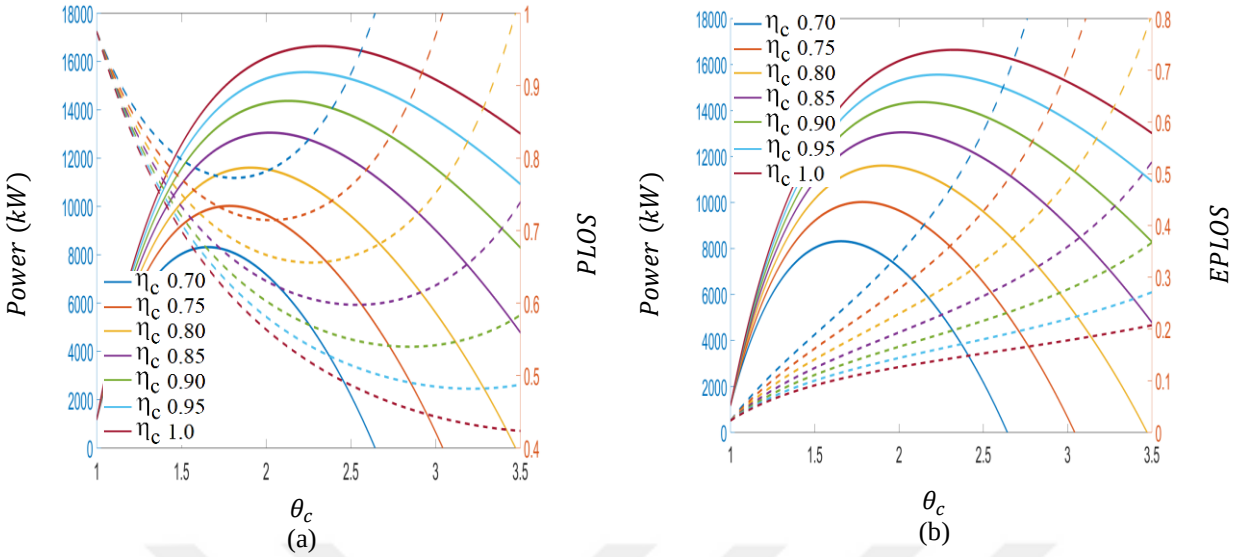

Figure 2.6: Contours of power and PLOS (a) and EPLOS for variations of $\boldsymbol{\theta_c}$ for dsitinct quantities of $\boldsymbol{\eta_c} = \boldsymbol{\eta_t}$[1]

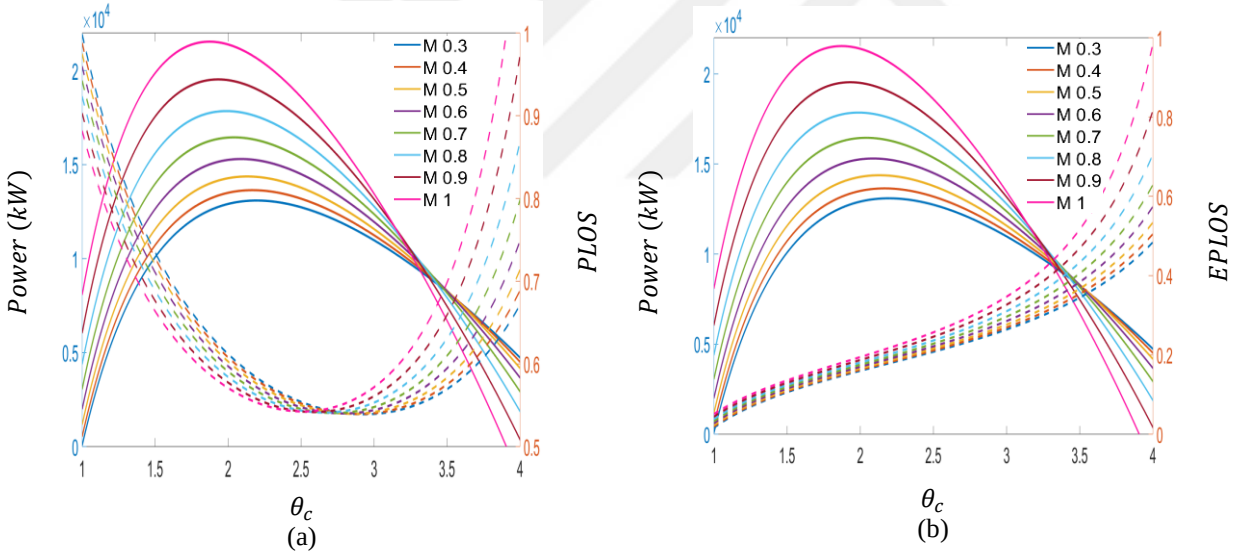

Figure 2.7: Contours of power and PLOS (a) EPLOS for variaitons of $\boldsymbol{\theta_c}$ for distinct quantities of $\boldsymbol{M_\infty}$

[1]: Figure 2.6 to Figure 2.9: Dashed lines lie on the secondary y-axis (right) and represent values of PLOS and EPLOS only.

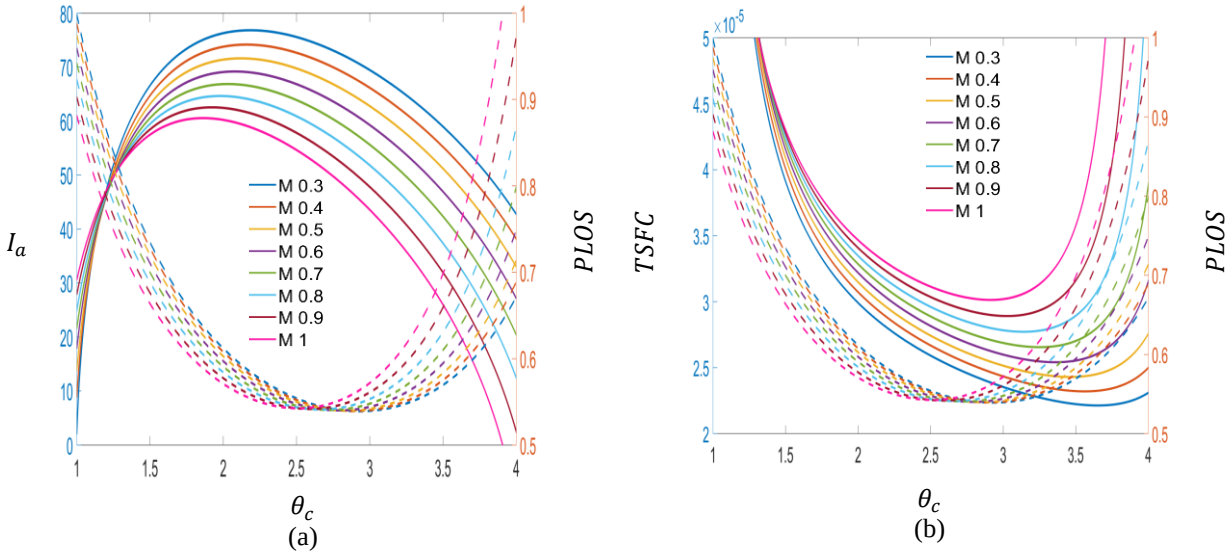

Figure 2.8: Contours of $\boldsymbol{I_a}$and PLOS (a) and TSFC (b) $\boldsymbol{\theta_c}$ for distinct quantities $\boldsymbol{M_\infty}$

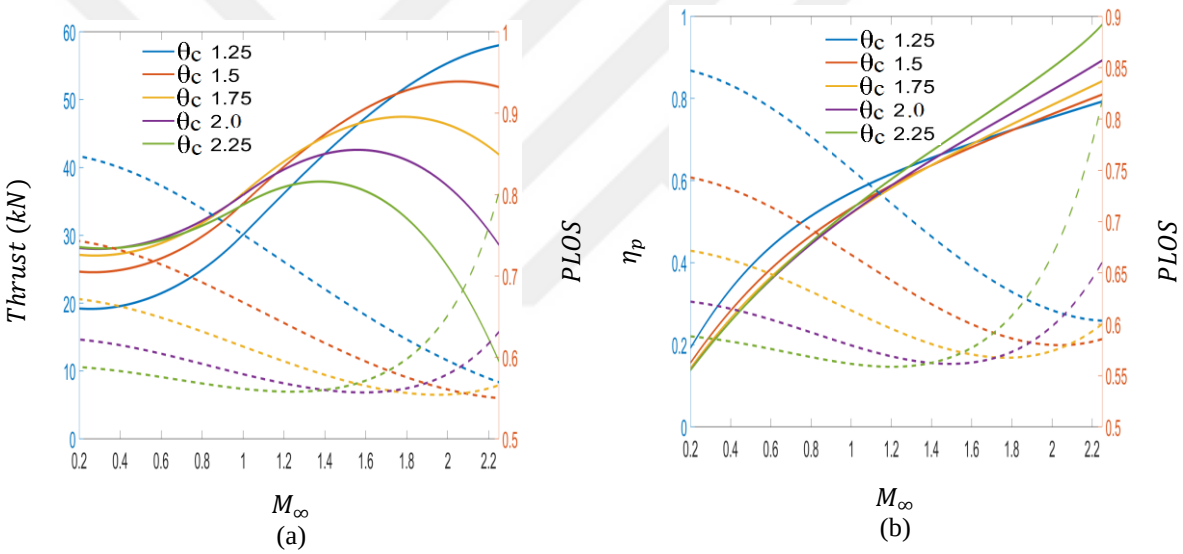

Figure 2.9: Contours of thrust and PLOS (a) and $\boldsymbol{\eta_p}$ (b) for variaitons of $\boldsymbol{M_\infty}$ for distinct quantities of $\boldsymbol{\theta_c}$

For a PLOS assessment for variations of power and for changes in compressor efficiency (Figure 2.10), power deficit decreases and the power output increases as η_c increases. It is worthy of noting that for a range of η_c from 70 to 100 percent, the power generated by the powerplant increases two-fold. For an increasing inlet flight Mach number, the required power generation from the powerplant must increase (Figure 2.11). While the power increases at increasing Mach number, quantities of minimum PLOS are not seen to vary for the selected operational condition under fixed irreversibilities. Moreover, Figure 2.12 illustrates that while the internal conductance

ξ for heat leakage drops PLOS also reduces; therefore, the working fluid is efficient in transforming the heat produced by the powerplant into accessible power at a minimum power deficit. Likewise, for engine operation at higher altitudes (Figure 2.13) both PLOS and the power generated by the turbojet decreases. Furthermore, for variations in altitude, the minimum quantities of PLOS for variations of power alludes to a linear association amongst the variables. Also, for M_∞ below sonic operation (Figure 2.14), there is a distictive benifit for the optimums of $TSFC^*$, I_a^* and f^* at maximum power and minimum PLOS of the powerplant.

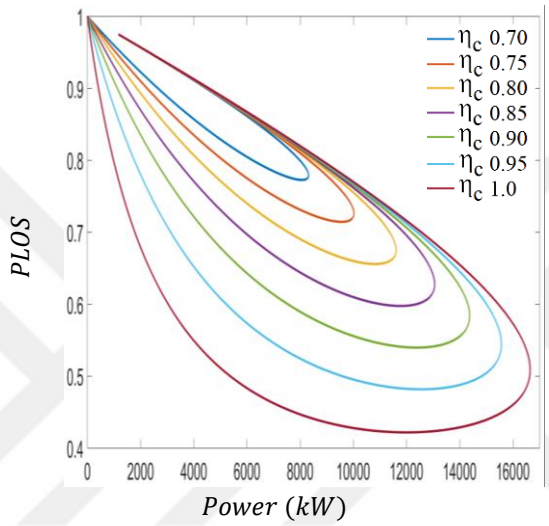

Figure 2.10: Contours of PLOS for variaitons of power for distinct quantities of $\boldsymbol{\eta_c = \eta_t}$

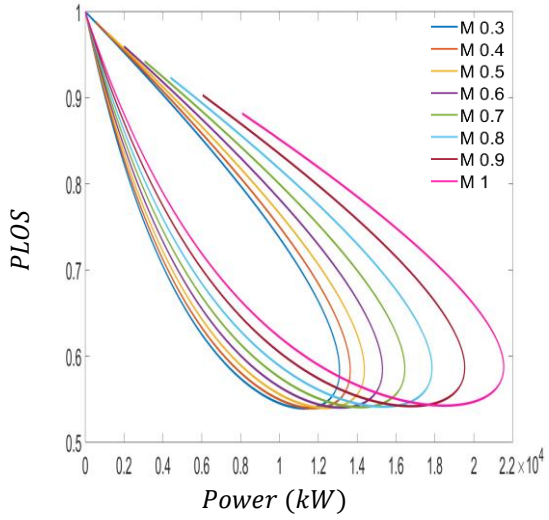

Figure 2.11: Contours of PLOS for variaitons of power for distinct quantities of $\boldsymbol{M_\infty}$

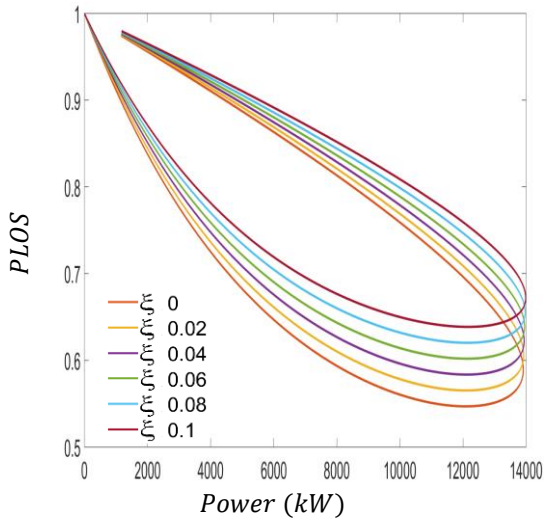

Figure 2.12: Contours of PLOS for variaitons of power for distinct quantities of heat leakage rates.

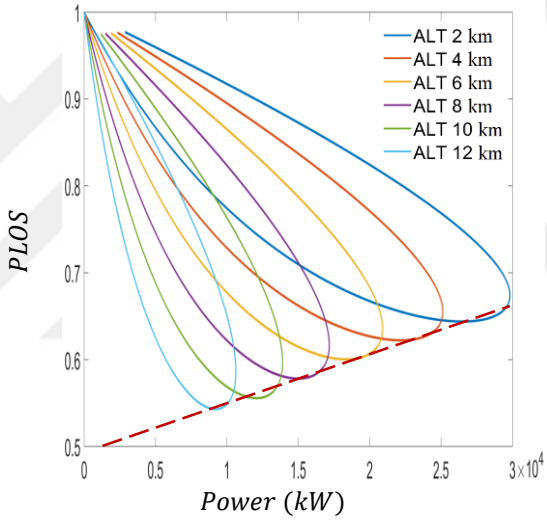

Figure 2.13: Contours of PLOS for variations of power for distinct quantities of altitudes

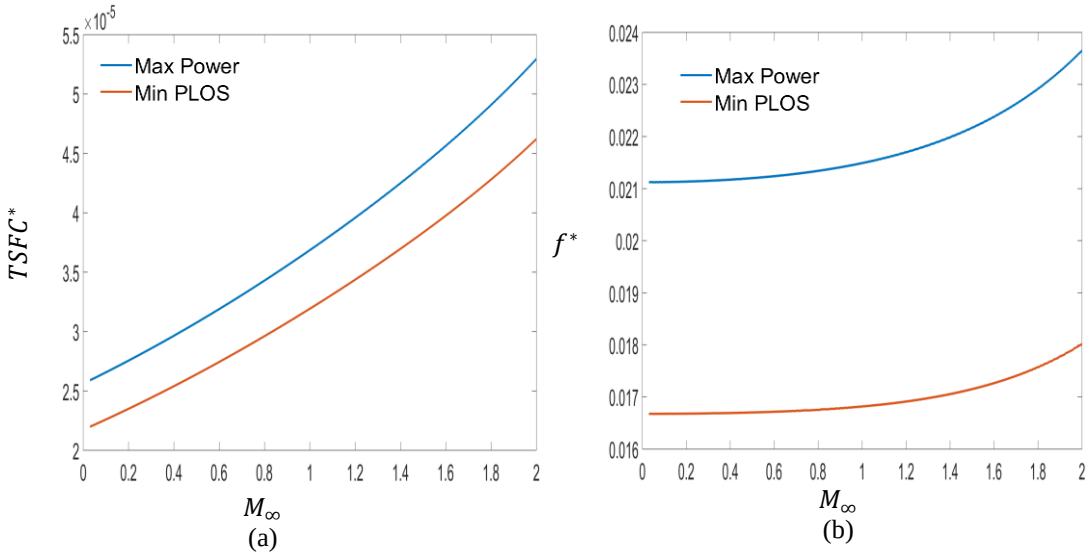

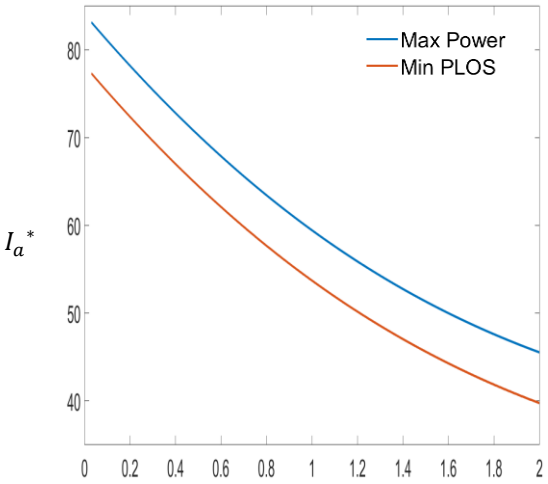

(c)

Figure 2.14: Contours of $\boldsymbol{TSFC}^*$ (a), $\boldsymbol{f}^*$ (b) and $\boldsymbol{I_a^*}$ (c) for variations of $\boldsymbol{M_\infty}$ at maximum power and minimum PLOS conditions

In Figure 2.15 through Figure 2.23, the optimum operational criterias of maximum power, maximum power density, ECOP and ECOL are evaluated amongst one another for selected principle performance variables as well as PLOS, EPLOS and CBSF. Figure 2.15 shows the contours of optimum EPLOS quantities with regards to altitude and flight Mach number. Maximum power operations indicate the minimal EPLOS quantities with regards to the remaining optimization theorems, in addition to stipulating a higher resiliance to internal irreversibilities. On the other hand, the maximum power conditions decreased thermal efficiencies and increased PLOS quantities (Figure 2.16 and Figure 2.17). Thus, maximum power operations are more detrimental for the environment, even if they exhibit the most reduced internal irreversibility impacts between the examined optimization theorems. Therefore, maximum power operation increased specific impulse and thrust (Figure 2.18 and Figure 2.19). In addition, maximum power operation have higher TSFC quantities (Figure 2.21) while producing the largest amount of power (Figure 2.22) for a moderate decrease in compression ratios (Figure 2.20) which results in reduced compressor sizes. The non-producible power owing to the configuration of the Carnot and Brayton configuration is portrayed in Figure 2.23; and is a comparitive assessment of the ideal Brayton configuration to the 100% scale of the Carnot configuration. Figure 2.23 indicates that for higher altitudes a reduced amount of power is forfeited, thus, the power generated by the Brayton cycle nears that of the Carnot cycle. Whereas,

M_∞ is seen to have a insignificant impact with regards to power generation; as a result, the forward speed of the aircraft is inconsequential. Depending on the design application, various testimonies can be obtained; operation at the maximum ECOL criteria renders higher EPLOS and lower PLOS quantities between the remaining optimization statements. Despite the impacts of the internal irreversibilities being moderately increased, the maximum ECOL criteria confers a more beneficial economical and environmental outcome.

The evaluation of Figure 2.17 reveals that for maximum power and ECOL operations, lower PLOS values are achieved at elevated altitudes and develope more beneficial circumstances for ecological deliberations; on the other hand M_∞ is seen to have marginal impact. However, if it is fundamental to have a larger power generation the turbojet must function at reduced altitudes and increased M_∞ when maximum power and ECOL operation are used, this is shown in Figure 2.22. Thus, it is up to the engineer to determine the design state of preference. Maximum power and ECOL operation can be more ecologically favourable (greater altitudes for reduced power generation) and alternatively present undesireable conditions (reduced altitudes higher M_∞ and increased power generation); or perhaps a consolidation amongst the operational altitudes and power generations.

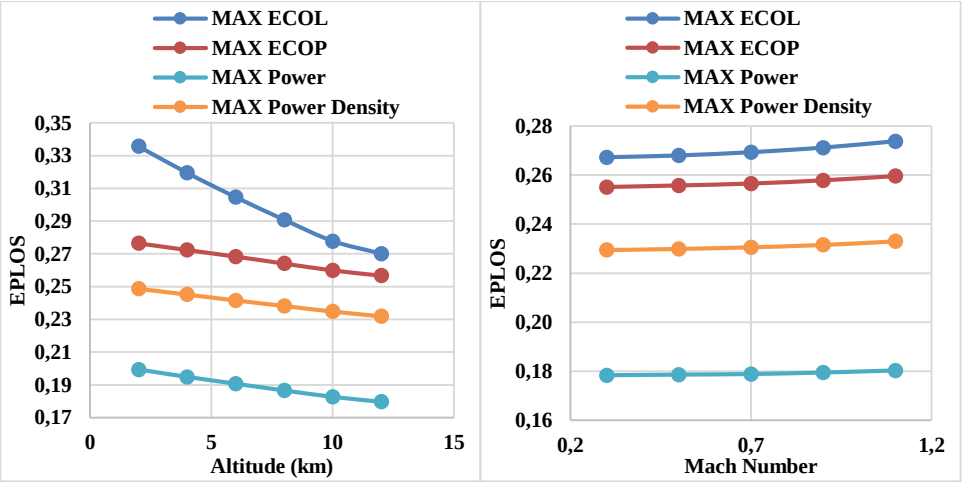

Figure 2.15: Optimum EPLOS contours for prescribed ALT and $\boldsymbol{M_\infty}$.

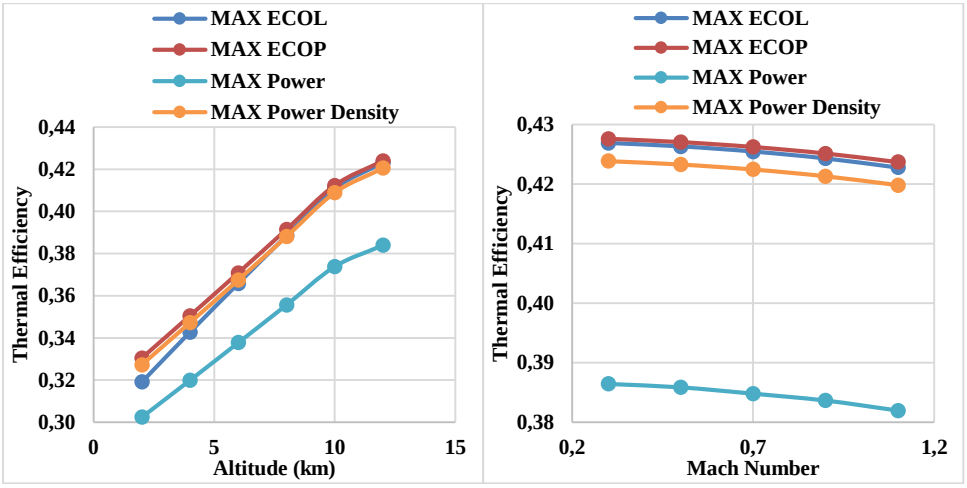

Figure 2.16: Optimum η_{th} contours for prescribed ALT and M_{∞}.

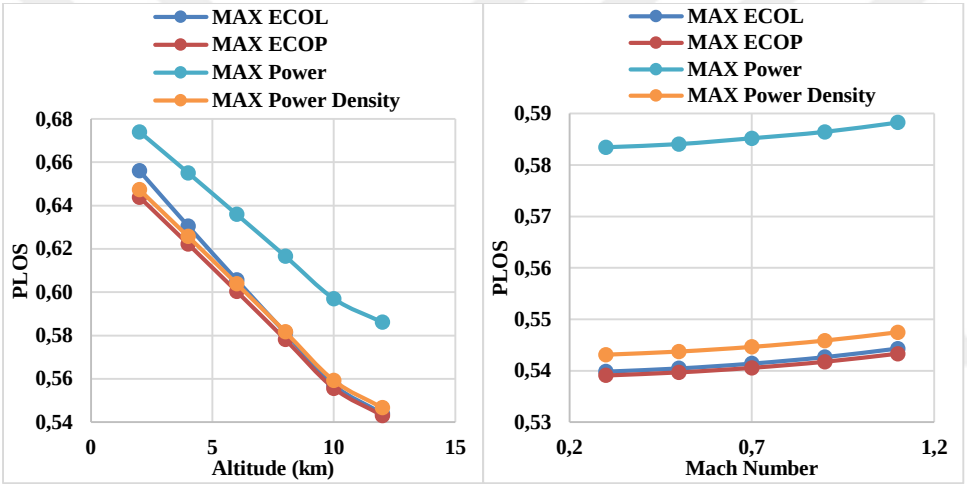

Figure 2.17: Optimum PLOS contours for prescribed ALT and M_{∞}.

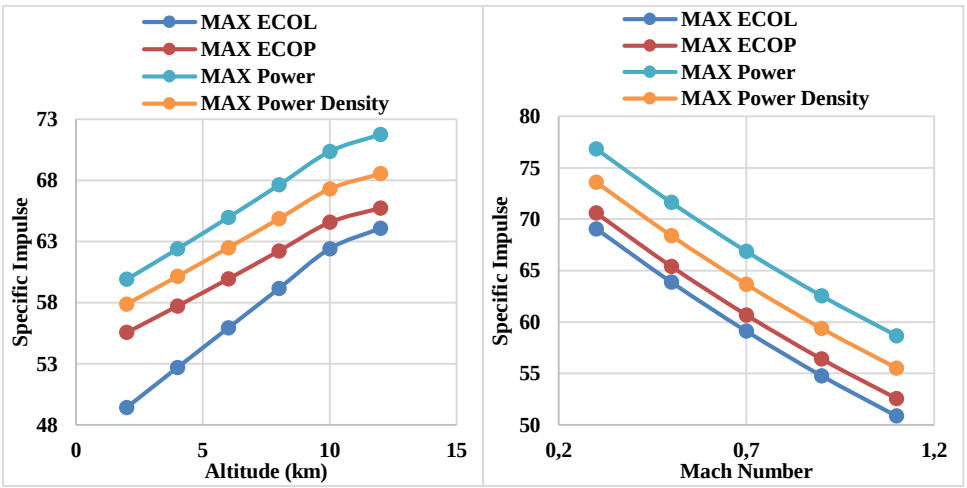

Figure 2.18: Optimum I_a contours for prescribed ALT and M_{∞}.

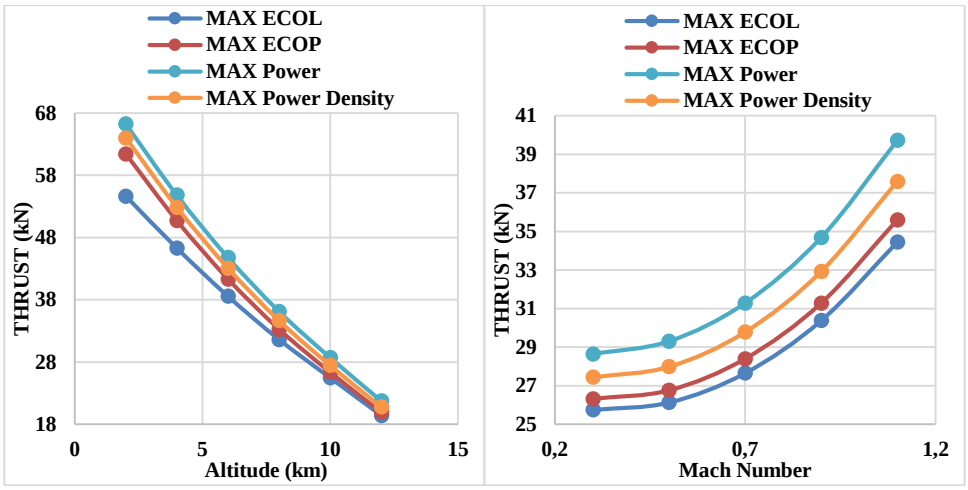

Figure 2.19: Optimum Thrust contours for prescribed ALT and M_∞

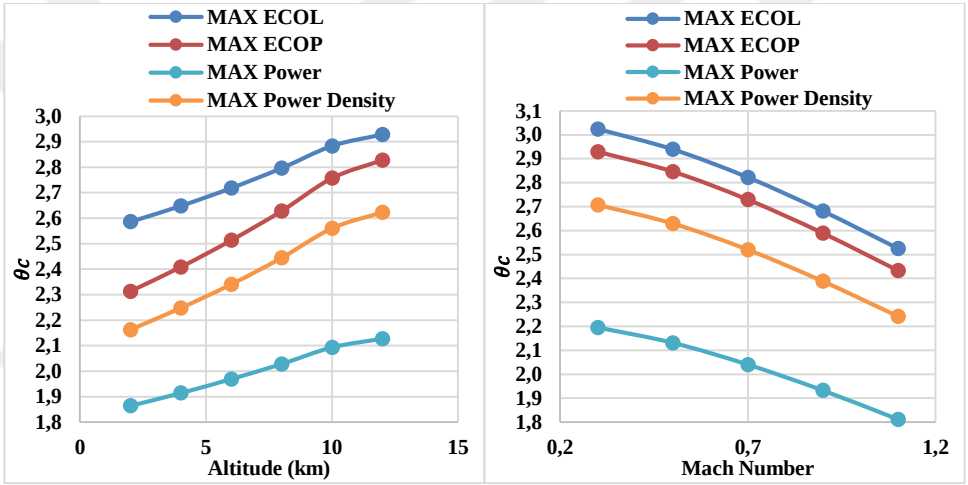

Figure 2.20: Optimum θ_c contours for prescribed ALT and M_∞.

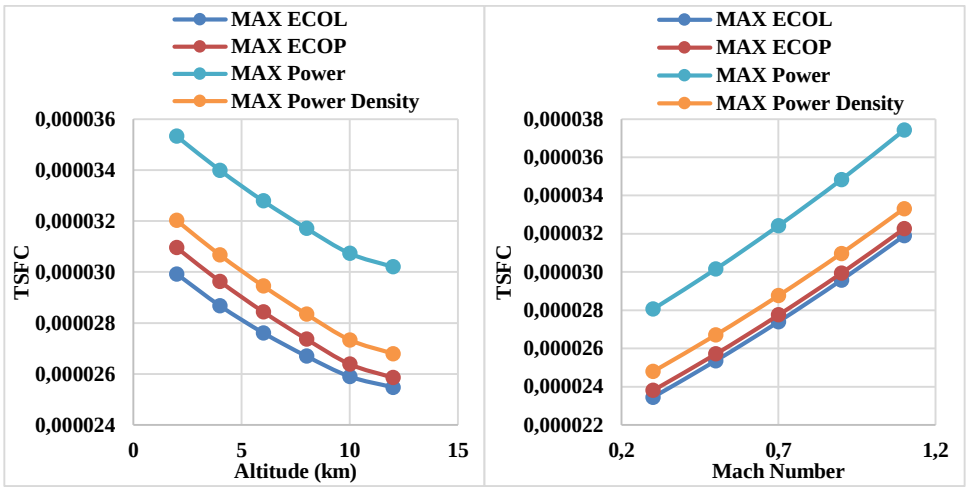

Figure 2.21: Optimum TSFC contours for prescribed ALT and M_∞.

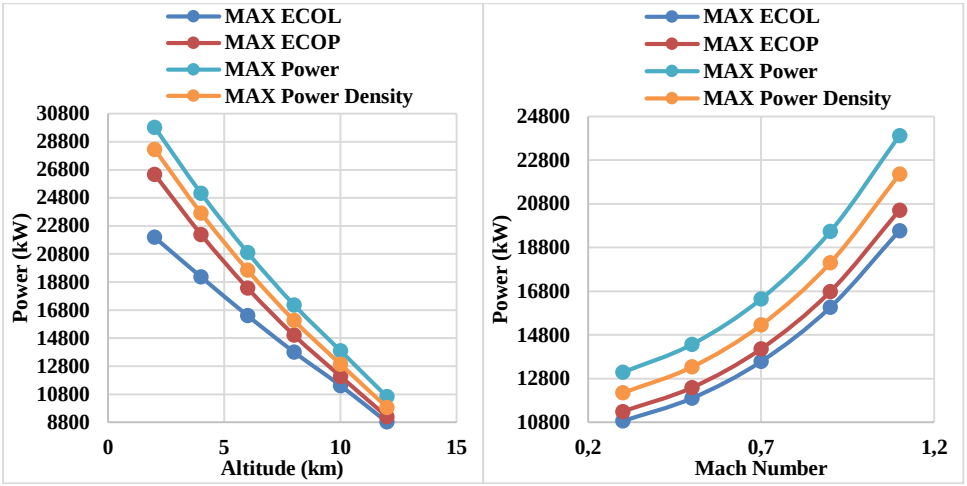

Figure 2.22: Optimum power contours for prescribed ALT and $\boldsymbol{M}_{\infty}$.

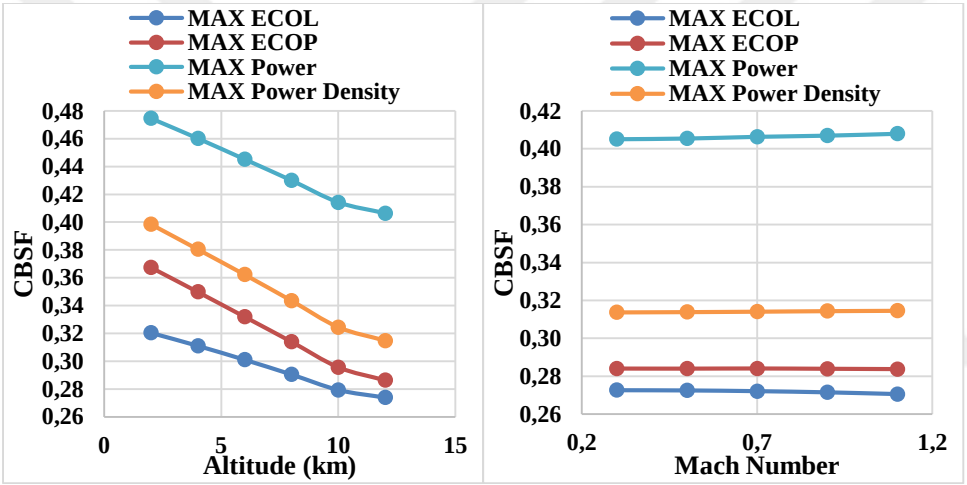

Figure 2.23: Optimum CBSF contours for prescribed ALT and $\boldsymbol{M}_{\infty}$.

The performance assessment, at flight conditions, of the irreversible Brayton turbojet engine was carried out utilizing power and power density approach in addition to ECOP and ECOL, selected variables were held constant while others varied. The ambient condition prescribed for the powerplant were at an initial: altitude of 10 km, inlet temperature of $T_a = 223.3\ K$, inlet pressure of $P_a = 26.5\ kPa$ and an inlet speed of sound of $a = 299.5\ m/s$. The given predetermined variables were: $M_{\infty} = 0.5$, $\eta_c = 0.87$, $\eta_t = 0.90$, $\eta_i = 0.93$, $\eta_j = 0.95$, $\eta_m = 0.99$, $\eta_b = 0.98$, $Q_R = 43000\ kJ/kg$ and a pressure drop from inlet to outlet of the combustor given as 4% (i.e. $\Delta P_b = 0.04$). Variations of certain criteria such as M_{∞}, are prescribed in the applicable graphic legends.

The contours of air specific impulse, I_a and thermal efficiency, η_{th} with regards to the compression ratio parameter, θ_c are illustrated in Figure 2.24a and Figure 2.24b for variations of compressor efficiencies. From Figure 2.25a, the air specific impulse is shown to pass through maximums with regards to the compressor pressure ratio parameter at all instances. The optimum value of θ_c that is commensurable with the maximum air specific impulse increases as the compressor efficiency increases. In addition, figure 4b also depicts maximum states of thermal efficiency for variations of θ_c; where the ideal case indicates an increase in value as θ_c increases. Figure 2.25a and Figure 2.25b also depict the positions where maximum power, power density, ECOP and ECOL (MP, MPD, MECOP and MECOL respectively) are obtained. Figure 2.24a indicates that at MP operations, peak rates of specific impulse may be achieved for a range of $1.5 < \theta_c < 2.5$ as. η_c increases; in addition, MP operations were beneficial than MPD, MECOP and MECOL. Moreover, for $\eta_c > 0.9$ MECOL operations indicate favourable situations over MECOP. Whereas Figure 2.24b showes that peak thermal efficiency rates were attained when MECOP operates between $1.5 < \theta_c < 4$ for increases in η_c.

Figure 2.25a and Figure 2.25b depict the contours of air specific impulse, I_a and thermal efficiency, η_{th} with regards to the cycle compression ratio parameter, θ_c and for variations in cycle temperature ratios, $\alpha = T_{03}/T_a$. As α increases, I_a and η_{th} increase and exhibit maximum operability limits at increased compression ratios. Cycle temperature ratio, α values between 6 and 7 indicate a substantial impact on the air specific impulse (I_a) and thermal efficiency (η_{th}) than the variations of η_c. Whereas, η_c has a higher effect on the air specific impulse (I_a) and thermal efficiency (η_{th}) when α is below 6. Similar to Figure 2.25a, Figure 2.26a also indicates that MP operations produce larger rates of specific impulse for a range of $1.5 < \theta_c < 2.7$ as.the altitude increases. Whereas Figure 2.26b shows that higher thermal efficiencis are attained under MECOP conditions for ranges of $1.5 < \theta_c < 4$ as the altitude increases. Both Figure 2.25b and Figure 2.26b illustrate that MECOL conditions are more beneficial than MECOP for $\alpha > 6$ and for altitudes ≥ 14 km repectively.

Figure 2.26 illustrates the contours of air specific impulse, I_a (a), thermal efficiency, η_{th} (b), TSFC (c) and Thrust (d) with regards to the cycle compression ratio parameter, θ_c for variations in altitude. Maximum rates of impulse and thrust were obtained utilizing maximum power conditions, whereas, higher η_{th} and reduced TSFC rates are

obtained for maximum ECOP operation. Moreover, for altitudes beyond 12 km maximum ECOL operation developes favourable outputs than maximum ECOP states.

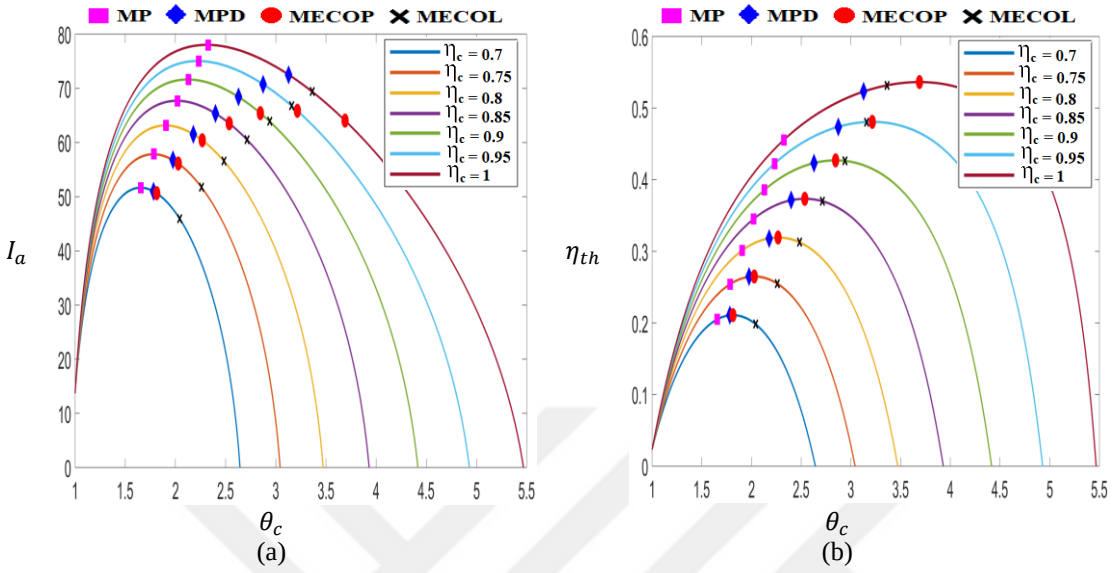

Figure 2.24: Contours of $\boldsymbol{I_a}$ (a) and $\boldsymbol{\eta_{th}}$ (b) for variaitons of $\boldsymbol{\theta_c}$ for distinct $\boldsymbol{\eta_c = \eta_t}$ quantities.

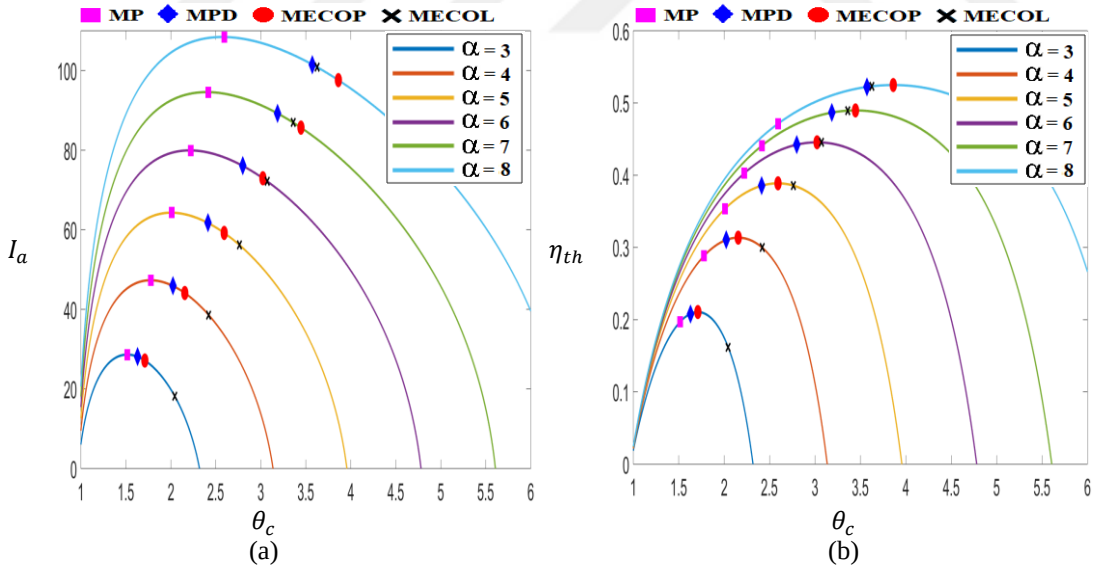

Figure 2.25: Contours of $\boldsymbol{I_a}$ (a) and $\boldsymbol{\eta_{th}}$ (b) for variations of $\boldsymbol{\theta_c}$ for distinct quantities of $\boldsymbol{\alpha}$.

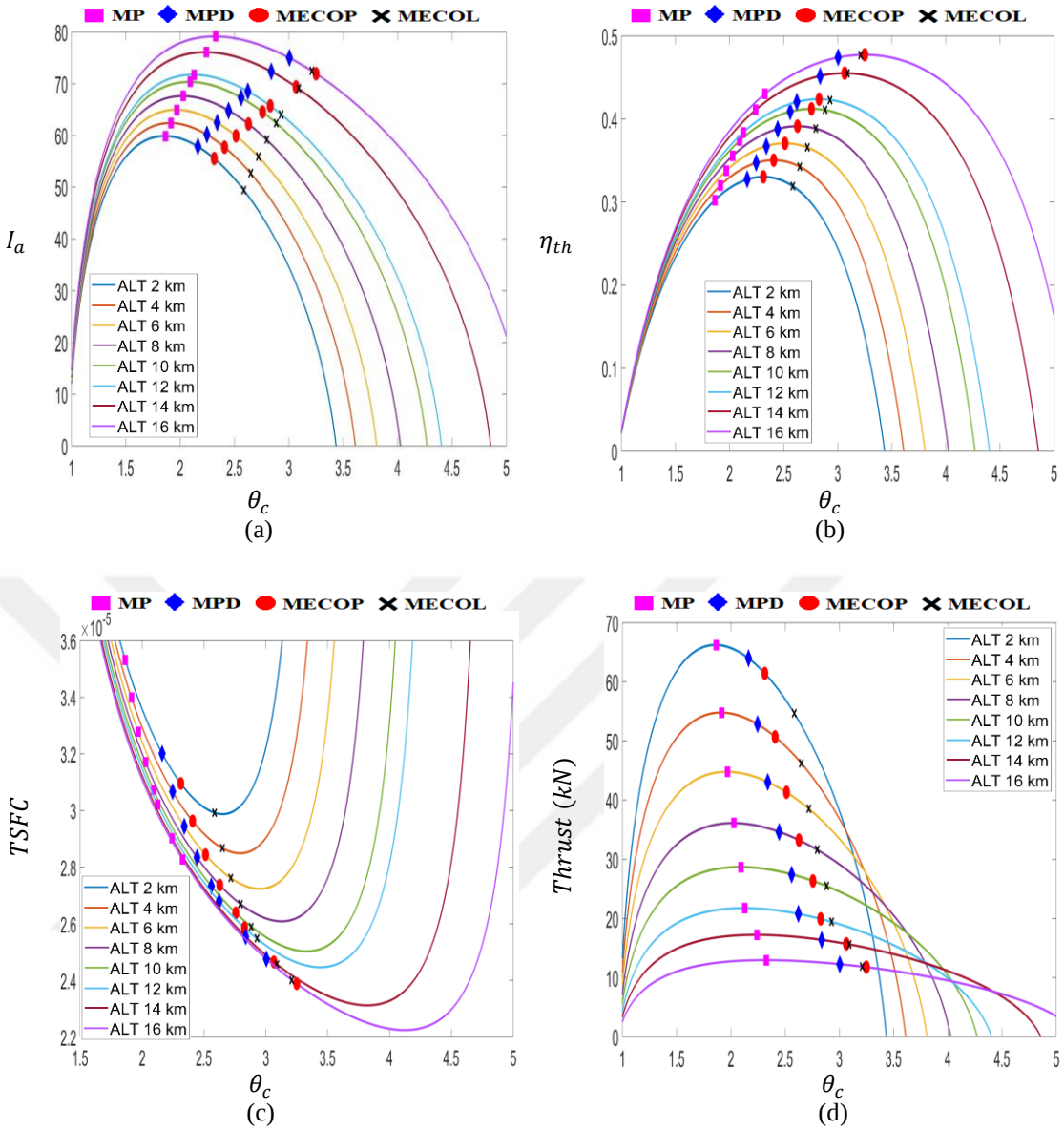

Figure 2.26: Contours of $\boldsymbol{I_a}$ (a) and $\boldsymbol{\eta_{th}}$ (b), TSFC (c) and Thrust (d) for variaitons of $\boldsymbol{\theta_c}$ for distinct quantities of altitude.

Figure 2.27 depicts the contours of the thermal efficiency (η_{th}), thrust specific fuel consumption (TSFC) and the specific volume difference ($(v_5 - v_a)/v_a$) for variations of cycle temperature ratio (α) at maximum power, maximum power density, maximum ECOP and maximum ECOL conditions. At maximum ECOP and power density operation the thermal efficiency, and TSFC shows improvement and differences of specific volumes were reduced; therefore an enhanced efficiency for a reduced volume and decreased TSFC. On the other hand, for $4.5 < \alpha < 6.5$ maximum ECOL operations were beneficial for TSFC, thermal efficiency and differences of specific volume.

Figure 2.28 depicts the contours of air specific impulse, I_a, propulsive efficiency (η_p), thermal efficiency (η_{th}) and difference of specific volume ($(v_5 - v_a)/v_a$) for variations of flight Mach number (M_∞) at maximum power, maximum power density, maximum ECOP and maximum ECOL states. The I_a incures a reduction at maximum power density, maximum ECOP and maximum ECOL than at the maximum power state, where the powerplant functioning at maximum power generation results in the highest propulsive force. Conversely, the difference of specific volume at maximum ECOL are reduced, establishing way to compact powerplant sizes than at maximum ECOP, maximum power density and maximum power; in addition, the propulsive efficiency at maximum ECOL is moderately enhanced than at maximum ECOP, maximum power density and maximum power. Whereas, the thermal efficiency at maximum ECOP more beneficial than at maximum ECOL, maximum power density and maximum power.

Figure 2.29 illustrates the contours of TSFC and fuel to air ratio (*f*) for variations of flight Mach number (M_∞) at maximum power, maximum power density, maximum ECOP and maximum ECOL operation. At maximum ECOL operation both the *f* and TSFC were lower than those for maximum ECOP, maximum power density and maximum power; therefore, eluding to more ecological fuel consumptions and conceivably lower green house gases and reduced quantities of fuel weight or larger payloads. Notwithstanding, the advantages of reduced TSFC and f occurs at an accomodation of lower engine thrust; whereas maximum power operation renders improved engine thrust generation than at maximum power density, maximum ECOP and maximum ECOL.

Figure 2.30 depicts the changes of power, TSFC and air specific impulse (I_a), for variations of compression ratio parameter, θ_c and flight Mach number (M_∞) at maximum power, maximum power density, maximum ECOP and maximum ECOL operation. While at maximum power operation, outputs of power and I_a were beneficial than for maximum power density, maximum ECOP and maximum ECOL. Whereas, at maximum ECOL the quantities of TSFC were favourable than for maximum ECOP, maximum power density and maximum power.

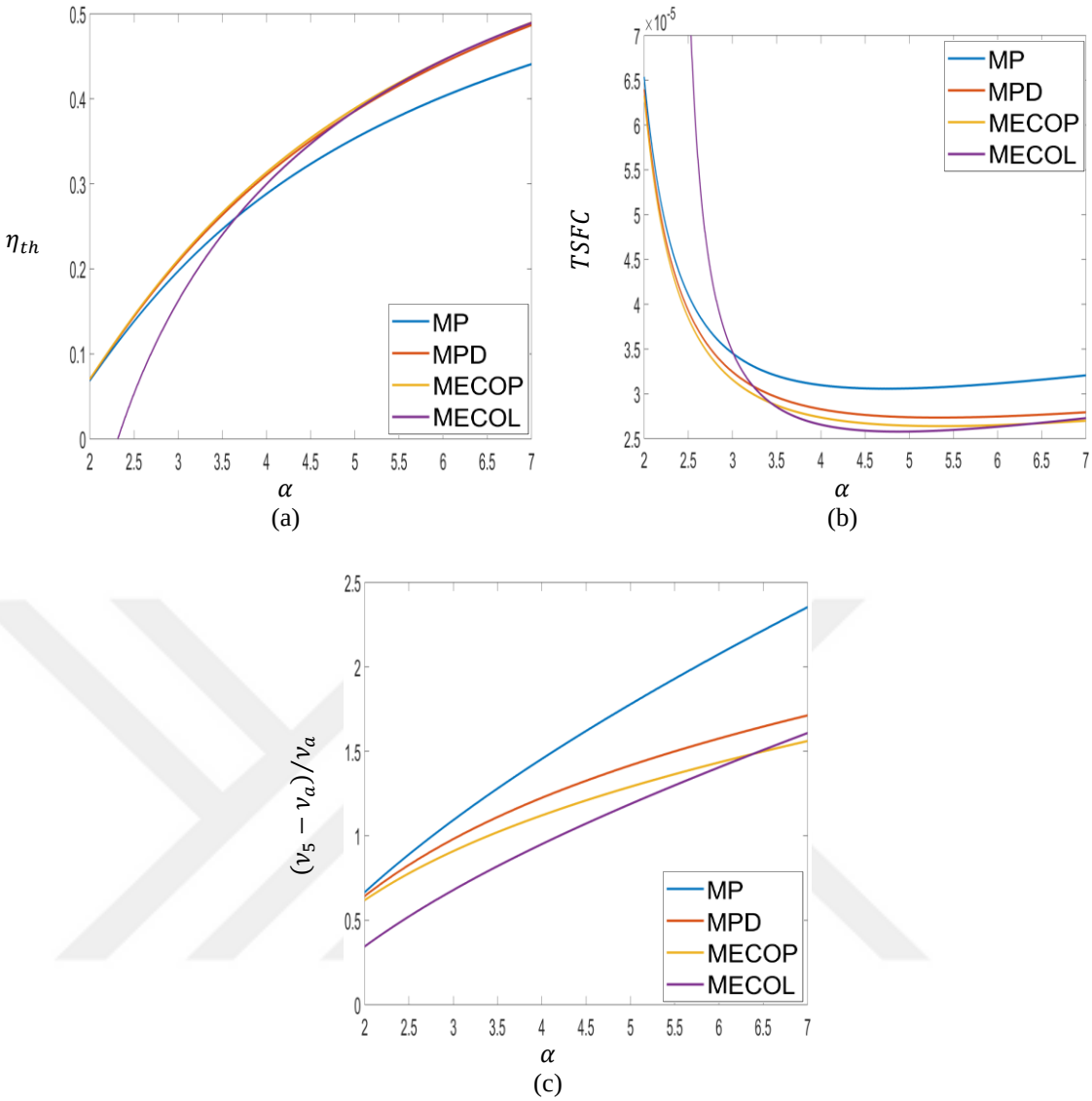

Figure 2.27: Contours of $\boldsymbol{\eta_{th}}$ (a), TSFC (b), and the specific volume variance (c) utilizing *MP, MPD, MECOP and MECOL* for varying $\boldsymbol{\alpha}$.

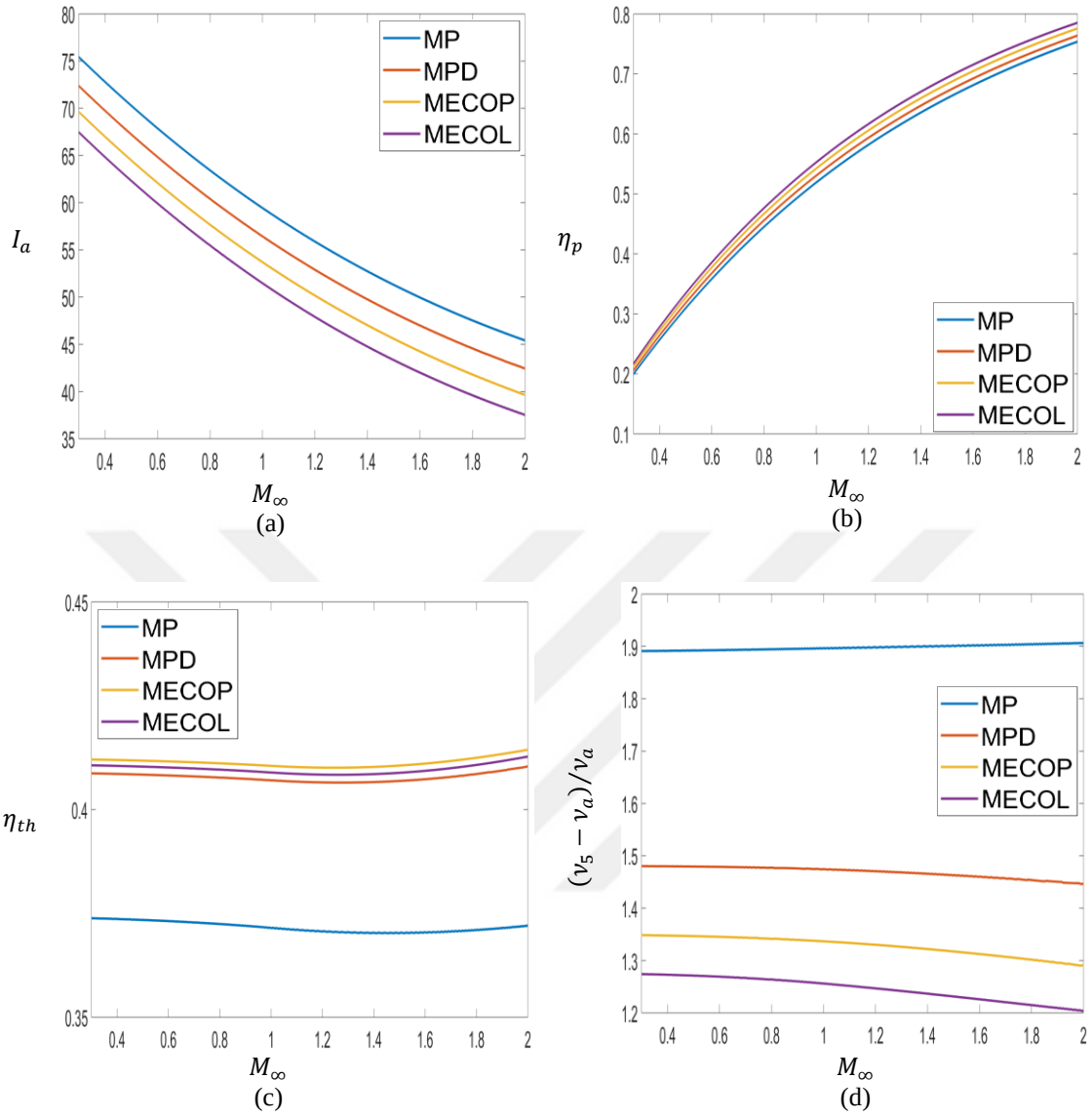

Figure 2.28: Contours of $\boldsymbol{I_a}$ (a), $\boldsymbol{\eta_p}$ (b), $\boldsymbol{\eta_{th}}$ (c),and the specific volume variance (d) utilizing *MP*, *MPD*, *MECOP and MECOL* for varying $\boldsymbol{M_\infty}$.

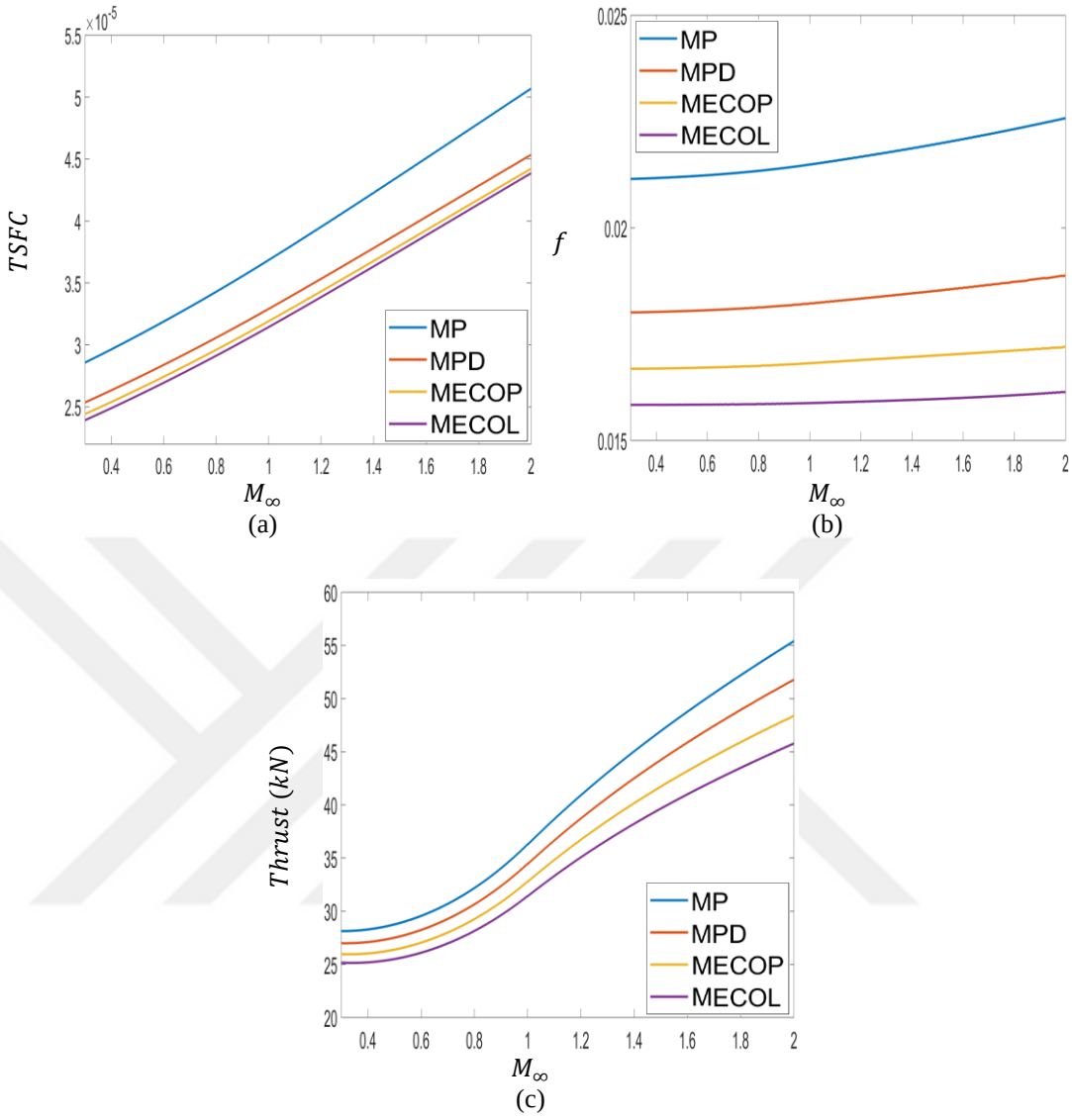

Figure 2.29: Contours of TSFC (a), *f* (b) and Thrust (c) utilizing *MP*, *MPD*, *MECOP and MECOL* for variations of $\boldsymbol{M}_{\infty}$.

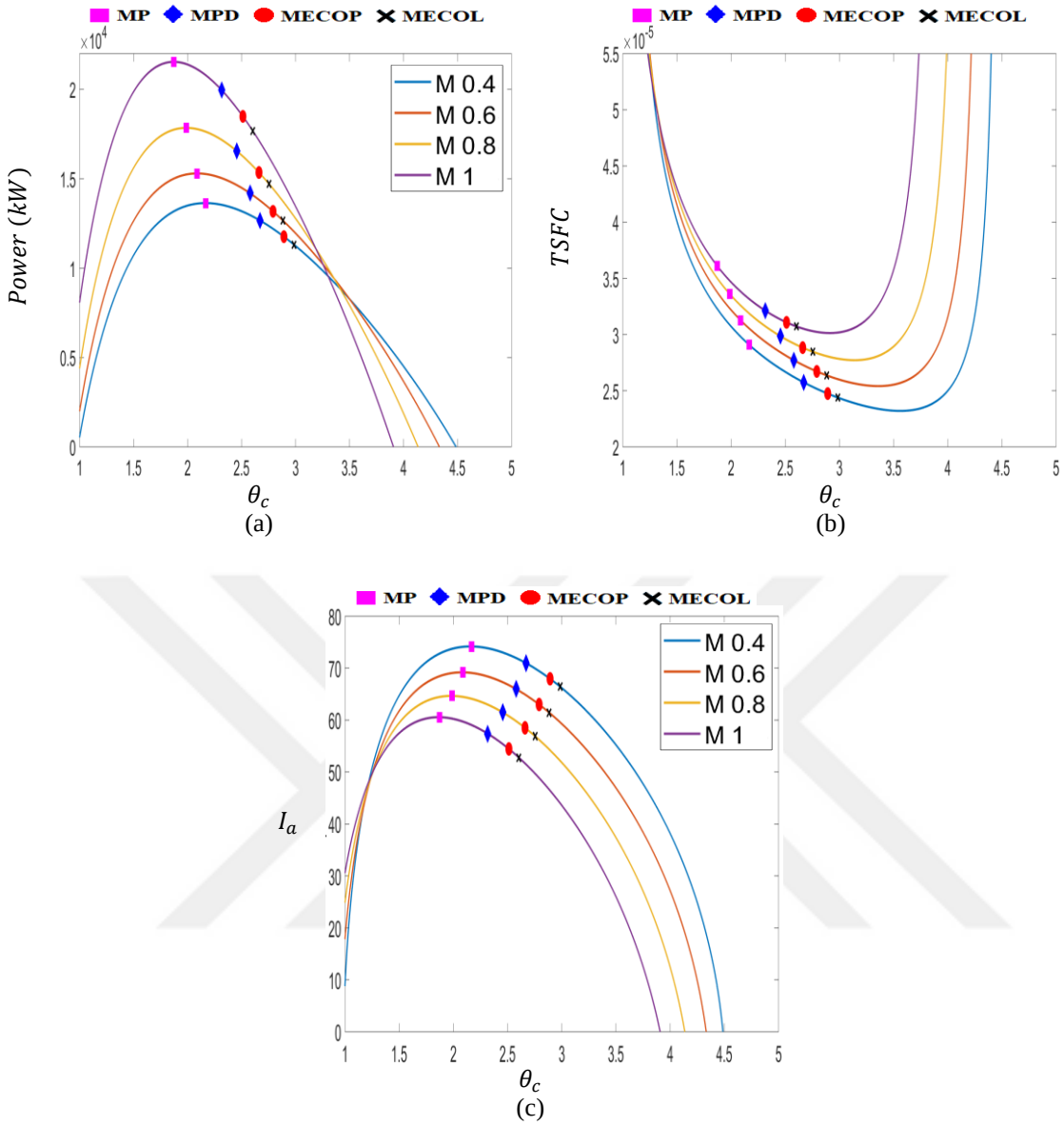

Figure 2.30: Contours of Power (a), TSFC (b) and $\boldsymbol{I_a}$ (c) for variaitons of $\boldsymbol{\theta_c}$ for distinct quantities of $\boldsymbol{M_\infty}$.

Performance ssessments for the seperate components, an overall evaluation for the optimum operating circumstances and respective theorems wre evaluated for the turbojet engine. Figure 2.31 and Figure 2.32 illustrates the variance of specific volume (Δv) amongst the seperate powerplant modules from inlet to exit states. Larger Δv quantities eludes to multitues of compression stages and therefore a sizeably dimensioned compressor. Variances of specific volume become larger for the compressor for changes in both altitude and temperature ratio parameter (α); however, reduces for variaitons of Mach number. Furthermore, for larger increments of α, Δv reaches a plateau and the variations in Δv contract. Moreover, conceptions at

maximum power operation demonstrates a reduced compressor size The combustion chamber also experiences an enlargement in $\Delta\nu$ for changes of altitude; on the other hand $\Delta\nu$ reduces for changes of α and experience minute changes for increases in Mach number. Likewise, the turbine experiences similar changes in $\Delta\nu$ as the combustion chamber; whereas, $\Delta\nu$ observes a minute reduction for changes in Mach number. The nozzle emulates variations of the compressor, with the exception for the deviation of $\Delta\nu$ as the Mach number varies depicting a minute enlargement. A reduced capacity for the combustor, turbine and nozzle are attainable when considering maximum ECOL operation. Variations of dimensionless pressure (Ṕ) at the inlet and exit of the compressor and turbine are demonstrated in Figure 2.33. Whereas the variations of the dimensionless temperature (Ť) for the combustion chamber are given in Figure 2.34. Every constituent of the engine observed an enlargement for the dimensionless parameter for variations of altitude and α and a reduction for changes of Mach number; however, changes for the combustion chamber are minute. Furthermore, constructions utilizing maximum power operation may render reducd compressor and turbine dimensions. However, designs for the combustion chamber are more beneficial utilizing the max ECOL function.

As a generalization, the overall $\Delta\nu$ of the entire engine and respective constituents $\Delta\nu$ experience an enlargement for changes of altitude; inevitably this generates an overall increased engine and individualistic constituents. On the other hand, as an accomodation, while the dimension of the compressor becomes larger the dimension and stretch of the combustor reduces. Moreover, flights at higher M_∞ induce reduced compressor and turbine dimensions but bigger nozzles. For higher α the dimension of the compressor and nozzle enlarge whereas the dimension of the combustor and turbine are reduced. For MP operation the compressor and turbine dimensions reduce while the combustor and nozzle experience an enlargemenet. To the contrary, at MECOL the contrast is observed in comparison to that at MP (i.e. the compressor and turbine dimensions increase whereas the combustor and nozzle dimensions decrease).

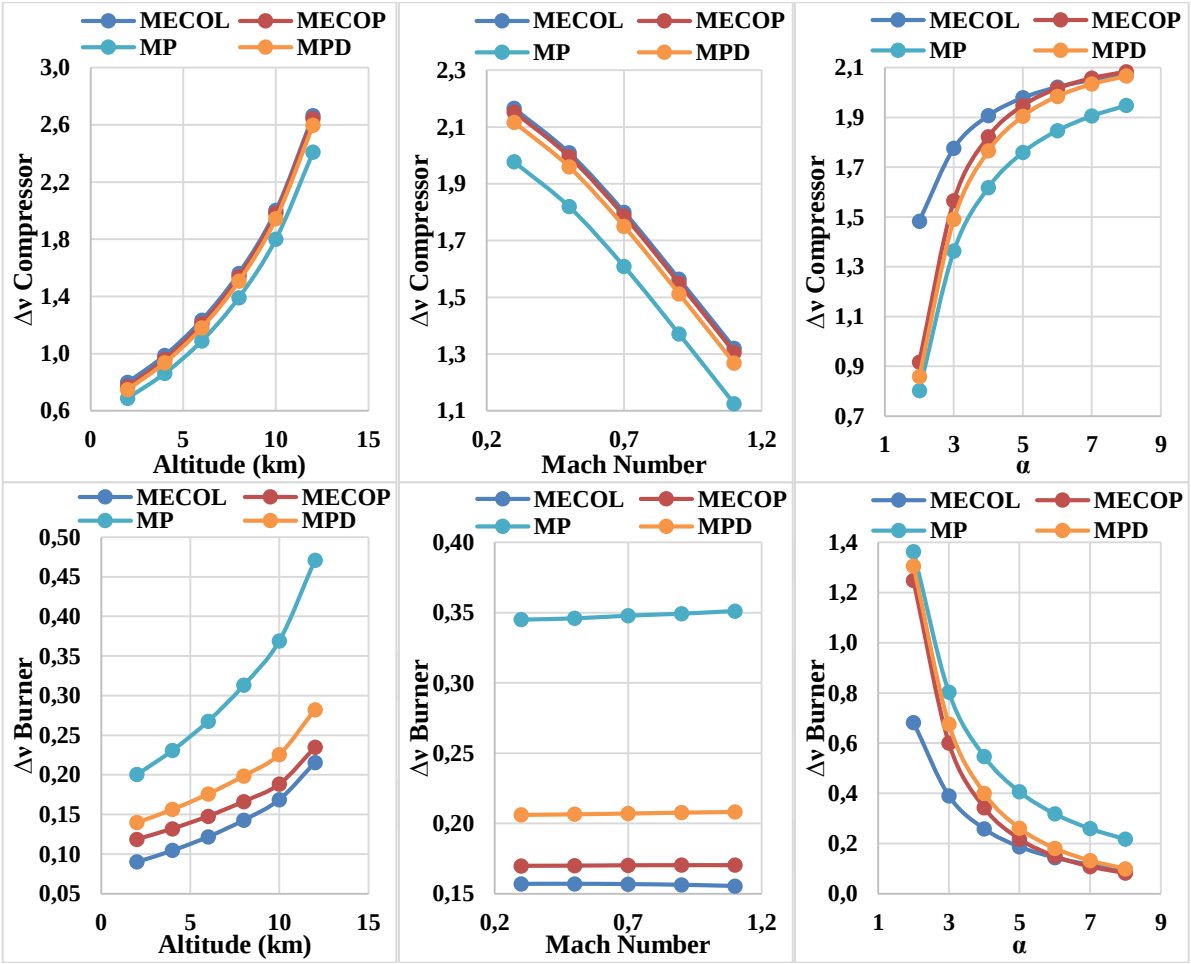

Figure 2.31: Contours of $\Delta\nu$ at the inlet and exit of the compressor and burner

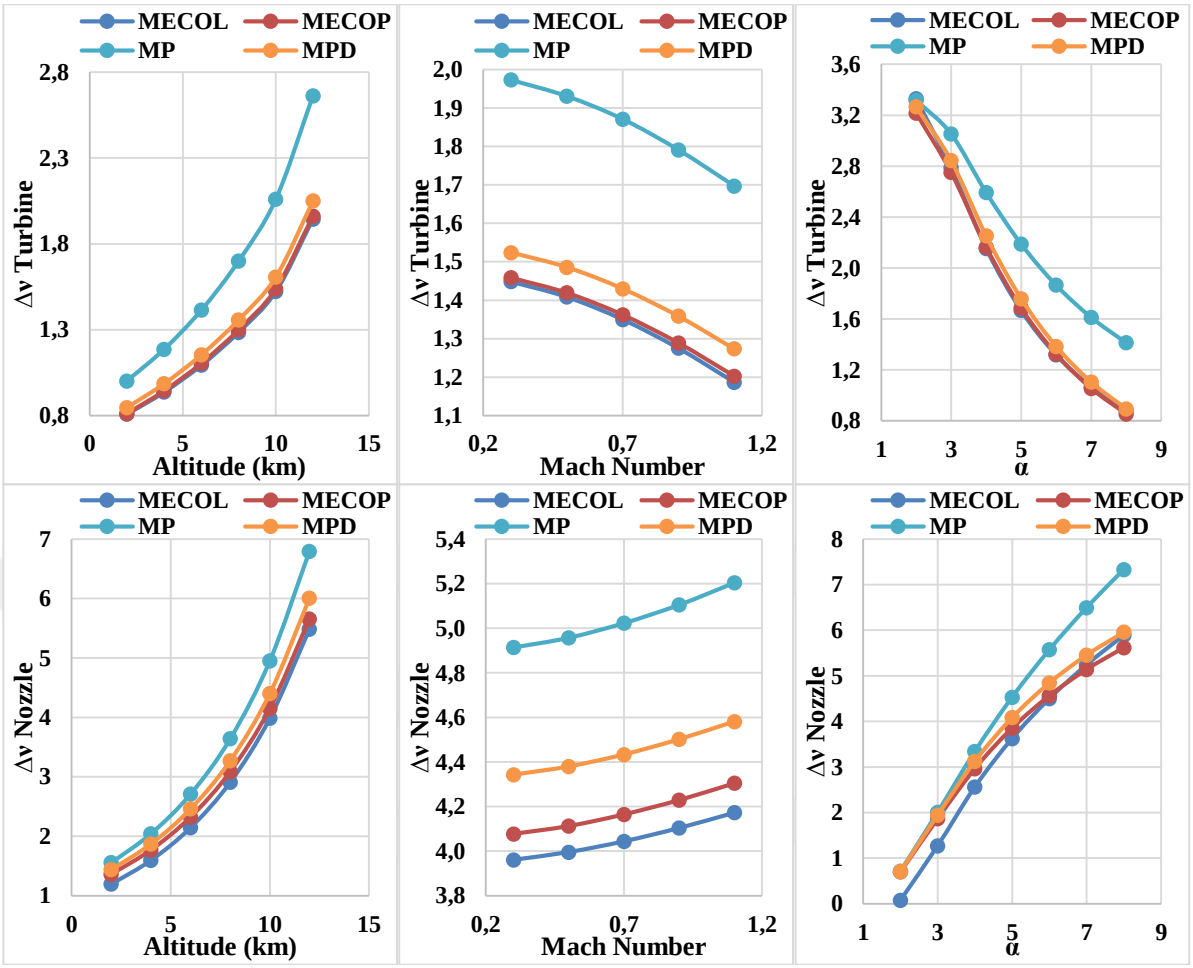

Figure 2.32: Contours of $\Delta\nu$ at the inlet and exit of the turbine and nozzle

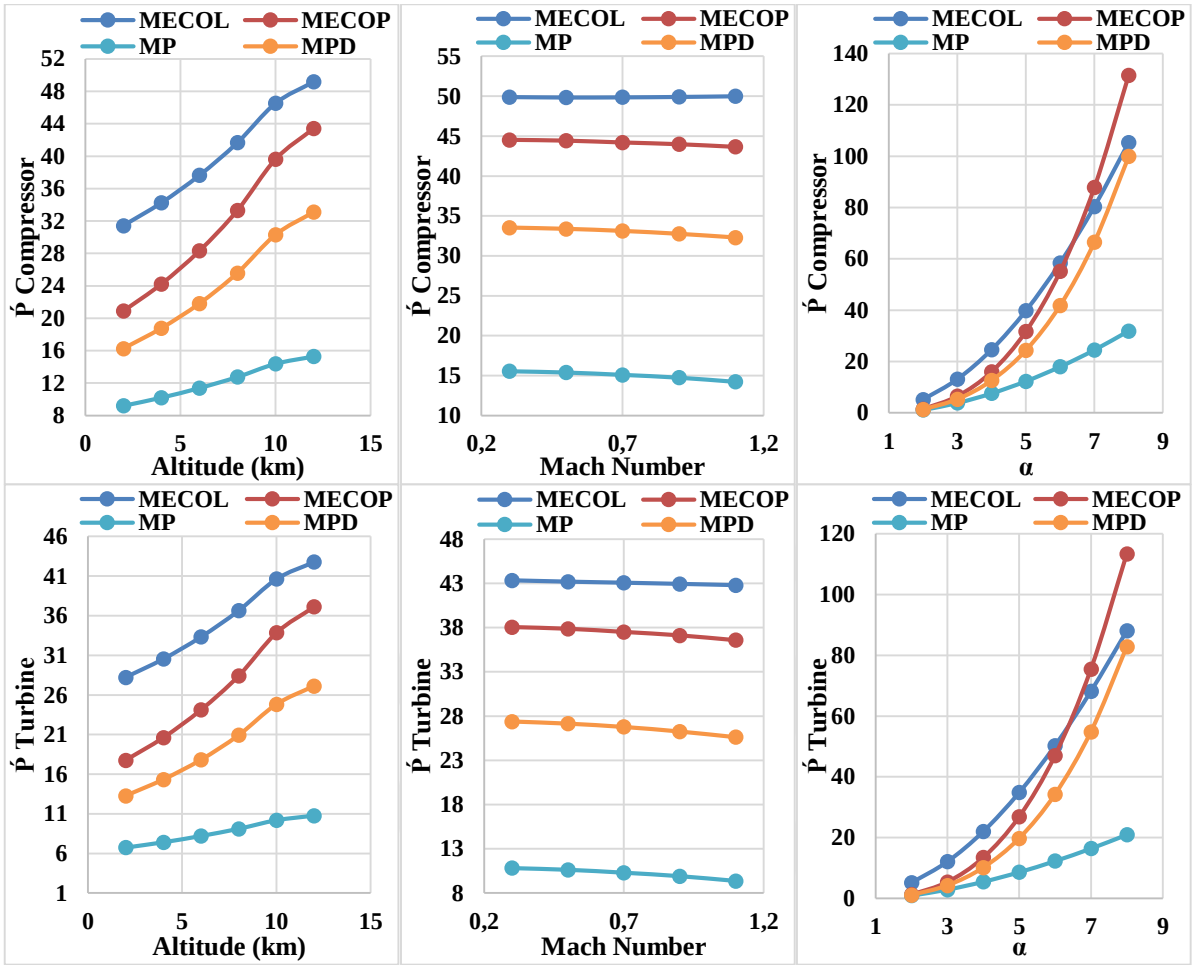

Figure 2.33: Non-dimensional pressure (***Ṕ***) across indicated engine component

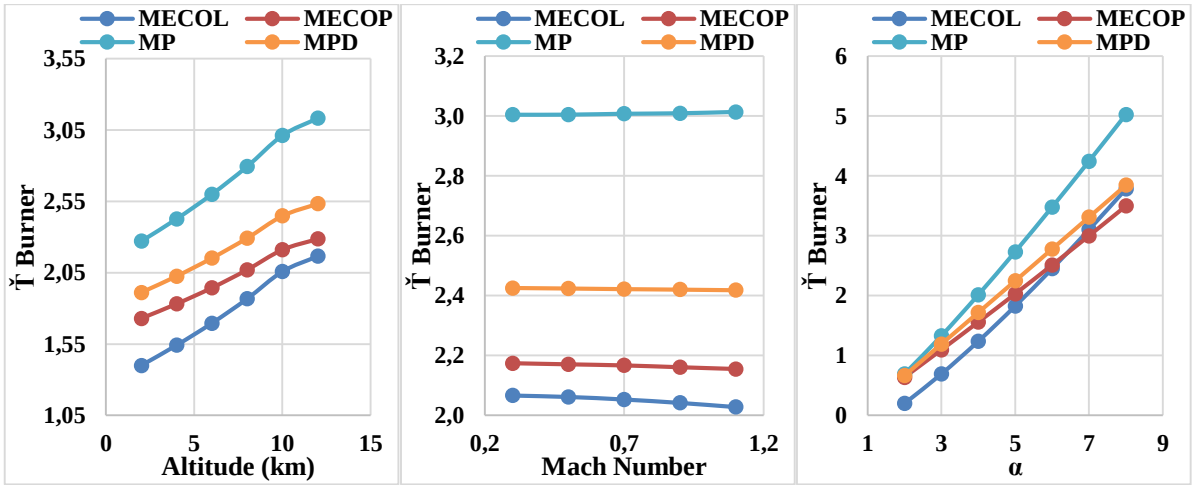

Figure 2.34: Non-dimensional temperature (***Ť***) across the burner

Figure 2.35 along with Table 2.2 and Figure 2.36 along with Table 2.3 are grouped together such that, the evaluation of the dimensional changes of turbojet powerplant on an overall and descrete module level for variations of altitude and Mach number respectively utilizing the optimization theorems of maximum power, power density, ECOP and ECOL are disclosed. Both tables and figures mentioned above dispense crucial insight for engine manufaturers at the premitive schematic construct of an airbreathing engine in the early design phase. The inventor is capable of anticipating the dimensional occupation of the individual components and can utilize precise optimization algorithms targeting reductions on mass and TSFC without detrimental accomodations on structural integrity and powerplant thrust.

By intentionally keeping the X-AXIS constant throughout Figure 2.35 and Figure 2.36 the extent of which the variations of the respective modules (i.e. on a scale difference) for changes of of altitude and Mach number are distinctively seen. Figure 2.35 gives an immediate realization with respect to the overall dimensional growth for changes of altitude and which respective module has experienced an enlargement or reduction in dimension for a chosen design state; the overall anticipated growth in engine dimension is a consequence to the reduction in air density at higher altitudes. It is understood that for increasing altitudes both the diffuser and combustor contribute a marginal part in correspondance to the compressor, turbine and nozzle. Furthermore, at a set altitude of 10 km and for changes in Mach number Figure 2.26 stipulates that the overall dimention of the powerplant remains constant; whereas, the dimension of the respective powerplant modules undergo metamorphisis. As the Mach number increases, the dimension of the diffuser and nozzle contribute a major influential aspect for design deliberations; where the design of the diffuser (ram recovery) has higher significance at increased Mach numbers than at reduced Mach values. Moreover, Table 2.2 and Table 2.3 highlights the effect on thrust (kN) and TSFC commensurative with Figure 2.35 and Figure 2.36 respectively. Where Table 2.2 reveals a reduction on both thrust and TSFC for changes of altitude and Table 2.3 show higher quantities for both thrust and TSFC for variations of Mach number. Eventhough, the optimization theorems were examined as a function of altitude and Mach number, they can, however, be utilized with regards to different variables.

Table 2.2: Thrust (kN) and TSFC (kg/N-s) at maximum ECOL, ECOP, MP and MPD for distinct quantities of altitude.

ALT	2 km		4 km		6 km	
	Thrust	**TSFC**	**Thrust**	**TSFC**	**Thrust**	**TSFC**
MECOL	55	2.99E-05	46	2.87E-05	39	2.76E-05
MECOP	61	3.10E-05	51	2.96E-05	41	2.84E-05
MP	66	3.53E-05	55	3.40E-05	45	3.28E-05
MPD	64	3.20E-05	53	3.07E-05	43	2.94E-05

ALT	8 km		10 km		12 km	
	Thrust	**TSFC**	**Thrust**	**TSFC**	**Thrust**	**TSFC**
MECOL	32	2.67E-05	25	2.59E-05	19	2.55E-05
MECOP	33	2.74E-05	26	2.64E-05	20	2.59E-05
MP	36	3.17E-05	29	3.07E-05	22	3.02E-05
MPD	35	2.83E-05	27	2.73E-05	21	2.68E-05

Table 2.3: Thrust (kN) and TSFC (kg/N-s) at maximum ECOL, ECOP, MP and MPD for distinct quantities of M_∞.

M_∞	0.3		0.5		0.7	
	Thrust	**TSFC**	**Thrust**	**TSFC**	**Thrust**	**TSFC**
MECOL	26	2.34E-05	26	2.54E-05	28	2.74E-05
MECOP	26	2.38E-05	27	2.57E-05	28	2.78E-05
MP	29	2.81E-05	29	3.02E-05	31	3.24E-05
MPD	27	2.48E-05	28	2.67E-05	30	2.88E-05

M_∞	0.9		1.1	
	Thrust	**TSFC**	**Thrust**	**TSFC**
MECOL	30	2.96E-05	34	3.19E-05
MECOP	31	2.99E-05	36	3.23E-05
MP	35	3.48E-05	40	3.74E-05
MPD	33	3.10E-05	38	3.33E-05

Table 2.4: State Investigation at M_∞0.5 and 0.9 for an Altitude of 10 km

State I M_∞ 0.5 ALT 10 km

	Thrust (kN)	**TSFC (kg/N-s)**	**Compressor**	**Burner**	**Turbine**	**Nozzle**
MECOP	27	2.57E-05	Larger	Smaller	Smaller	Smaller
MP	29	3.02E-05	Smaller	Larger	Larger	Larger

State II M_∞ 0.9 ALT 10 km

	Thrust (kN)	**TSFC (kg/N-s)**	**Compressor**	**Burner**	**Turbine**	**Nozzle**
MECOP	31	2.99E-05	Larger	Smaller	Smaller	Smaller
MP	35	3.48E-05	Smaller	Larger	Larger	Larger

Figure 2.37 and Figure 2.38 illustrates the stretch of the combustor at maximum optimization operation for changes of altitude and Mach number respectively. At decreased altitudes the length of the combustor increases, while developing into impracticle lengths (1.4 m at an altitude of 2 km) for operations at MP. On the other hand, increased altitudes reduces the stretch of the combustor to a practicle length even at MP operation (0.55 m at an altitude of 12 km, a 61% reduction from the 2 km altitude). Moreover, it is noteworthy to keep in mind that the target design of a turbojet materialzes at increased altitudes. Conversely, the stretch of the combustor at higher Mach number (at an altitude of 10 km) also grows. Likewise, at MP operation the stretch of the combustor grows into impracticle lengths (1.33 m at a Mach number of 1.1 vs. 0.5 m at a Mach number of 0.3; a 62.4% length growth). On the other hand, for supersonic Mach numbers, usually addressed for military operation, an afterburner is mandatory to keep the combustor within a reduced dimensional scale. Exceptionally, military implementations circumscribe engine design utilizing MP or MPD operation for an acommodation on TSFC where the unprecedented target design locus is for maximum power generation. However, civil aviation powerplants constructs are best when utilizing MECOL or MECOP operation where quantities of TSCF are more beneficial. This has been illustrated in Table 2.4 for two states of investigation at Mach numbers of 0.5 and 0.9. Utilizing MECOP, thrust and TSFC exhibit reductions compared to MP operations at both Mach numbers of 0.5 and 0.9. Moreover, at MECOP the combustion chamber, turbine and nozzle are reduced when compared to MP operation. On the other hand, the accomodations utilizing MECOP is an increased compressor while MP portrays reduced compressor dimensions.

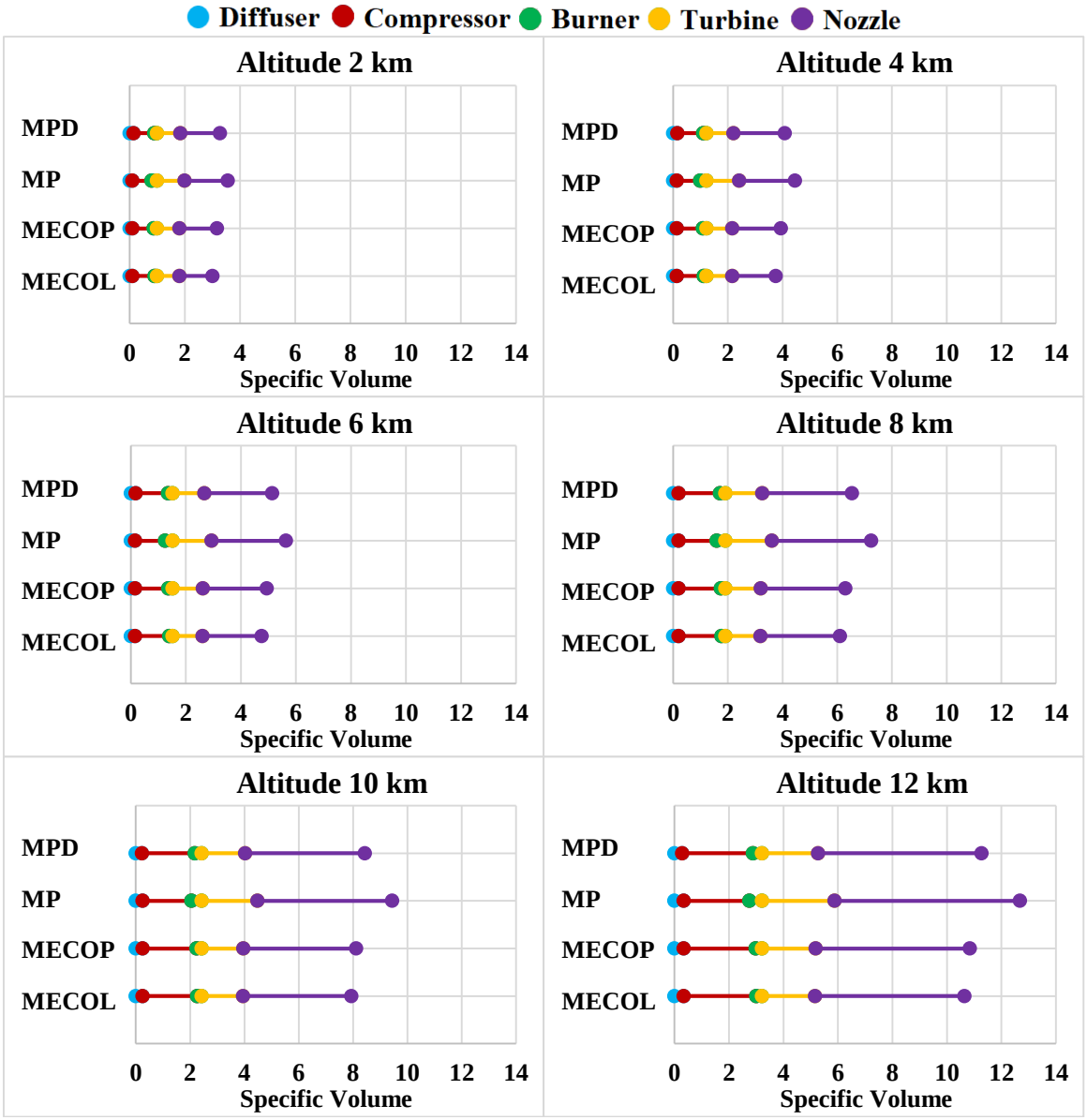

Figure 2.35: Component size variation at maximum ECOL, ECOP, MP and MPD for changes of altitude.

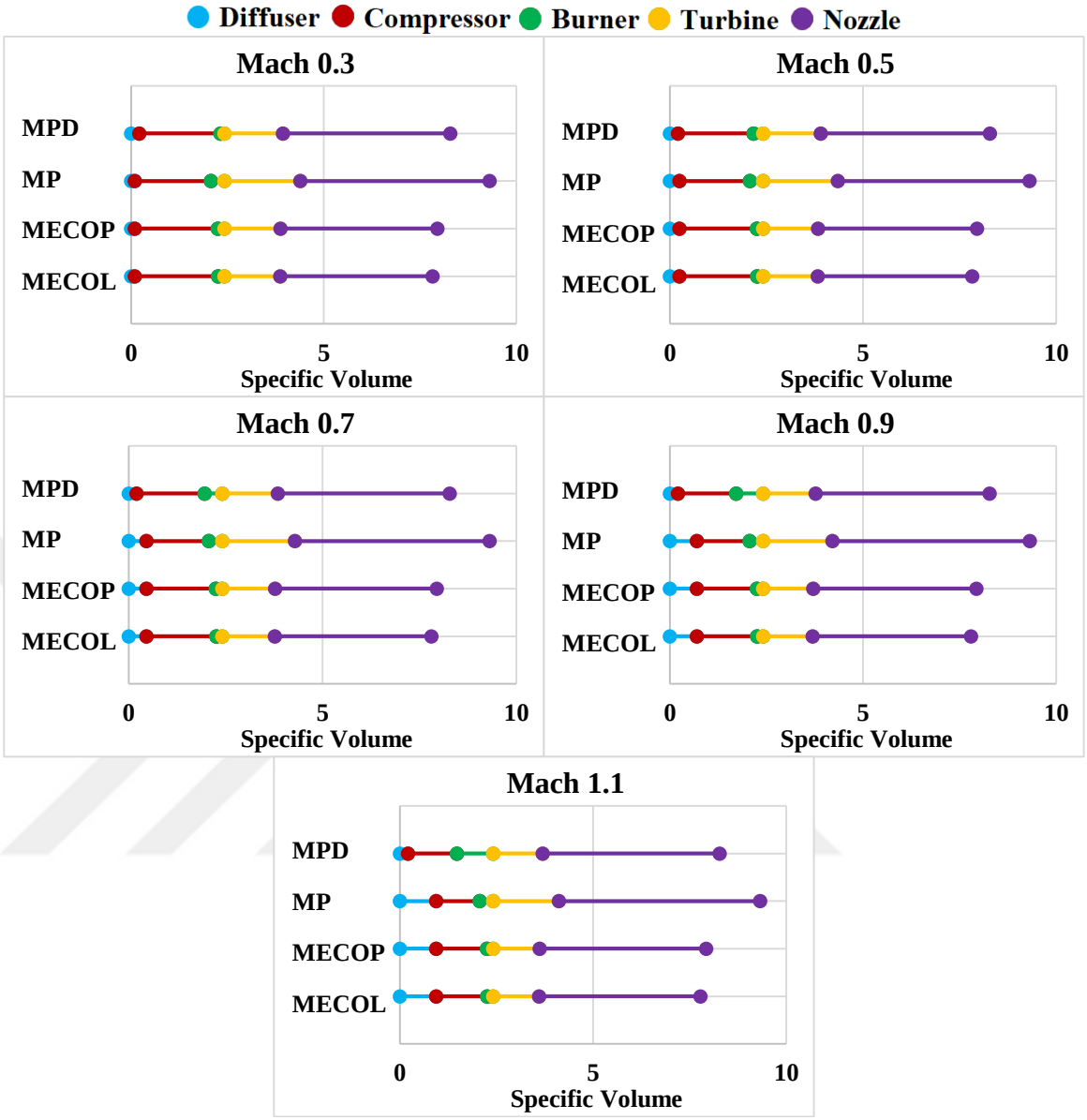

Figure 2.36: Varying Module dimensions at maximum ECOL, ECOP, MP and MPD for distinct vales of $\boldsymbol{M}_{\infty}$.

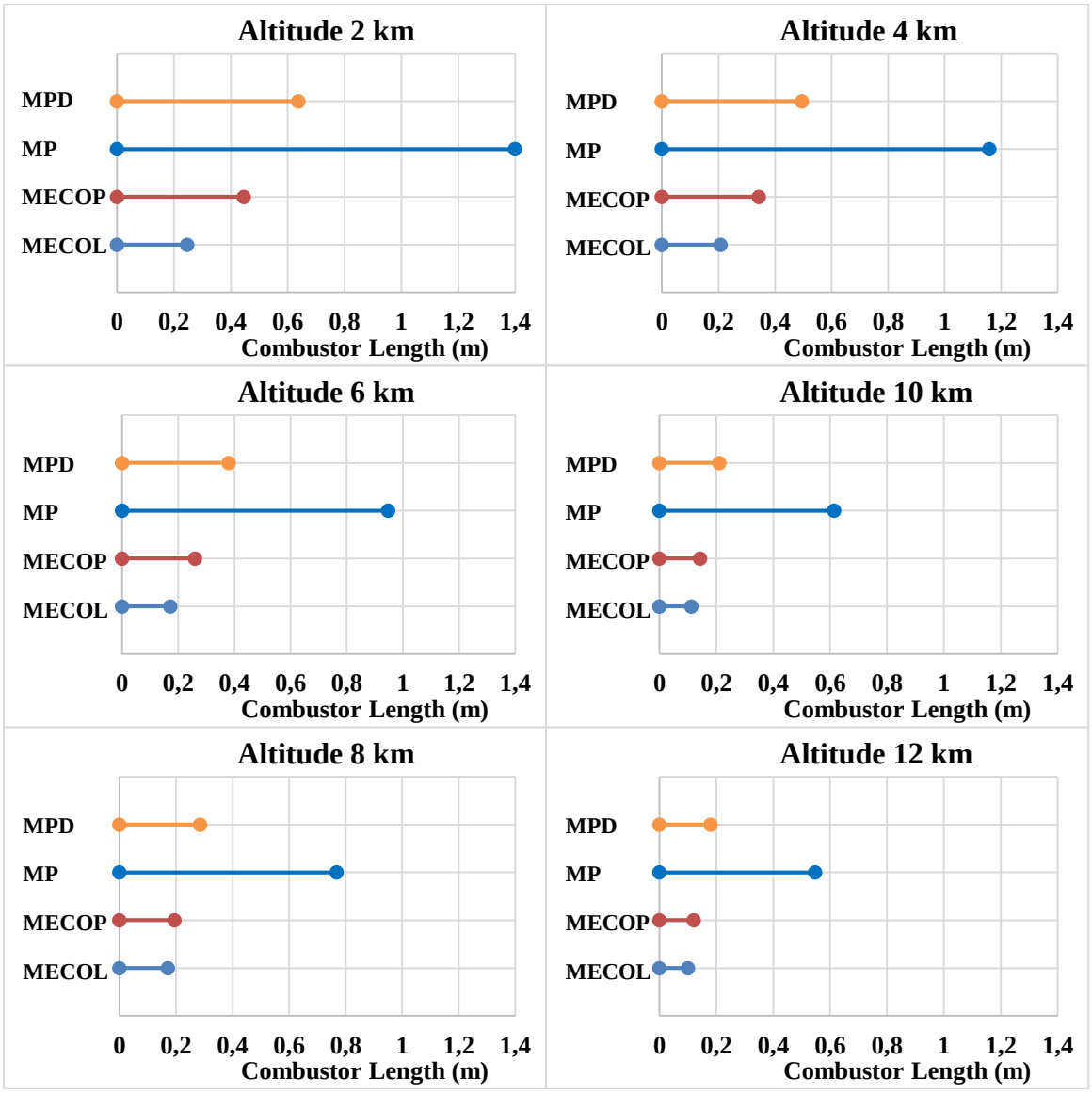

Figure 2.37: Length of the combustion chamber at maximum ECOL, ECOP, MP and MPD for distinct quantities of altitude.

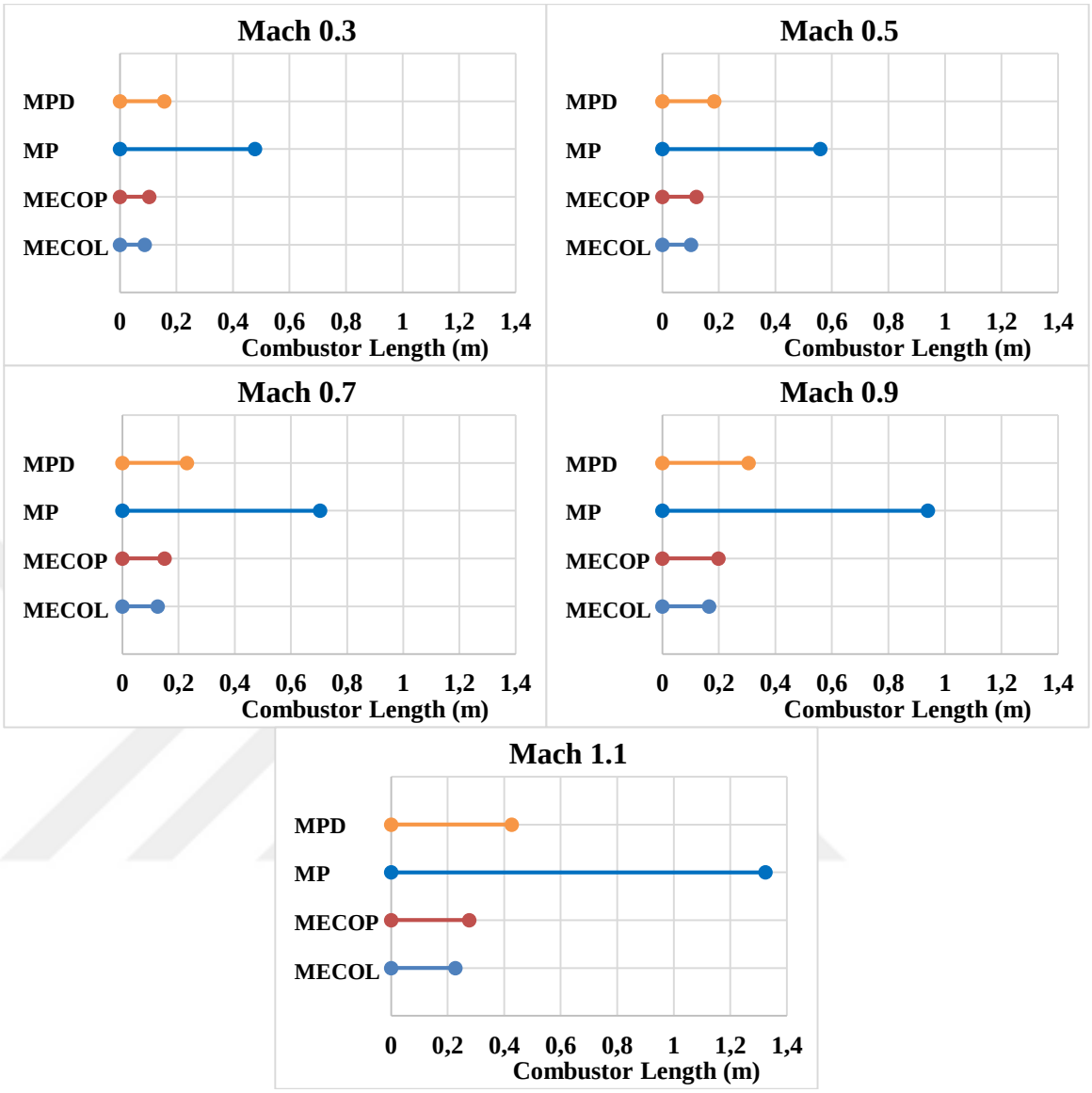

Figure 2.38: Length of the combustion chamber at maximum ECOL, ECOP, MP and MPD for distinct quantities of $\boldsymbol{M}_{\infty}$.

2.5 Prospects of Turbojets: No Afterburner

Assessments were carried out utilizing newly characterized performance optimization functions (PLOS, EPLOS and CBSF) in association with the current objective theorems of maximum power, maximum power density, ECOP and ECOL. The classical irreversible Brayton configuration included both the diffuser and nozzle as a part of the turbojet engine numerical formulation. Variations of the constants influencing the cycle performance were examined including the: compressor pressure ratio parameter, cycle temperature ratio, compressor and turbine efficiencies, altitude and flight Mach number. For variations of compressor and turbine efficiency, indicates a beneficial advantage for the construction of a turbojet powerplant configuration for efficiencies of $\eta_c \geq 85\%$ with regards to PLOS, Power, NG and shaft force; operating at reduced NG speeds stipulates reduced engine dimensions for increased shaft force and power generation for minimal system deficit. Evaluating power generations for variations of M_∞, a favourable region for $\theta_c = 2 \pm 0.4$ is attained. For a prescribed compressor ratio (θ_c) design state, the Mach number shifts to the operational condition of preference; where the working region of $1.4 < M_\infty < 1.6$ can fulfill ecological obligations while attaining larger thrust outputs. Furthermore, maximum power operation benefits a decreased impact of internal irreversibilities for a compromise of larger exergy destruction encouraging ecology. Whereas, maximum ECOL operation illustrates a contrary outcome; favourable towards ecology however nonbeneficial for internal irreversibility impacts. Moreover, a noticable benefit at maximum power and minimum PLOS for the optimals $TSFC^*$, I_a^* and f^* for engine operation lower than sonic conditions.

The variations of the optimization functions of MP, MPD, MECOP and MECOL were examined in addition to their effect on the turbojet performance variables including: I_a, TSFC, η_{th}, η_p, thrust, power, volume, specific volume, pressure and temperature difference for dimensional assessments and f. The correlations indicate that the design variables at MECOL and MECOP operation portray reduced, more efficient and decreased fuel consumption for turbojet engines with regards to civil implementations. In addition, a substantial benefit occurs at MECOL and MECOP and larger compression and temperature ratios than those at MP and MPD; where an optimal

compression ratio as high as 30 ($\theta_c \approx 2.64$) and a maximum cycle temperature ratio of 7 can be obtained for the turbojet engine. Furthermore, developing engines at MECOL or MECOP stipulates in smaller of combustor, turbine and nozzle dimensions and reduced TSCF for an acommodation of an enlarged compressor. On the other hand, for military implementations MP and MPD operation (enlarged combustor, turbine and nozzle dimension and reduced compressor) are beneficial particularly at supersonic speeds and when amalgmated with an afterburner for a compromise on TSFC.

Notwithstanding, regardless if a developer utilizes maximum power or ECOL theorems, a decision msy be made if the intended target design state of preference is beneficial and respecting the environment or presents harmful operating situations (higher altitudes and reduced power generation vs. lower altitudes higher M_∞ and larger power generation respectively); conceivably, a concession amongst operational altitude and power generation may be attained. Deliberations from this investigation may be utilized for the determination of optimum operational circumstances and design variables for thrust producing powerplants.

3. THEORETICAL MODEL OF TURBOJET: WITH AFTERBURNER

3.1 Objective Formulations and Established Variables

The turbojet with an afterburner (AB) based on the irreversible Brayton configuration arrangement and its T-s diagram are depicted in Figure 3.1. The elementary foundations of this Brayton configuration has all the same processes as the turbojet without an afterburner up to station numbering 04 (exit of turbine), where the remaining processes are: the air may or may not be further heated by the addition and burning of fuel at the afterurner (**indicated in red**); the air is then accelerated and purged to the atmosphere through the exhausted nozzle. The turbojet engine with an AB uses the same model and operates amongst a heat source at high temperature, T_H, and a heat sink at low temperature, T_L. However, in the AB configuration there are two ($\dot{Q}_H$) rates of heat disseminated from the high temperature source to the turbojet engine; but there is still only one ($\dot{Q}_L$) rate of heat discarded to the heat sink from the turbojet powerlant with an AB.

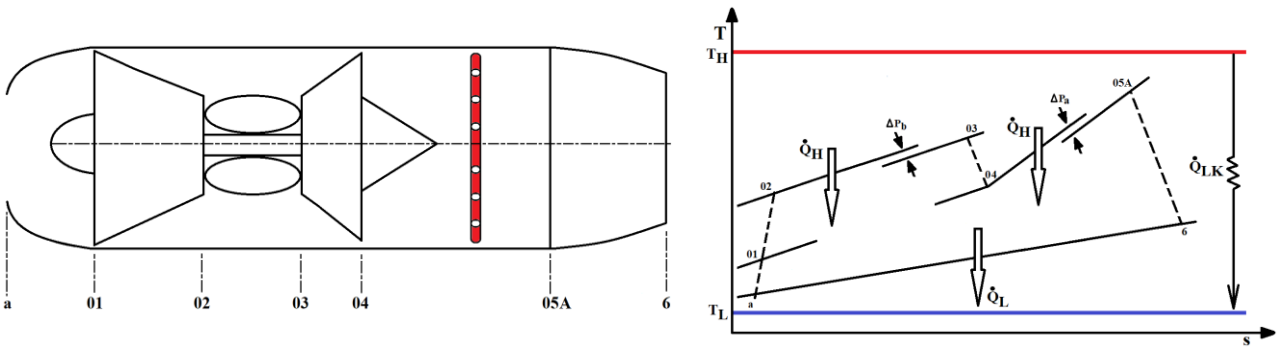

(a) (b)

Figure 3.1: Engine arrangement (a) and T-s schematic representation of a turbojet cycle (b) with an afterburner

Similar to the turbojet engine without an AB, the power generated by the turbojet powerplant configuration with an AB can still be defined as:

$$\dot{W} = \dot{Q}_{HT} - \dot{Q}_{LT} = \dot{Q}_H - \dot{Q}_L \,. \qquad (3.1)$$

However, the total heat dissipation rates from the high temperature reservoirs to the combustion chamber and the AB are now defined as:

$$\dot{Q}_{HT} = \dot{m}_{fb} Q_R \eta_b + \dot{m}_{fAB} Q_R \eta_{AB} \quad (3.2)$$

Here we assume that the fuel used for the combustion chamber is the same as for the AB, therefore, Q_R is still the fuel heat liberated per unit mass for both the combustion chamber and the AB, $\dot{m}_{fb}$ is the fuel mass flow rate and η_b is the efficiency for the combustion chamber, $\dot{m}_{fAB}$ is the fuel mass flow rate and η_{ab} is the efficiency for the AB.

Compression ratio parameter, θ_c is still given as before and taken to be: $\theta_c = (P_{02}/P_{01})^{(\gamma-1)/\gamma}$.

By applying an energy balance across the combustion chamber and the after burner the total fuel to air ratio, f_{Total} is determined as:

$$f_{Total} = f_b + f_{ab} = \frac{C_{pt}T_{03} - C_{pa}T_{02}}{Q_R \eta_b - C_{pt}T_{03}} + \frac{(1+f)C_{pt}(T_{05} - T_{04})}{\eta_{ab} Q_R - C_{pt} T_{05}} \quad (3.3)$$

The equations of the propulsion variables including: thrust (F), specific thrust (F_S) and thermal (η_{th}) are now redefined for the incorporation of the AB. The thrust specific fuel consumption (TSFC), air specific impulse (I_a), propulsive (η_p) efficiencies, power density ($\dot{W}_d$), rate of entropy generation ($\dot{S}_G$), ECOL, ECOP and PLOS formulations do not change as previously stated for the turbojet engine without an AB, however they now also consolidate the AB component within the mathematical statements.

The thermal efficiency of the turbojet cycle with an AB becomes:

$$\eta_{th} = \frac{\dot{W}}{\dot{Q}_{HT}} = \frac{\dot{W}}{\dot{m}_{fb} Q_R \eta_b + \dot{m}_{fAB} Q_R \eta_{AB}}. \quad (3.4)$$

The thrust equation is reobtained by applying integral momentum equation through the appropriate selection of the new control volume across the engine.

$$F = \dot{m}_a[(1 + f_b + f_{ab})C_6 - C_a] + A_6(p_6 - p_a) \quad (3.5)$$

where C_6 is now the new exit velocity at the exhaust nozzle after the AB, C_a is the flight speed, A_6 is the exhaust nozzle exit cross section area and f_b *and* f_{ab} are the fuel to air mass flow rate ratio of the combustion chamber and AB respectively. As before, by presuming perfect expansion and taking into account a per unit mass basis, the specific thrust is rewritten as:

$$\mathbf{F_S = (1 + f_b + f_{ab})C_6 - C_a}. \quad (3.6)$$

In addition to the numerical optimization procedures, the Mass Flow, Gas Generator Speed, Shaft Force, Altitude models and propulsion equations are still applicable to the turbojet with an AB.

3.2 Outcomes and Considerations

When considering a turbojet engine with an operative afterburner, the performance analysis and comparision takes a shift towards the more constraining paramters which are primarily the Mach number and altitude. Performance evaluations have been assessed on under a maximum power regieme for the Turbojet without with an AB and compared to the turbojet without an AB under the same condition. Table 3.1 represents the values previosly taken for the turbojet without an AB in addition to the complementary values for the AB conditions (**in blue**); divergences from these quantities are represented within the respective figures. The essential propulsion equations for the powerplant state point evaluations may be obtained from El-Sayed [71].

Table 3.1: Additional delegated variable inputs for Afterburner condition.

Inputs		
T_L = 200 K	η_j = 0.95	γ_g = 1.333
T_H = 2200 K	η_m = 0.99	R = 287 J/kg K
T_a = 223.3 K P_a = 26.5 kPa	η_b = 0.98	Di = 0.8 m
ALT = 10000 m	C_{pa} = 1.005 kJ/kg K	Q_R = 43000 kJ/kg
ξ = 0.01	C_{pg} = 1. 148 kJ/kg K	η_c = 0.87
η_i = 0.93	γ_a = 1.4	η_t = 0.9
M = 0.5	ΔP_b = 0.96	T_{03} = 1200 K
η_{ab} = 0.9	**ΔP_{ab} = 0.97**	**T_{05} = 2000 K**

Figure 3.2 expresses the variations of thermal η_{th} (a), overall η_o (b) and propulsive η_p (c) efficiency for changes in altitude as a function of flight Mach number, M_∞. For

Mach numbers higher than unity the thermal efficincy of the turbojet with an AB becomes more advantageous at all altitudes; this is due to the much higher work / thrust output of the turbojet with an AB in comparison to the turbojet without an AB (see Figure 3.4). In addition, the thermal efficiency for a turbojet with an AB show an increase with increasing Mach number, whereas the turbojet without an AB show a slight decrease with increasing Mach number. Onthe other hand, the propulsive efficiency for a turbojet without an AB are about 20% higher for flight Mach numbers above 0.8 and at all altitudes than the turbojet with an AB; for Mach numbers below 0.8 the propuslive efficiency for a turbojet without an AB become about 10% higher than that of the turbojet with an AB, below Mach number of 0.4 the difference between the two configurations becomes increasingly smaller. The overall efficiency for a turbojet without an AB still show greater advantage up to a Mach number of ~ 1.6; above this value the turbojet with an AB show a comparible advantage where the difference between the two engine configurations is around 5%. Figure 3.3 clearly shows that for a turbojet with an AB both the fuel to air ratio and TSFC are higher than that of a turbojet without an AB; this is an unavoidable consequence for the tradeoff in increased thrust.

It is important to keep in mind that the purpose of using a turbojet with an AB is the significant increase in thrust, power and impulse of the system at all altitudes and flight Mach numbers (Figure 3.4). However, this comes at the expenditure for higher fuel consupmtion and heavier weight due to the increase in exhaust nozzle specific volume (Figure 3.4d). For altitudes higher than 6 km the thrust and power of both engine configurations intersect at a point. For example at an altitude of 12 km the red dot on Figure 3.4b corresponds to the two red dots on Figure 3.4a; what is seen is that the turbojet with an AB can achieve the same thust and power as the tubojet without an AB at a much lower Mach number (0.6 vs. 1.6 respectively).

As previously mentioned, the main objective of the turbojet with an AB is the higher power output of the system, this can be seen again from Figure 3.5 and Figure 3.6. From both figures it can be seen that the difference in effective power loss parameter (EPLOS) between both engine configurations is quite small; in addition, as the Mach number is increased from 0.8 to 1 the difference in EPLOS decreases. Therefore, from an EPLOS perspective (ignoring the marin of pwer gain) there is no significant advantage as to which engine configuration is used. On the other hand, from a PLOS

point of view the, the exergy destruction of the turbojet with an AB is overall higher than a turbojet without an AB. In addition the difference at minimum PLOS between both engine configurations is about 10%. Moreover, minimum PLOS for the turbojet with an AB occurs at the maximum power output and lower compressor ratio parameter θ_c, whereas the minimum PLOS for the turbojet witout an AB is slightly shifted towards the right at lower power output and higher compressor ratio parameter θ_c, means an increase in compressor size and inevitably weight. Therefore, the turbojet with an AB displays an advantage of: lower θ_c and compressor weight and higher power output at the expence of higher exergy destruction. However, the turbojet with an AB having a lower θ_c and lower compressor weight needs to be compared to the increase in weight gain due to the AB components and exhaust nozzle.

From Figure 3.7, for a constant altitude of 10 km and chnages in Mach number and as previously stated, that the overall dimension of the powerplant does not change while the repective powerplant constituents undergo size metamorphisis. For both engine configurations, at higher Mach numbers dimensions for diffuser increases, therefore, the selectiom of diffuser (ram recovery) develops as a crutial role than at reduced Mach numbers. In addition, the exhaust nozzle for the turbojet with an AB is on average ~85% larger than that of the turbojet without an AB, which inevitably corresponds to an increase in engine weight. Therefore, a comparative and tradeoff study of the decreas in θ_c and thus compressor weight, the ~85% increase in exhaust nozzle specific volume and the AB fuel components need to be examined.

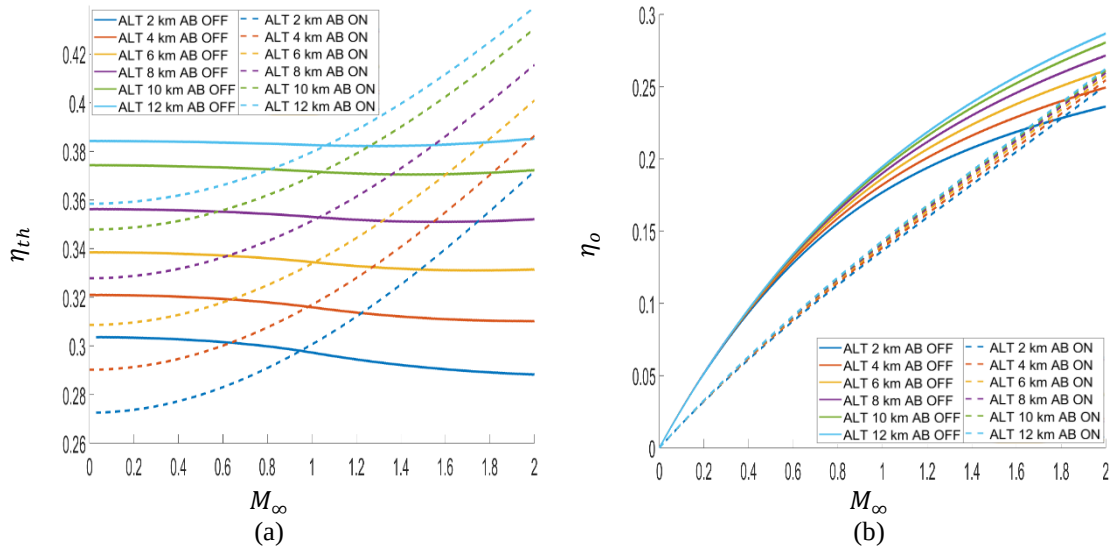

(a) (b)

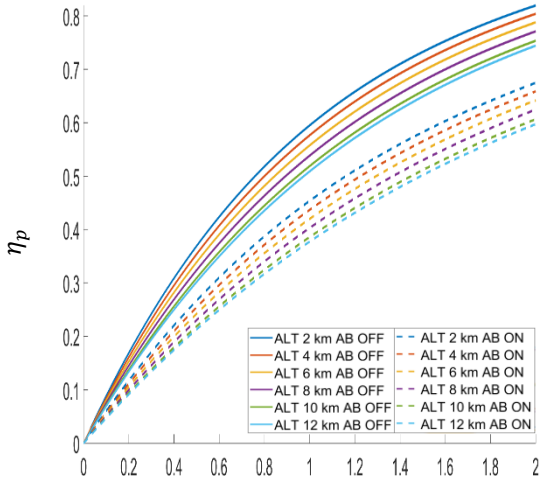

(c)

Figure 3.2: η_{th}, η_o and η_p efficiency for variations of altitude as a function of flight Mach number, M_∞.

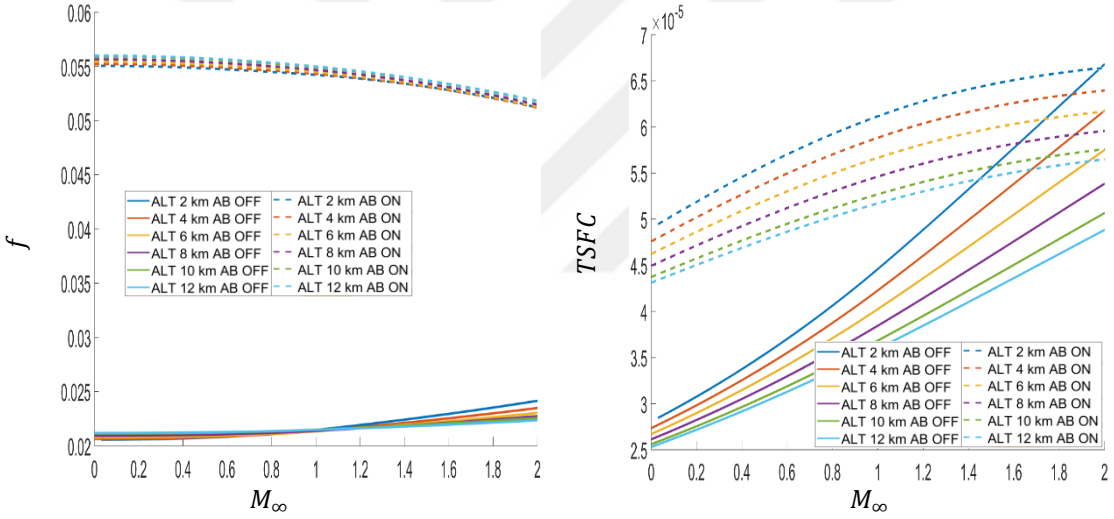

(a) (b)

Figure 3.3: f and $TSFC$ efficiency for distinct quantities of altitude for variaitons M_∞.

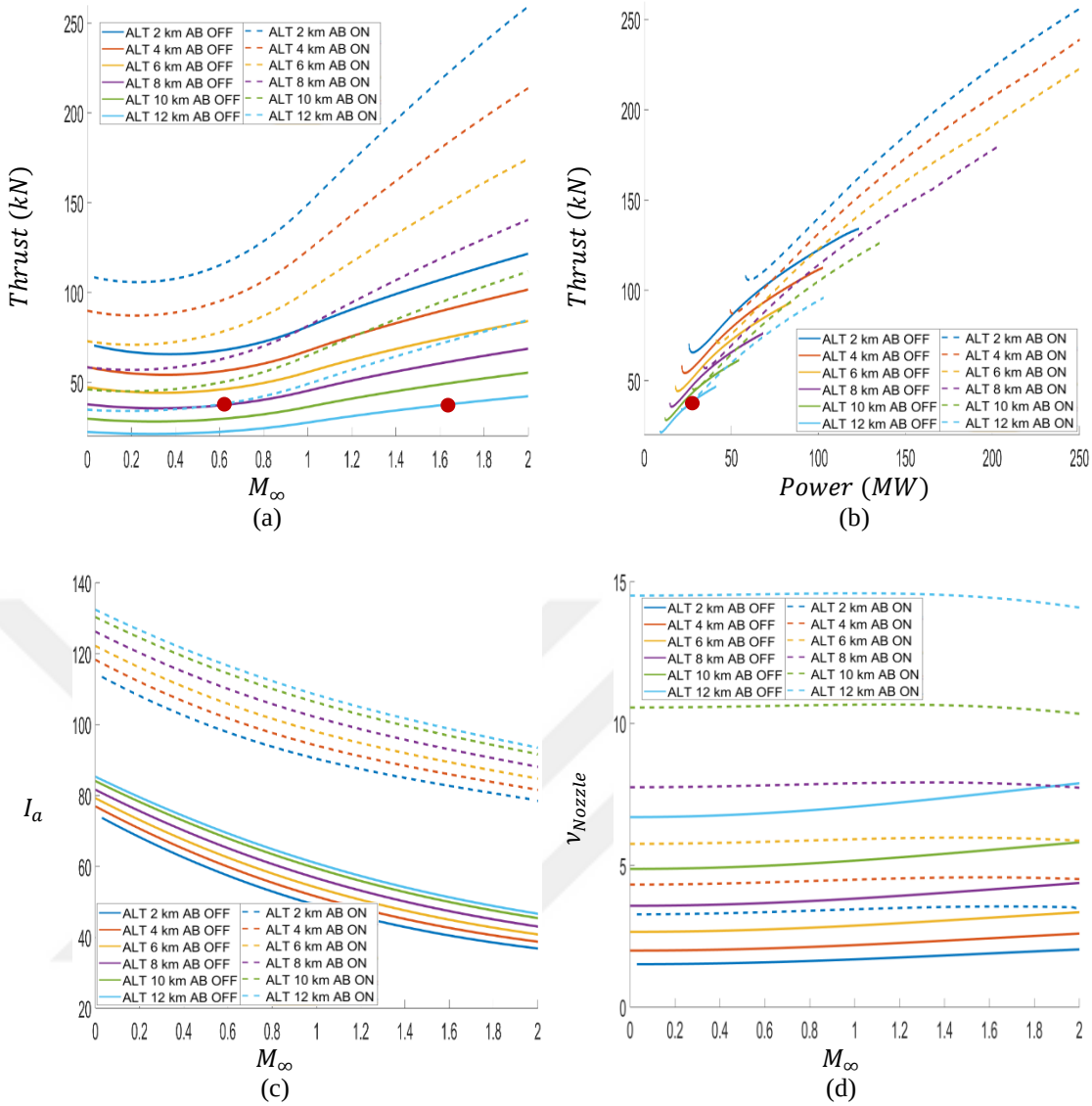

Figure 3.4: ***Thrust*** (a), $\boldsymbol{I_a}$ (c) and $\boldsymbol{\nu_{Nozzle}}$ (d) for variations of altitude as a function of $\boldsymbol{M_\infty}$ and ***Thrust*** (b) as a function of ***Power***.

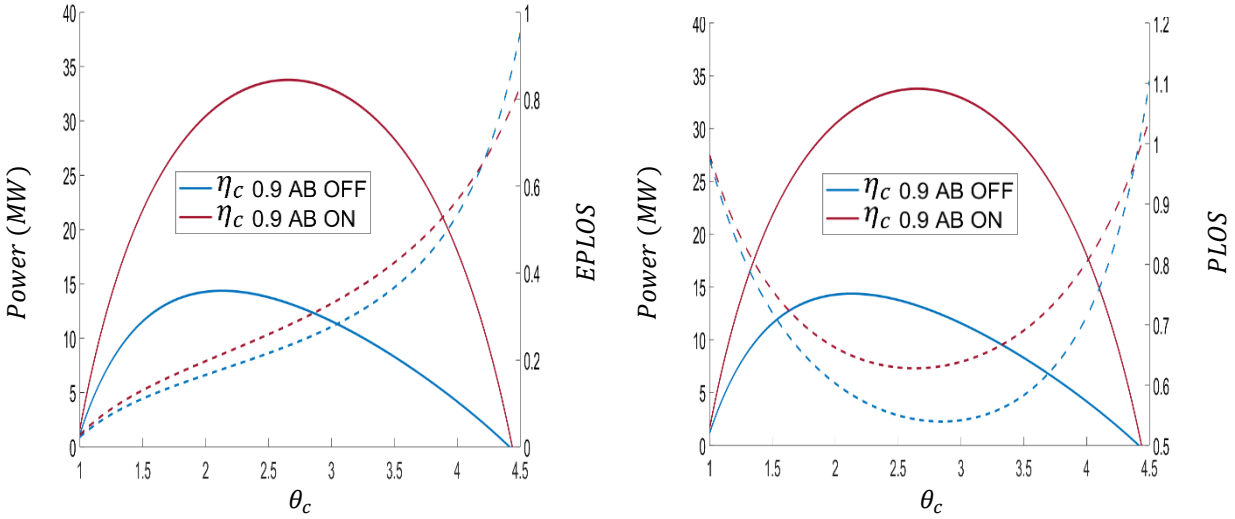

Figure 3.5: *Power*, *EPLOS* and *PLOS* for distinct quantitis of η_c for variations of θ_c.

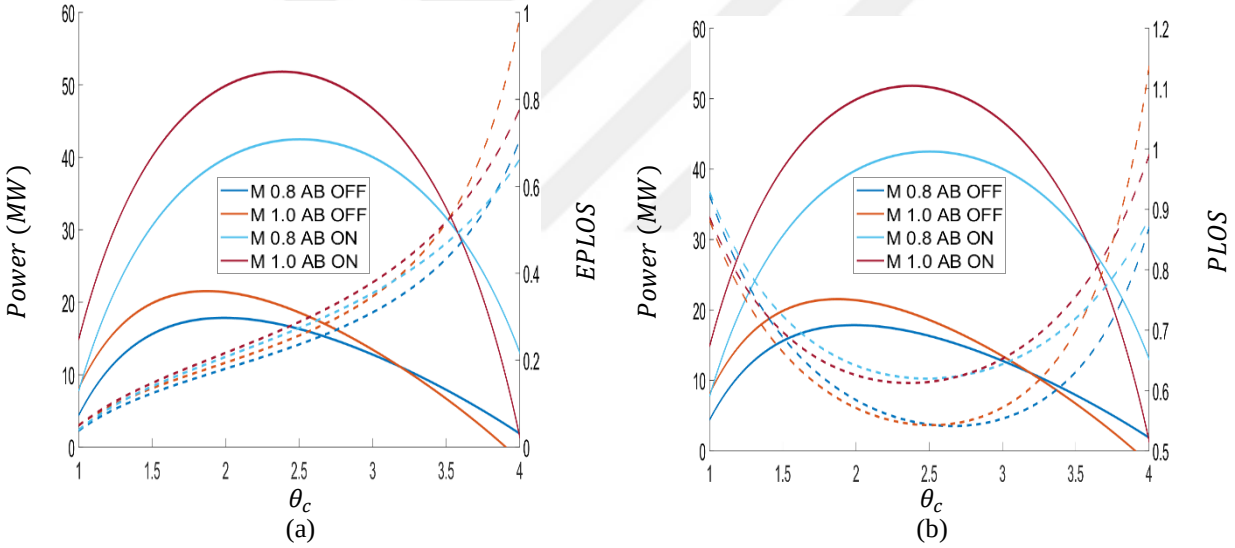

Figure 3.6: *Power*, *EPLOS* and *PLOS* for distinct quantities of M_∞ as a function of θ_c.

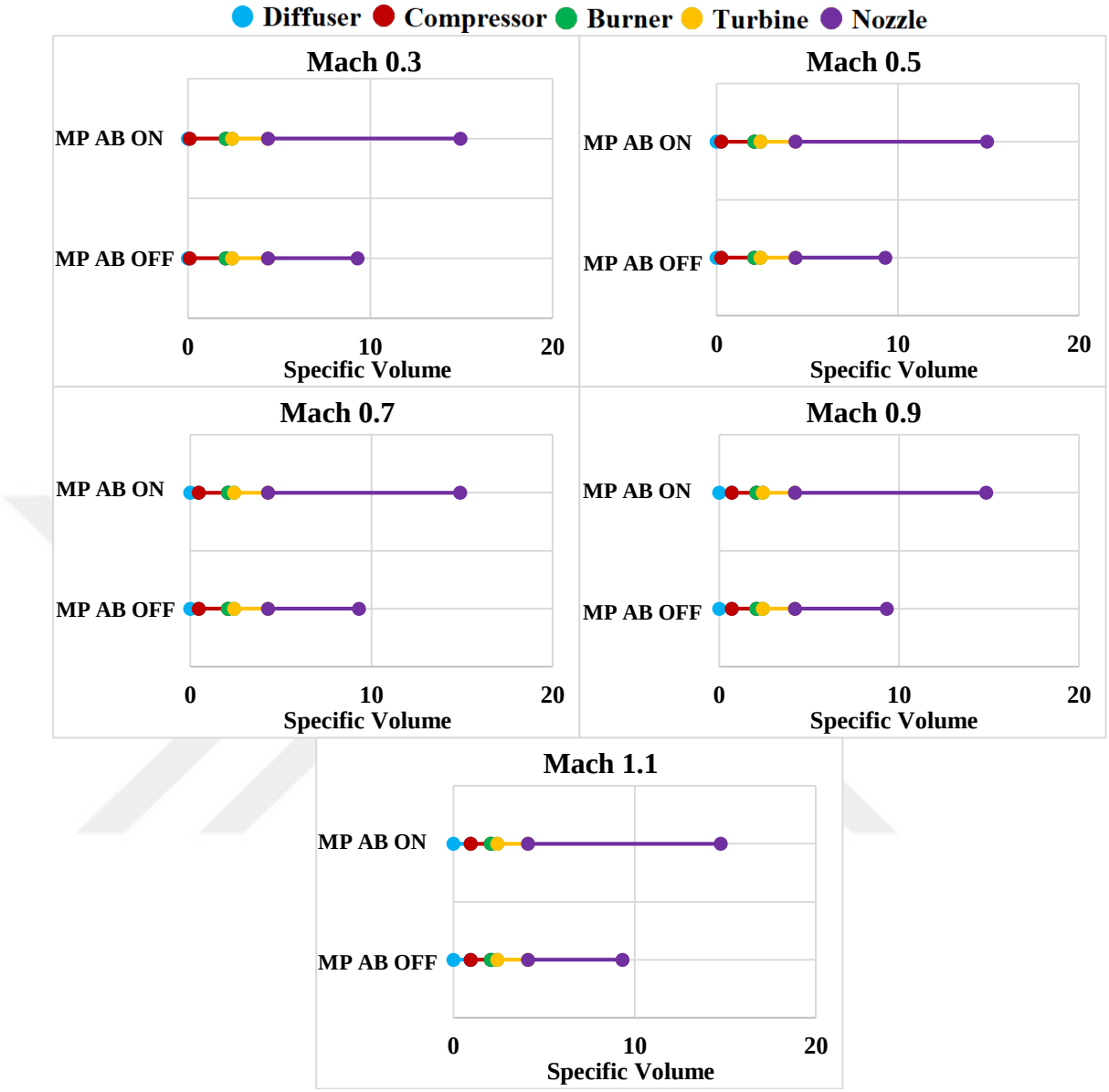

Figure 3.7: Dimensional metamorphisis of respective engine modules at maximum MP for variations $\boldsymbol{M}_{\infty}$.

3.3 Prospects of Turbojets: With Afterburner

The primary purpose of a turbojet with an AB is to increase thust, power, specific impulse at the expence of higher fuel to air ratio, exergy destruction and ***perhaps*** overall weight of the engine configuration. As mentioned a concessional study of the decreas in θ_c and thus compressor weight, the ~85% increase in exhaust nozzle specific volume and the AB fuel components must be conducted. Although the turbojet with an AB has a significant advantage of increase in thrust at all altitudes and Mach

numbers, it is only beyond a Mach number of unity does the thermal efficiency of the engine configuration portray higher relevance. On the other hand, it was also seen that for a given altitude, the turbojet with an AB was able to attain the same power and thrust output as the turbojet without an AB at a much lower Mach number. Therefore, when considering lower mach numbers the turbojet with AB has a higher advantage in attaining shorter Take-Off distances, especially for military aircrfts on aircraft carriers (i.e. warships). In addition, at higher Mach numbers, the turbojet with an AB has a significantly higher amount of thrust which becomes critical for military type aircrafts in combat mode.

4. THEORETICAL MODEL OF RAMJET

4.1 Objective Formulations and Established Variables

The basis of the ramjet powerplant also depends on the irreversible Brayton configuration and its T-s diagram are illustrated in Figure 4.1. The fundamental precepts of this Brayton configuration operation are:

1. Diffusion takes place as a two step process: first, from far upstream (a) to the engine entrance (1); second, from the engine inle (1) to the end of the diffusion section (2).
2. Air enters the combustion chamber at a subsonic speed. This is achieved through multiple oblique shock waves pinging at the cone / wedge tip and then followed by a normal shock wave located at state (1). Fuel is then injected at state (2) and ignited with a spark.
3. The ignited flames pass through the flame holders (**indicated as a red bar**) at state (3) for improved combustion (compelete combustion) and flame stabilization. The end of the combustion chamber is defined as state (4). Generally the temperature at this state can be as high as 3000 K.
4. The propelling exit of the ramjet consists of a convergent-divergent (CD) exhaust nozzle. The convergent section startes from state (4) and ends at the nozzle throat at state (5) and the divergent section ends at stae (6). The CD nozzle is designed such that the exit velocity is greater than the free stream velocity, thus, thrust is accomplished.

The ramjet uses the same model and operates between a heat source at high temperature, T_H, and a heat sink at low temperature, T_L. Simlar to the turbojet without an AB configuration there is one ($\dot{Q}_H$) rate of heat transferred from the heat source to the turbojet engine and one ($\dot{Q}_L$) rate of heat is rejected to the heat sink from the ramjet engine.

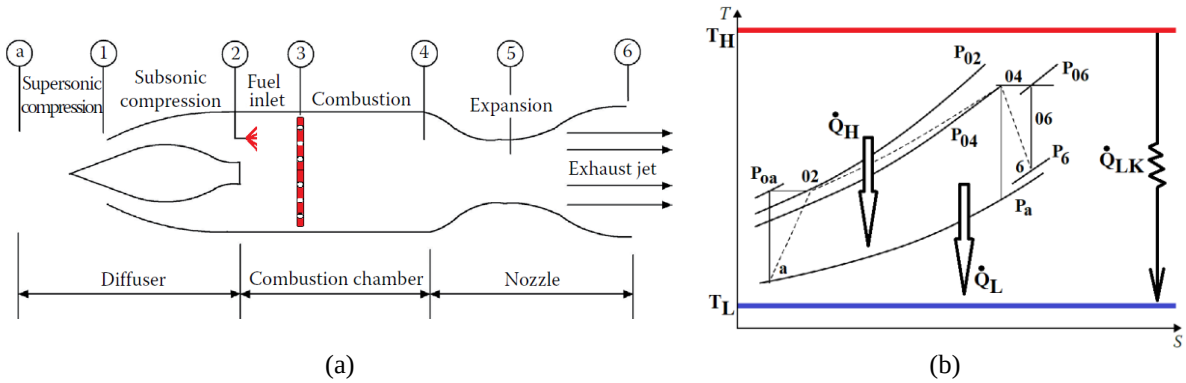

(a) (b)

Figure 4.1: Engine arrangement (a) and T-s schematic representation of a ramjet cycle (b)

Similar to the turbojet engine with and without an AB, the power produced and the total heat transfer rate from the hot reservoirs to the combustion chamber by the ramjet engine cycle are also written as:

$$\dot{W} = \dot{Q}_{HT} - \dot{Q}_{LT} = \dot{Q}_H - \dot{Q}_L \quad (4.1)$$

$$\dot{Q}_{HT} = \dot{m}_f Q_R \eta_b \quad (4.2)$$

Here we also assume that the fuel used for the combustion chamber is the same as for the turbojet engine with and without an AB; therefore, Q_R is still the fuel heat dissipation per unit mass for the combustion chamber, where $\dot{m}_f$ is the fuel mass flow rate and η_b is the efficiency for the combustion chamber.

Here, as with the turbojet engine with and without an AB, the compression ratio parameter ($\theta_c = (P_{02}/P_{01})^{(\gamma-1)/\gamma}$) is no longer used for the ramjet engine cycle. Rather, stagnation pressure ratios for the intake, combustion chamber, nozzle and for the overall engine are defined as:

Stagnation pressure ratio in the intake:

$$r_d = \frac{P_{02}}{P_{oa}} \quad (4.3)$$

Stagnation pressure ratio in the combustion chamber:

$$r_c = \frac{P_{03}}{P_{o2}} \quad (4.4)$$

Stagnation pressure ratio in the nozzle:

$$r_n = \frac{P_{05}}{P_{o3}} \quad (4.5)$$

Overall engine stagnation pressure ratio:

$$\frac{P_{05}}{P_{oa}} = r_d\, r_c\, r_n \qquad (4.6)$$

Implementing an energy balance at the inlet nd exit of the combustor the fuel to air ratio, *f* for the ramjet is derived as:

$$f = \frac{C_{pa}(T_{04} - T_{0a})}{Q_R \eta_b - C_{pa} T_{04}} \qquad (4.7)$$

The equations of the propulsion variables including: thrust (F), specific thrust (F_S), thrust specific fuel consumption (TSFC), air specific impulse (I_a), thermal (η_{th}) and propulsive (η_p) efficiency, power density ($\dot{W}_d$), rate of entropy generation ($\dot{S}_G$), ECOL, ECOP and PLOS formulations do not change as previously stated for the turbojet engine without an AB, however they now consolidate the ramjet configuration within the mathematical statements. Therefore, the reader can refer to Secion 2.1 for these formulations. In addition to the numerical optimization procedures and Altitude model are still applicable to the ramjet engine; whereas the Mass Flow, Shaft Force and Engine Speed models are no longer applicable.

The mass flow for the ramjet engine is now defined from free stream conditions as:

$$W_a = \rho_a A_1 C_a \qquad (4.8)$$

4.2 Outcomes and Considerations

Similar to the turbojet with an AB the performance analysis and comparision for the ramjet engine also takes a trasnformation towards the more constraining paramters of Mach number and altitude. In addition the performance evaluations have also been assessed on under a maximum power regieme for the ramjet and compared to the Turbojet without with an AB to the turbojet without an AB under the same condition. Table 4.1 represents the values previosly taken for the turbojet with (**in blue**) and without (black) an AB in addition to the values for the ramjet condition (**in red**); departures from these quantities are represented within the necessary figures. The essential propulsion theorems for the powerplant state point computations may be obtained from El-Sayed [71]. Note, that for the ramjet there is no compressor, turbine nor shaft, therefore, the values of these component efficiencies are not used for the

ramjet cycle analysi. In addition, the ramjet was assessed at a higher altitude (16.2 km vs. 10 km) and the heat source at high temperature, T_H, had to be raised in order to accomodate the maximum cycle temperature of the ramjet.

Table 4.1: Additional delegated variable inputs for Ramjet condition.

Inputs		
T_L = 200 K	**η_j = 0.96**	γ_g = 1.333
T_H = 2500 K	η_m = 0.99	R = 287 J/kg K
T_a = 216.6 K	**η_b = 0.96**	Di = 0.8 m
P_a = 10.01 kPa	C_{pa} = 1.005 kJ/kg K	Q_R = 43000 kJ/kg
ξ = 0.01	C_{pg} = 1. 148 kJ/kg K	η_c = 0.87
η_i = 0.93	γ_a = 1.4	η_t = 0.9
M = 0.5	ΔP_b = 0.96	T_{03} = 1200 K
η_{ab} = 0.9	**ΔP_{ab} = 0.97**	**T_{05} = 2000 K**
δ = 12	**A_i = 0.2 m^2**	**ALT = 16200 m**

4.2.1 Single oblique and normal shock solution

As the title of this section advocates, the figures below (Figure 4.2 to Figure 4.5) are based on a single oblique and normal shock solution for the ramjet cycle analysis. The oblique shock at the wedge tip, normal shock at the inlet and the Rayleigh flow solutions are based on the tables and formulations of gas dynamics and can be found in Keith et al. [104]. In addition, the oblique shock was assumed to be a weak shock occuring at the wede tip such that a higher pressure recovery can be obtained. The weak shock angle solution also ensures that the flow downstream remains supersonic.

From Figure 4.2 it can be seen that both the fuel to air ratio, *f*, and TSFC decrease with increasing Mach number; in addition the TSFC also shows a decrease with increasing wedge angle, δ. However, at a given Mach numer the fuel to air ratio is constant; this is due to the fact that *f* is calculated on the basis of maximum (T_{04}) and atmospheric (T_a) cycle temperature conditions and completely independent of the wedge angle, δ, and thus remains constant for a given Mach number (see 4.7).

Figure 4.3 shows both an increase in thurst and power as both the wedge angle and Mach number increases. In addition, the thermal and overall efficiency of the ramjet

increases with increasing Mach number and wedge angle; however, the propulsive efficiency shows an increase with increasing Mach number and a slight decrease, ~1%, with increasing wedge angle.

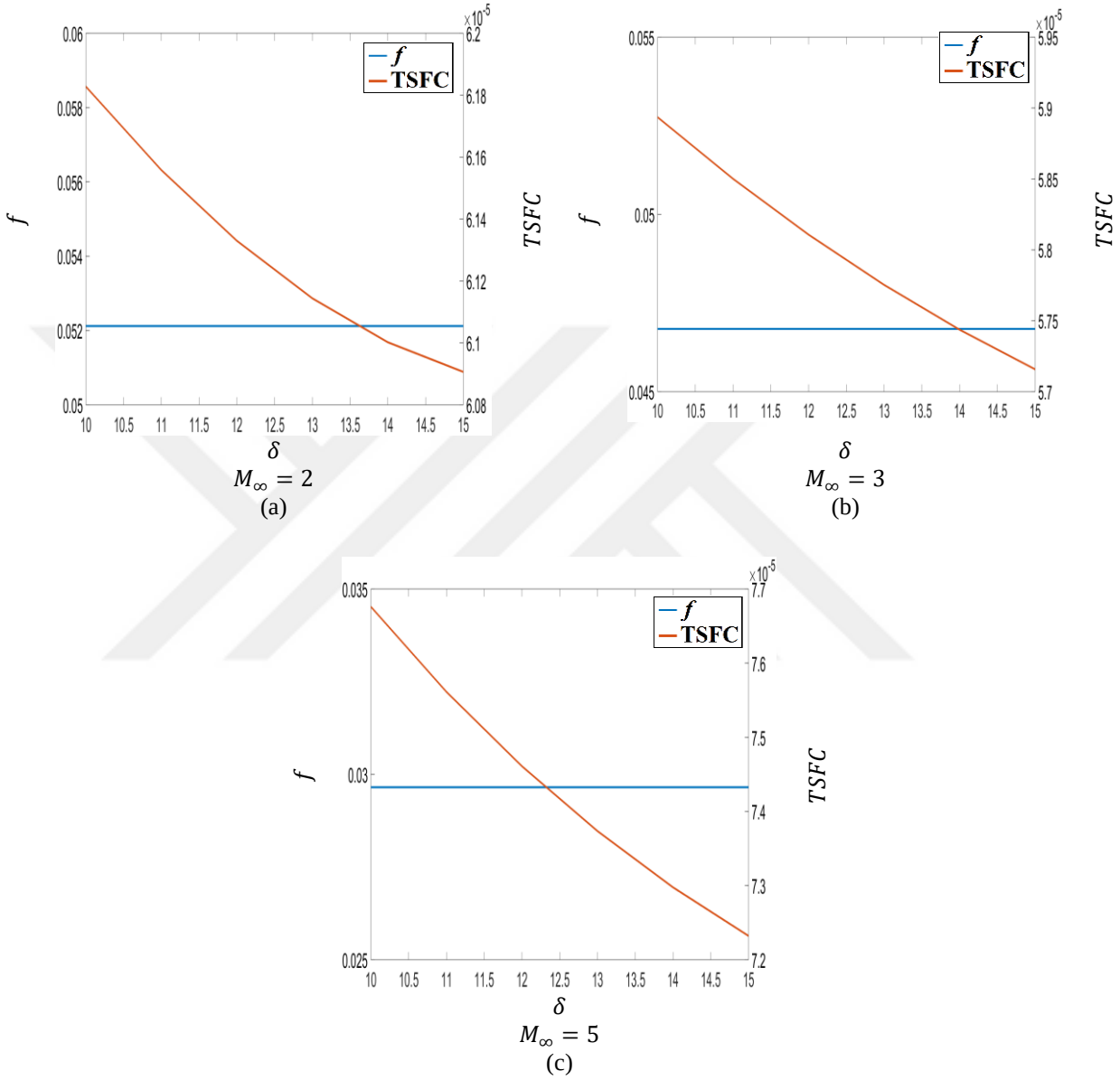

Figure 4.2: *f*, and TSFC for variations of δ and for distinct quantities of $\boldsymbol{M}_\infty$

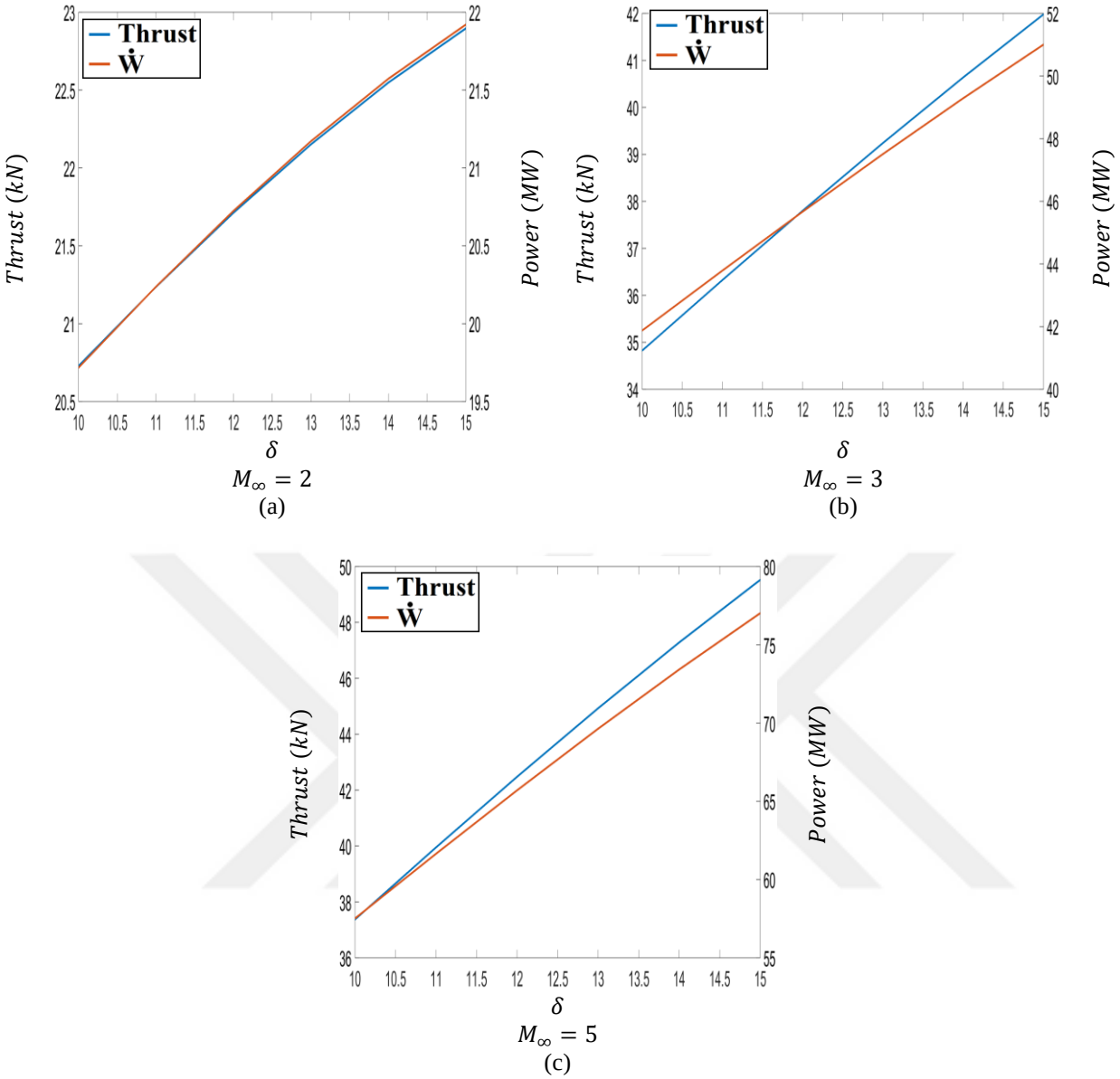

Figure 4.3: Thrust and $\boldsymbol{W_a}$ for variaitons of δ and for distinct quantities of $\boldsymbol{M_\infty}$

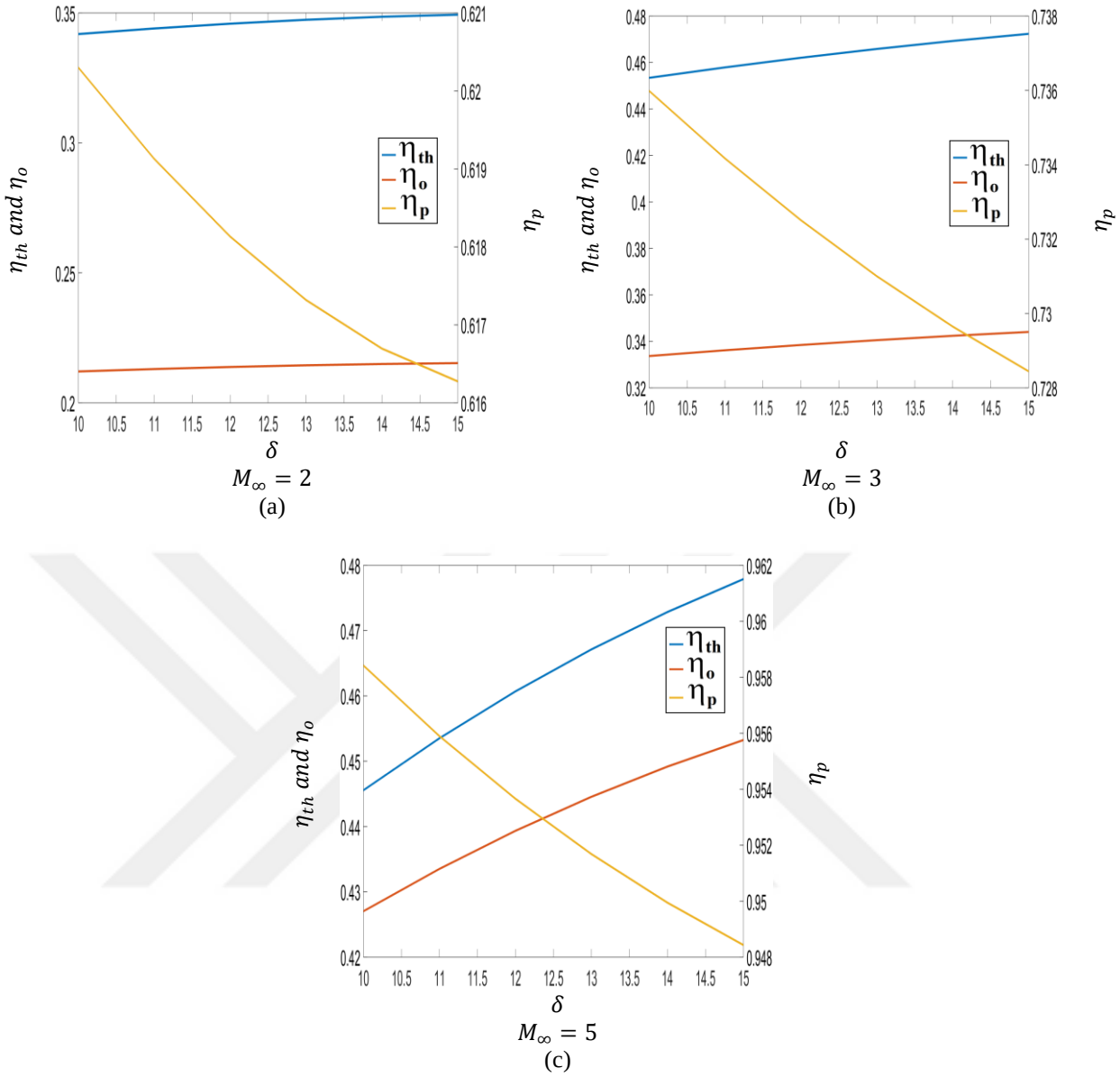

Figure 4.4: η_{th}, η_o and **η_p** efficiencies for variations of δ and for distinct quantities of **M_∞**

Figure 4.5 below shows that as the wedge angle inceases the oblique shock angle increases, however, as the Mach number increases the oblique shock angle decreases. In addition, for all wedge angles and with increasing Mach number, the wedge length increases and purtrubes outwards towrds the left; this occurs such that, for a weak oblique shock and higher pressure recovery, the shock wave remains attached at the wedge tip and inlet lip.

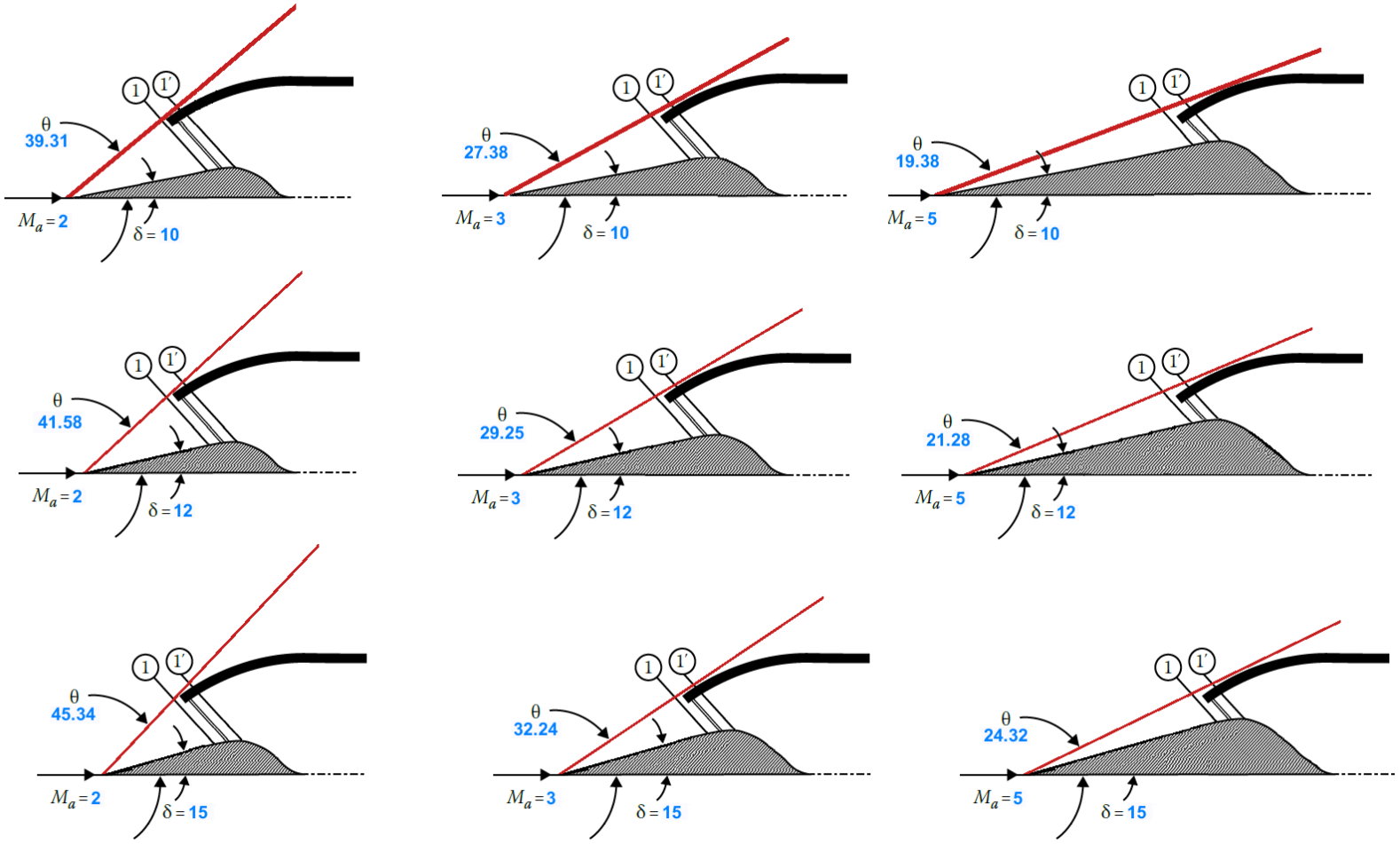

Figure 4.5: Representation of Oblique and Normal Shock angles for variations of wedge angles δ and Mach number $\boldsymbol{M}_{\infty}$

4.2.2 Multiple oblique and single normal shock solution

In this section the analysis of the turbojet with and without an AB and the ramjet cycle has been based on a maximum power (MP) performance spectrum.

In the previous sectiom (4.2.1) solutions were given based on a single oblique and normal shock solution, however this assumtion drives a much higher stagnation pressure drop for the inlet and is not a representation of real gas turbine inlet pressure recovery (ram recovery) design characteristics. Therefore, the MIL-E-5007D [103] specification is now used for the definition of the diffuser stagnation pressure ratio and valid for Mach numbers between 1-5:

$$r_d = 1 \quad For\ Mach\ Number < 1 \tag{4.9}$$

$$r_d = 1 - 0.075(M_\infty - 1)^{1.35} \quad From\ 1\ to\ 5\ Mach\ Number \tag{4.10}$$

$$r_d = 800/(M^4 + 938) \quad For\ Mach\ Number > 5 \tag{4.11}$$

The results forn the single oblique and normal shock solution (SOSN) vs. the multiple oblique and single normal (MOSN) shock solution for the diffuser stagnation pressure ratio can be seen from Figure 4.6. At a Mach number of 5 the SOSN and MOSN solutions give a pressure stagnation ratio of 0.14 and 0.52 respectiely.

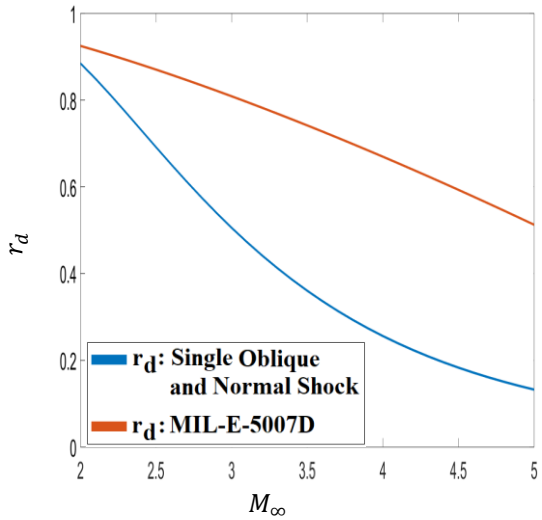

Figure 4.6: Single Oblique and Normal Shock vs. Multiple Oblique and Single Shock solution.

Figure 4.7 represents the thermal, overall and propulsive eficiencies of the turbojet with and witout an AB in comparison to the ramjet engine. As previously mentioned the turbojet with an AB has a better advantage on thermal efficiency for Mach numbers geater than 1. Overall the ramjet shows much better performane on thernmal and overall efficiency; however, the propulsive efficiency of the ramjet engine is not competitive with that of the turbojet with and without an AB until the free stream Mach number reaches beyond 4.

Figure 4.8 shows the fuel to air ratio, TSFC and impulse of all three engine configurations. In terms of *f*, the ramjet cycle is still competitive with that of a turbojet with an AB, however, cannot compete with the turbojet without an AB. Both the TSFC and impulse of the ramjet engine show larger benefits over the turbojet with and without an AB; however, for Mach numbers beyond 5 both the TSFC and impulse of the ramjet become disadvntageous.

The thrust and power (Figure 4.9) for the ramjet cycle becomes more substantial for ranges of Mach numbers between 2 to 5, on the other hand the turbojet with and without an AB are still much more advantageous in terms of thrust and power. In addition, the specific volume of the exhaust nozzle for the ramjet is much larger than the turbojet with and with out an AB, therfore, represents an issue of increased weight.

However, since the ramjet cycle has no compressor nor turbine (i.e. no moving parts) the tradoff in nozzle length and weight may be more than acceptable. Also, that fact that the ramjet has higher thermal and overall efficiency and can attain much higher Mach numbers that the turbojet with and without an AB makes the ramjet more compelling for propulsive use.

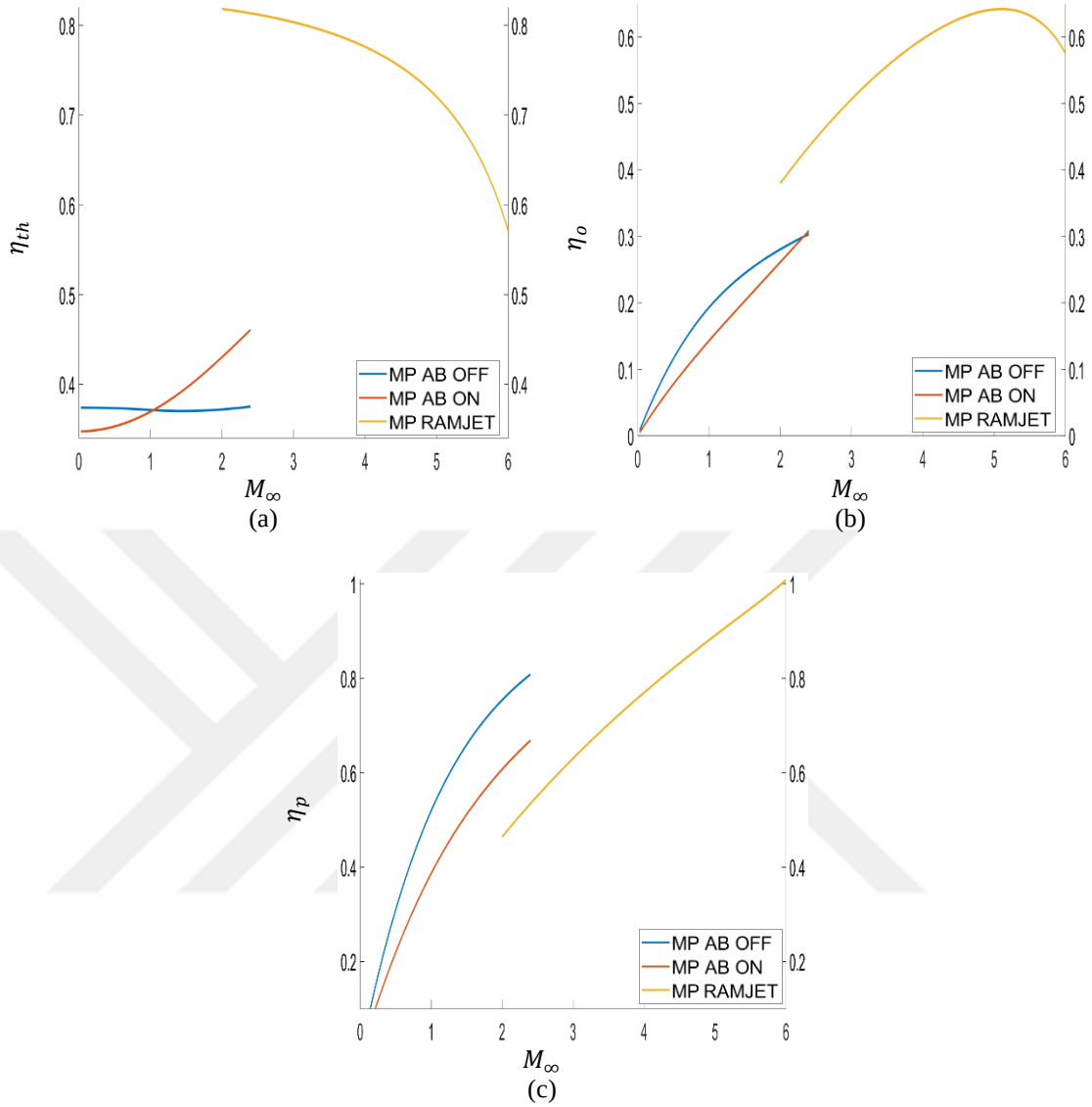

Figure 4.7: η_{th}, η_0 and η_p for turbojet with and without an AB vs. ramjet engine as a function of M_∞.

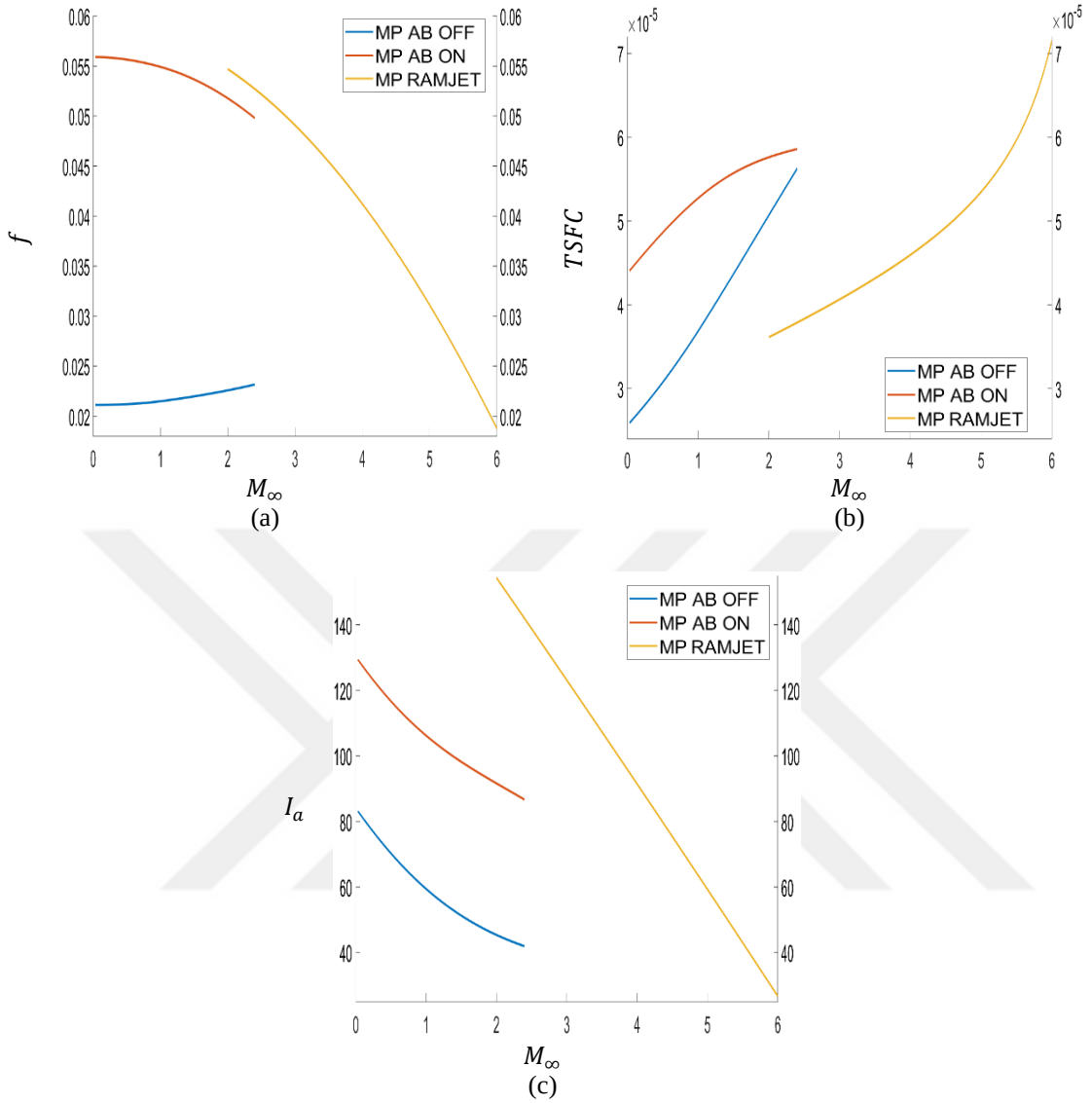

Figure 4.8: f, TSFC and I_a for turbojet with and without an AB vs. ramjet engine as a function of M_∞.

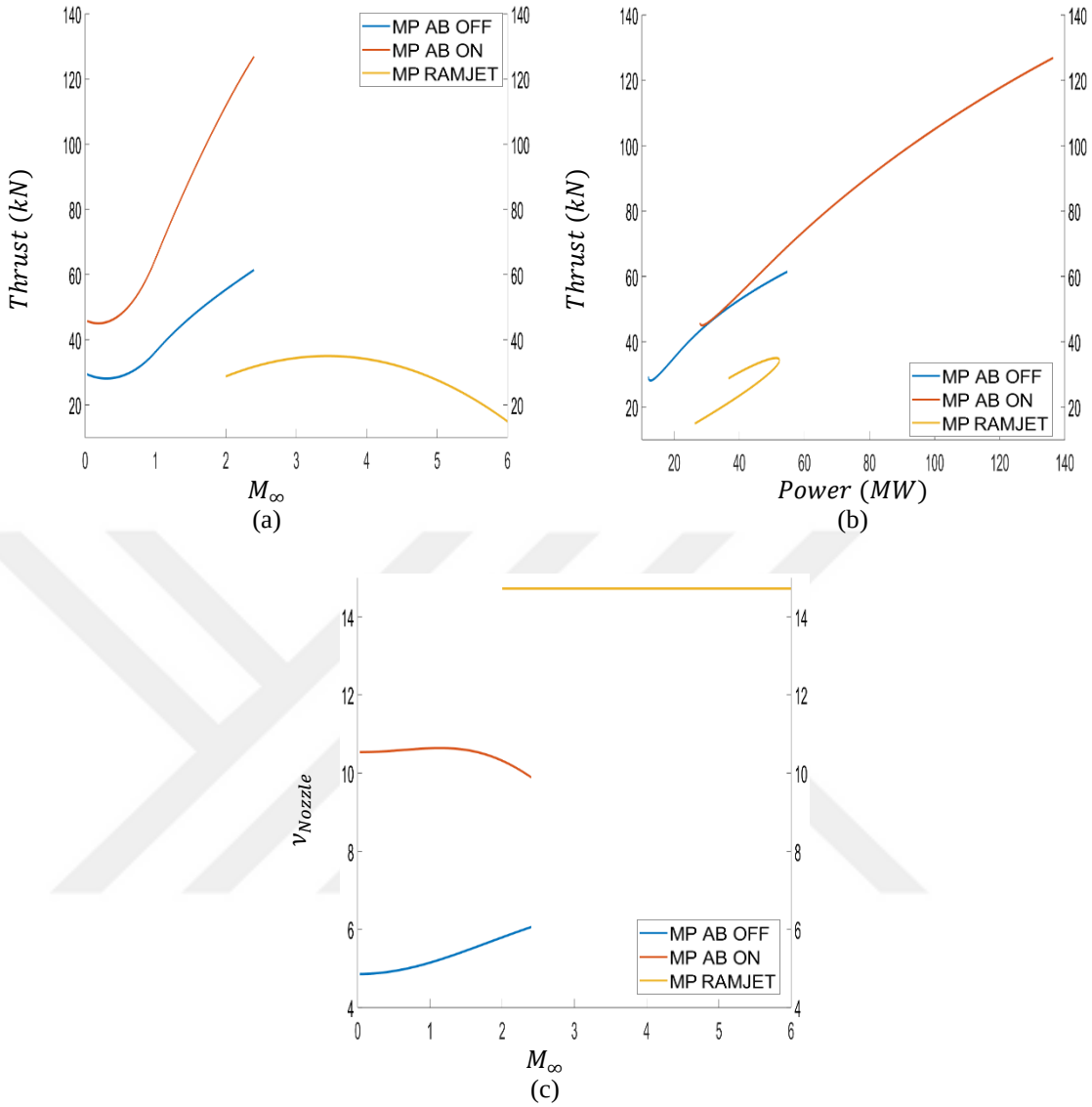

Figure 4.9: Thrust (a) and $\boldsymbol{v_{Nozzle}}$ (c) as a function of $\boldsymbol{M_\infty}$ and Thrust vs. Power for turbojet with and without an AB vs. ramjet engine.

Figure 4.10 to Figure 4.12 represent the variation on the performance parameters of the ramjet engine as a function of the Mach number for deviations in the fuel's LHV(Q_R). All the performance parametes show an increase as the LHV is decresed. This is intrinsically due to the increase of the fuel to air ratio which is inversly proportional to the LHV of the fuel (see Equation 4.7), thus showing an impat on all the remaining performance parameters. However, the specific volume of the exhaust nozzle does not show any variation for changing values of LHV. This is due to the fact that the calculation of the specific volume becomes independent of the LHV at a maxmimum power performance analysis. In adition, it is important to note that when

reducing or increasing the LHV of the fuel an effect should be seen on the maximum temperature of the cycle; however, since the maximum temperature of the cycle is kept constant throughout the analysis, this inter-relationship is lost. Moreover, the effect og the LHV on the maximum temperature of the cycle has not been studied nor provided in any textbook or research article.

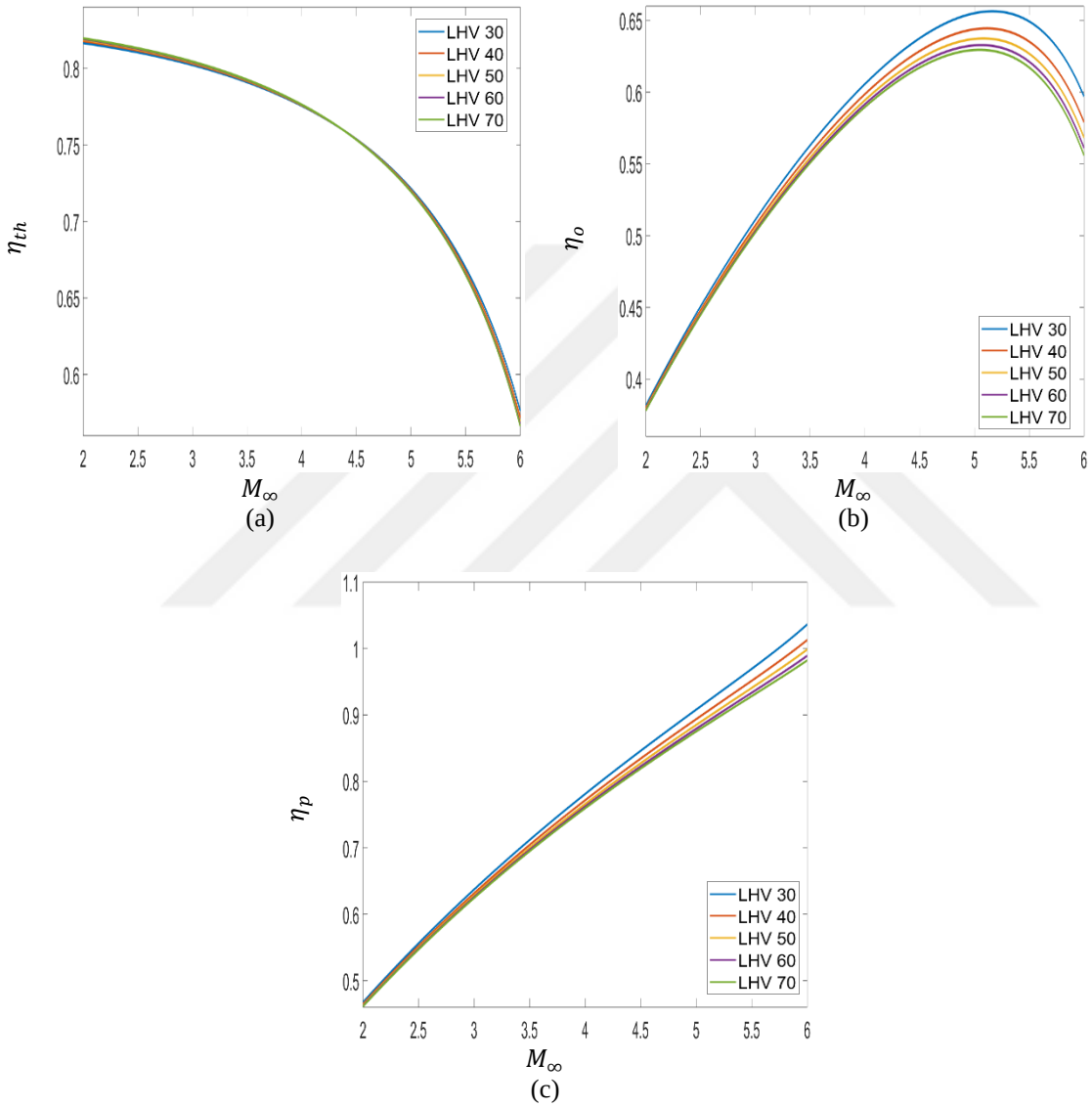

Figure 4.10: η_{th}, η_0 and **η_p** for variations of LHV for ramjet engine as a function of **M_∞**.

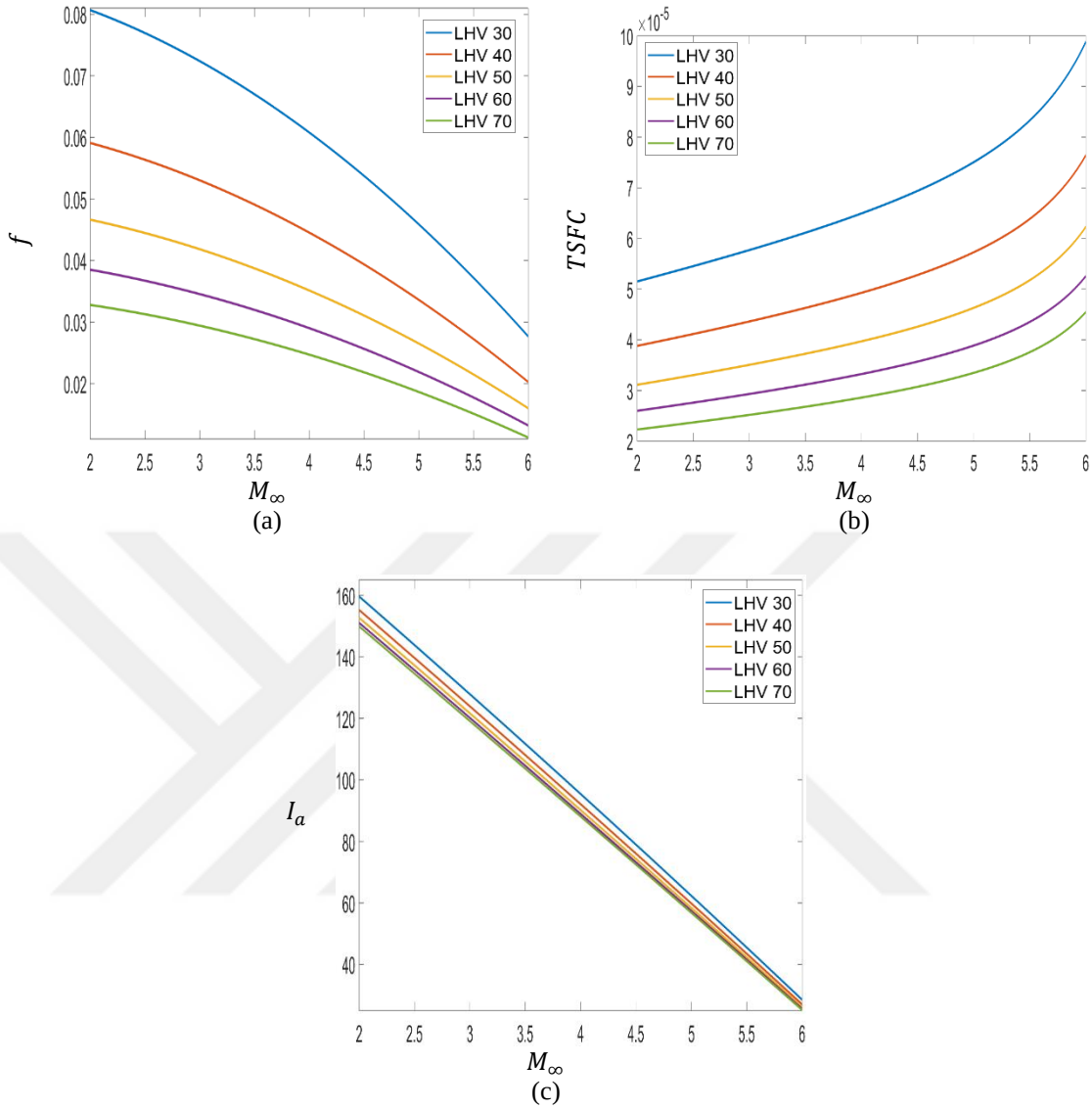

Figure 4.11: f, $TSFC$ and I_a for.variations of LHV for ramjet engine as a function of M_∞.

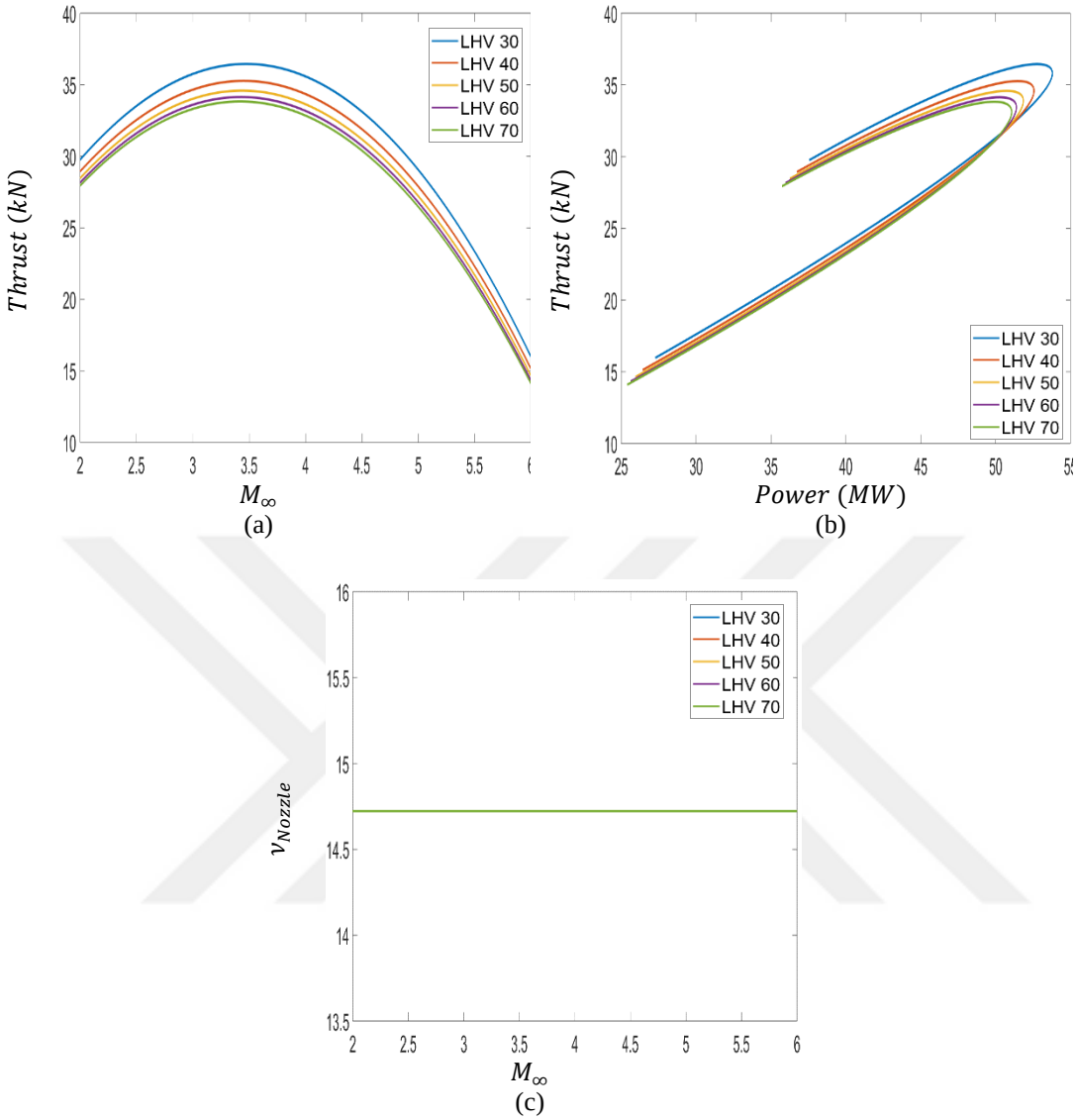

Figure 4.12: Thrust (a) and $\boldsymbol{\nu_{Nozzle}}$ (c) as a function of $\boldsymbol{M_\infty}$ and Thrust vs. Power for variations in LHV.

4.3 Prospects of Ramjets

The evaluation of the ramjet was undertaken on a maximum power (MP) basis and compare to that of the turbojet with and without an AB. It is clear that the advantages of the ramjet are its attainability of much higher thermal and Mach numbers, lower weight due to the abscence of moving parts (compressor, turbine, shaft, etc.) and the ability to have a higher maximum operating cycle temperature.

However, the performance of the ramjet is only realized at Mach numbers between 4-5, especially in terms of propulsive efficiency. Beyond a Mach number of 5 the ramjet cycle becomes quite disadvantagous for any applicable use. Moreover, the ramjet has a much higher fuel consumption in comparison to the turbojet with and without an AB. In addition due to the higher attainable maximum cycle temperatures, higher-temperature materials would be requiered.

Despite the disadvantages of the ramjet cycle on its own, the propulsion cycle of the ramjet can be combined with a turbine based cycle such that the performance benifits from both can be incorporated. This is the subjet of the following and final section of the thesis, Turbine Based Combined Cycles (TBCC).

5. TURBINE BASED COMBINED CYCLE (TBCC): THE TURBORAMJET ENGINE

5.1 Objective Formulations and Established Variables

Turbine Based Combined Cycles (TBCC) assimilate the advantages of both states of of operation from the turbojet / turbofan and ramjet / scramjet such that:

1. The turbojet / turbofan can takeoff, climb, cruise, descent and land, and thrust can still be generated up to Mach numbers of 2 to 3.
2. The ramjet is capable of generating thrust from Mach numbers of 1 in addition to reaching Mach numbers of 5 to 6.
3. Whereas the scramjet is capable of generating thrust from Mach numbers of 2.5 in addition to reaching Mach numbers of 20.

In the first segment of flght the engine works as a turbojet / turbofan and then switches to the ramjet / scramjet in accordance to aircraft mission.

The hybrid engine (TBCC) considered for this section is the Turboramjet engine. The turboramjet can be run in either turbojet (AB being ON or OFF), ramjet and even dual mode operation. In addition, the construction of the turboramjet engine can be in the form of: Wraparound or Over / Under type. Moreover, either construction carries the same thermodynamic cycle analysis (see Figure 5.1). In the turbojet mode the engine generates all the thrust needed for the aircraft and the states and governing equations are the same as prescribed in section 3 and section 2 for a turbojet with and without an afterburner respectively. In the dual mode both the turbojet and ramjet are operating simultaneously. The thrust generated by the turbojet starts to decline as the inlet air mass flow rate is reduced and diverted for ramjet operation by adding fuel and igniting the mixture for thrust generation. In the ramjet mode the inlet air mass flow is now fully diverted to the ramjet and the turbojet stops working and no longer contributes to thrust generation; thus, thrust generation is exclusively achieved by the ramjet. The ramjet states and governing equations are the same as prescibed in section 4.2.2 for

multi-oblique shock and single normal shock solution and Rayleigh flow calculation for the combustion chamber.

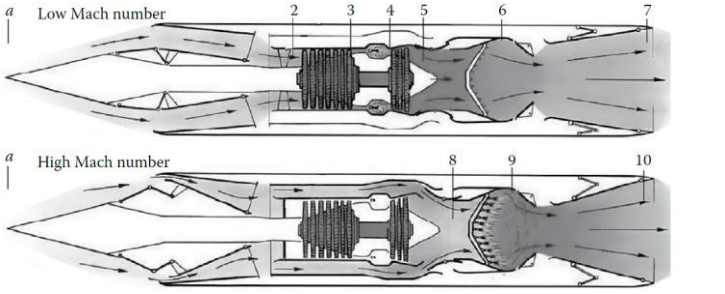

Wraparound Turboramjet
(a)

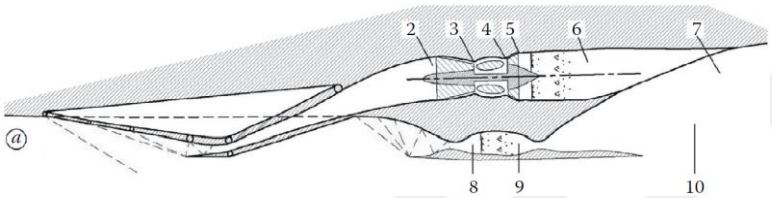

Over / Under Turboramjet
(b)

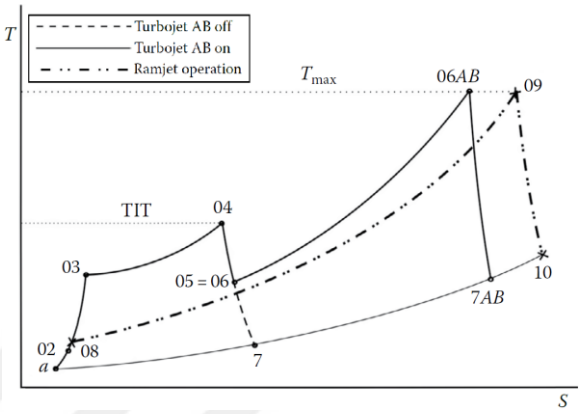

Thermodynamic Cycle of Turboramjet
(c)

Figure 5.1: Wraparound (a), Over/Under (b) and Thermodynamic Cycle (c) of Turboramjet Engine

5.2 Outcomes and Considerations

This section considers the analysis of a wraparound turboramjet model. In addition, the reader is to refer to section 2, sections 3 and 4.2.2 for the objective functions and prescribed parmeters of the turbojet without and with an AB and ramjet respectively.

The basis of the turboramjet powerplant with an afterburner (AB) depends on the irreversible Brayton configuration and its T-s diagram are illustrated in Figure 5.2. The fundamental precept of this Brayton configuration has all the same processes as the turbojet with and without an AB and the ramjet. As previously stated the turboramjet engine with an AB operates amongst a heat source at high temperature, T_H, and a heat sink at low temperature, T_L. In the AB configuration there are two ($\dot{Q}_H$) rates of heat transferred from the heat source to the turbojet engine; in the ramjet mode only one ($\dot{Q}_H$) rate of heat is transfered from the high temperature source; however, there is still only one ($\dot{Q}_L$) rate of heat is dissipated to the heat sink from the turboramjet powerplant with an AB. Figure 5.2 (b) aslo depicts the various engine therodynamic cycle

configurations: turbojet without an AB (**orang**); turbojet with an AB (**black**) and ramjet (**green**).

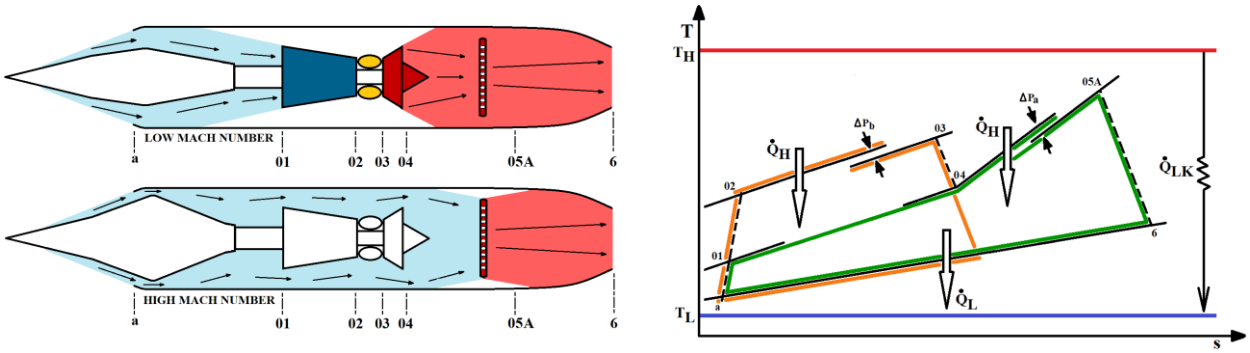

(a) (b)

Figure 5.2: Engine arrangement (a) and T-s schematic representation of a turboramjet cycle (b) with an afterburner

Similar to the turbojet with an AB and ramjet engines the performance analysis and comparision for the turboramjet engine also takes a trasnformation towards Mach number and altitude. Moreover, the **dual** mode operation was considered and assessed as variations of altitude and inlet air mass flow; the split of air mass flow between the turbojet and ramjet. Note that in dual mode operation the turbojet engine AB are considered to be ON. In addition the performance evaluations have also been assessed under a maximum power regieme for the turboramjet. Table 5.1 represents the combination of values taken for the turbojet with and without an AB as well as the values for the ramjet condition (the inlet area of the ramjet is now considered as $0.5m^2$); departures from these quantities are represented within the necessary figures. The essential propulsion equations for the powerplant state point computations may be obtained from El-Sayed [71].

Table 5.1: Delegated variable inputs for Turboramjet condition.

Inputs		
T_L = 200 K	η_j = 0.95	γ_g = 1.333
T_H = 2200 K	η_m = 0.99	R = 287 J/kg K
T_a = 223.3 K	η_b = 0.98	Di = 0.8 m
P_a = 26.5 kPa	C_{pa} = 1.005 kJ/kg K	Q_R = 43000 kJ/kg
ξ = 0.01	C_{pg} = 1. 148 kJ/kg K	η_c = 0.87
η_i = 0.93	γ_a = 1.4	η_t = 0.9
M = 0.5	ΔP_b = 0.96	T_{03} = 1200 K
η_{ab} = 0.9	ΔP_{ab} = 0.97	T_{05} = 2000 K

δ = 12	**A_i = 0.5 m^2**	ALT = 10000 m

Figure 5.3 to Figure 5.5 is an altitude assessment of the turboramjet in dual mode operation as a function of Mach number for a 25% to 75% inlet air mass flow split between the turbojet and ramjet respectively. The performance parameters of: thermal, propulsive and overall efficiency; fuel to air ratio, TSFC, impulse, thrust, power and specific volume were evaluated.

Figure 5.3 distinctly shows the limitation of turbojet operation as a function of altitude and Mach number. The maximum feasible operating range in terms of Mach number at an altitude of 2 km, 4 km, 6 km, 8 km, 10 km and 12 km to 20 km are 1.97, 2.08, 2.19, 2.31, 2.44 and 2.51 respectively, after which a divergence in the propulsion solutions are encountered. The propulsive efficiency of the turbojet still outweighs the use of the ramjet up to a Mach number of 2.5. However, falls short in terms of thermal and overall efficiency in the overlapping region of Mach 1.97 and 2.51. In terms of overall efficiency, the ramjet indicates highest performance at 3.36, 3.55, 3.74, 3.94, 4.15, 4.34, 4.47, 4.63, 4.73 and 4.89 Mach with 0.52, 0.54, 0.56, 0.58, 0.60, 0.63, 0.65, 0.68, 0.70 and 0.73 overall efficiencies for each altitude from 2 km to 20 km respectively. Whereas the turbojet reaches its maximum performance capability at 1.97, 2.08, 2.19, 2.31, 2.44 and 2.51 Mach with 0.25, 0.26, 0.28, 0.30, 0.31 and 0.32 overall efficiencies respectively for each altitude from 2 km to 12 km; note that beyond 12 km the overall efficiency and Mach number remains the same. The thermal efficiency of the ramjet depicts a gradual decrease and takes a sharp decline beyond a Mach number of 4; thus, at 4.09, 4.24, 4.41, 4.6, 4.76, 4.9, 5.03, 5.16, 5.26, and 5.38 Mach with 0.48, 0.51, 0.54, 0.56, 0.60, 0.62, 0.64, 0.66, 0.68 and 0.70 thermal efficiencies are achieved. Whereas the turbojet reaches its maximum performance capability at 1.97, 2.08, 2.19, 2.31, 2.44 and 2.51 Mach with 0.37, 0.39, 0.42, 0.44, 0.46 and 0.48 thermal efficiencies respectively for each altitude from 2 km to 12 km; similarly, beyond 12 km the thermal efficiency and Mach number remains the same. The propulsive efficiency of the ramjet is nearly linear and illustrates an upper saturation limit for 2 km and 20 km at Mach numbers of 4.27, 4.45, 4.65, 4.85, 5.07, 5.22, 5.3, 5.37, 5.44 and 5.5 respectively; in addition, at a Mach number of 2 the propulsive efficiency decreases from 0.59 to 0.50 as the altitude increases from 2 km to 20 km. Whereas the turbojet reaches its maximum performance capability at 1.97, 2.08, 2.19, 2.31, 2.44 and 2.51 Mach with 0.67 propulsive efficiency respectively for

each altitude from 2 km to 20 km; also the Mach number and propulsive efficiency does not change beyond 12 km.

Figure 5.4 shows the *f*, *TSFC* (kg/N-s) and I_a (s) of the dual mode operating system. For all altitudes the ramjet indicates lower *f* and *TSFC* and higher I_a than the turbojet. The minimum attainable *f* for the turbojet ranges from 0.05137, 0.0508, 0.05033, 0.04993 and 0.04861 for the previously specified Mach numbers and altitudes; in addition to showing a decrease if *f* for increasing altitude. On the other hand, the ramjet experiences an increase in *f* as the altitude increases. Nevertheless, at a Mach number of 2 the *f* increases from 0.04122 to 0.0441 which is still much lower than the *f* of the turbojet. Evidently this is due to the turbojet fuel contribution stemming from both the combustion chamber and afterburner, whereas the ramjet only utilizes the afterburner fuel for thrust generation. In addition, the ramjet exhibits a much greater advantage of attaining higher Mach numbers for even lower values of fuel to air ratio; i.e. as the Mach number increases the *f* also decreases. The turbojet reaches a maximum TSFC capability at 1.97, 2.08, 2.19, 2.31, 2.44 and 2.51 Mach with 6.637e-05, 6.415 e-05, 6.215 e-05, 6.032 e-05, 5.865 e-05 and 5.694 e-05 TSFC respectively for each altitude from 2 km to 12 km; in addition to a decrease in TSFC with increasing altitude notwithstanding that the Mach number and TSFC do not changing beyond 12 km. For a TSFC of 5.694 e-05, the operating range for the ramjet in term of Mach numbers are: 3.46, 3.67, 3.9, 4.14, 4.4, 4.62, 4.79, 4.96, 5.11 and 5.26 for altitudes from 2 km to 20 km respectively; where beyond a TSFC of 5.694 e-05 operation becomes unrealistic.

Figure 5.5 depicts the thrust (kN) for variations of Mach number and power and the exit nozzle specific volume (m^3/kg) for variations of Mach number. In terms of thrust the turbojet is capable of achieving 64, 55, 47, 39, 32, 25, 18, 13, 10 and 7 kN of thrust at Mach numbers of 1.97, 2.08, 2.19, 2.31, 2.44, and 2.51 respectively for each altitude from 2 km to 20 km. Whereas the ramjet can produce 257, 213, 174, 140, 111, 85, 63, 47, 34 and 25 kN of thrust at a Mach number of 2 for each altitude from 2 km to 20 km. As expected, the thrust and power of the dual system decreases with altitude. Nonetheless, the ramjet is still capable of producing 7 kN of thrust at a Mach number of 5.73. When examining the specific volume, the ramjet has a lower exit nozzle specific volume than the turbojet at all altitudes. For the turbojet, specific volumes of 3.5, 4.5, 5.8, 7.5, 9.9, 13.3, 18.3, 25, 34.3 and 46.9 are achieved at Mach numbers of 1.97, 2.08, 2.19, 2.31, 2.44, and 2.51 respectively for each altitude from 2 km to 20

km. Whereas the ramjet experiences limitations in specific volumes of 2.4, 2.9, 3.6, 4.5, 5.7, 7.3, 9.4, 12.0, 15.4 and 19.8 for operable Mach number maximums of 4.87, 5.07, 5.28, 5.5, 5.73, 5.89, 5.95 and 6 as the altitude increases from 2 km to 20 km. Moreover, as the altitude increases the specific volume of the turbojet becomes far too large for efficient operation and therefore too heavy. Altitudes at and above 10 km show approximately twice the increase in specific volume for the turbojet than the ramjet. Therefore, the turbojet can be used up to an altitude of 8 km and then completely switch to ramjet operation for altitudes of 10 km and beyond. Where at 20 km the specific volume of the ramjet is ~20 (which is obtained at 14 km for the turbojet) and ~47 for the turbojet respectively.

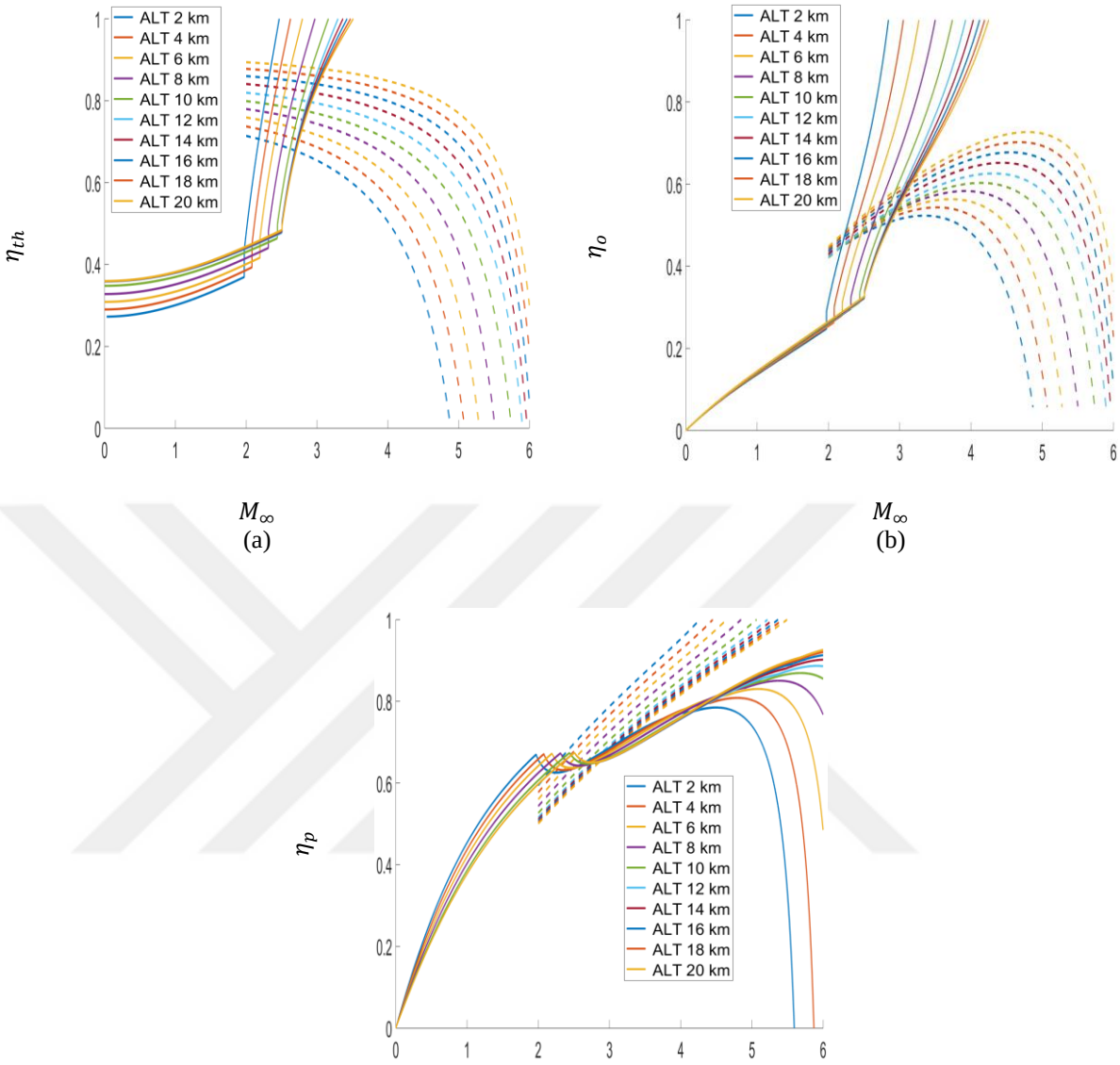

Figure 5.3: η_{th}, η_0 and η_p for variations of altitude for turboramjet engine as a function of M_∞.

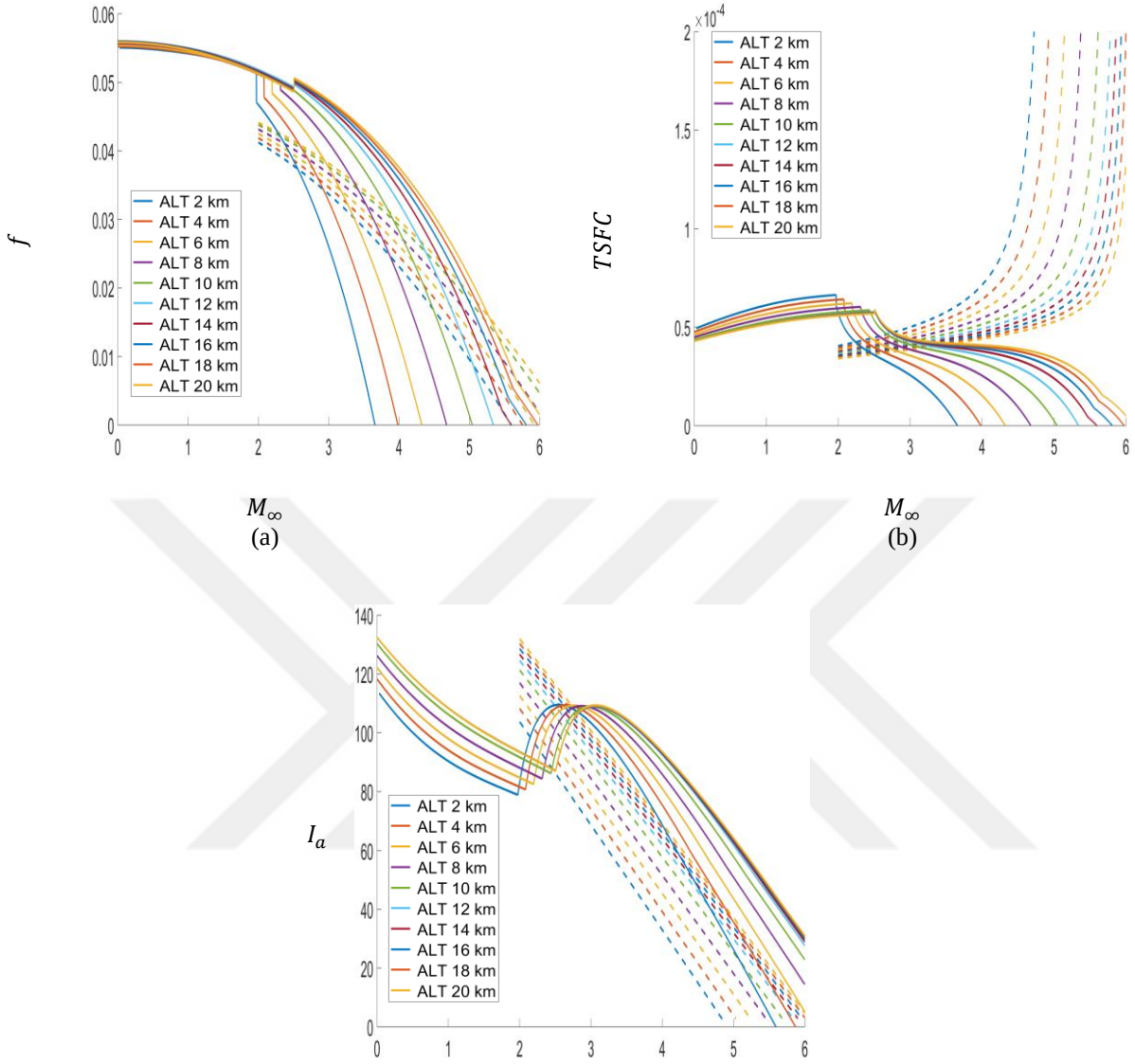

Figure 5.4: f, $TSFC$ and I_a for.variations of altitude for turboramjet engine as a function of M_∞.

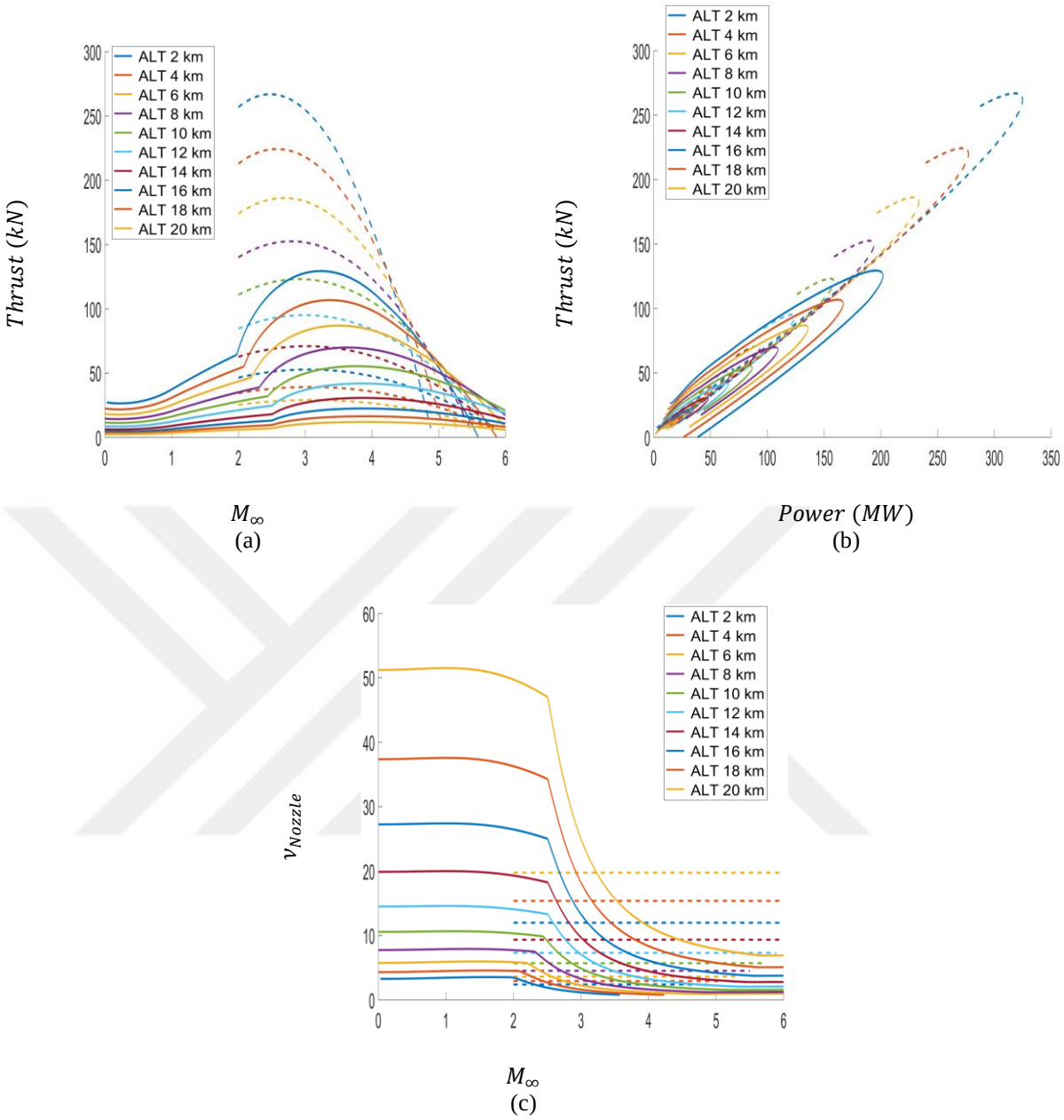

Figure 5.5: Thrust (a) and $\boldsymbol{\nu_{Nozzle}}$ (c) as a function of $\boldsymbol{M_\infty}$ and Thrust vs. Power for variations in altitude.

Figure 5.6 to Figure 5.14 is an assessment of variations of inlet air mass flow split between the turbojet and ramjet as a function of Mach number at 10 km and 20 km (all figures on the right and left respectively). The legend in these figures indicates the percentage of air mass flow being diverted to the ramjet (-- **dashed lines**) and the remaining percentage being directed to the turbojet (**— solid lines**). It is also to note that curves of the same colour are complementary to each other; for example, the blue curves imply a 25% to 75% inlet air mass flow split between the ramjet and turbojet respectively. However, the exception to the previous statement are the **purple** curves, where 100% inlet air mass flow to the ramjet means 0% to the turbojet and vice versa. In addition, this part of the analysis has restricted the operation of the turbojet up to a Mach number of 2.5; as has previously mentioned the limitation of the turbojet application reaches a maximum operable Mach number of 2.4 for both altitudes of 10 km and 20 km respectively. Whereas, the constraint for the discussion of the ramjet analysis will be kept to a maximum Mach number of 4.4 and 5.26 for the altitudes of 10 km and 20 km respectively; this is due to the feasibility in terms of *TSFC* as stated previously. Also to note, the pressure and temperature at 10 km vs. 20 km are: 26.43 kPa and 223.15 K vs. 5.47 kPa and 216.65 K respectively.

Figure 5.6 and Figure 5.7 show that at 25% inlet air mass flow the turbojet is economically more effective in terms of both thermal and overall efficiency respectively at Mach 2. As the split of mass flow to the ramjet is increased (50% to 100%) it becomes quite distinct that the ramjet is much more beneficial. Also, in general, as the inlet mass flow of either system increases, so do the thermal and overall efficiencies. For the altitudes of 10 km and 20 km the maximum attainable thermal efficiencies are: 0.23, 0.34, 0.41 and 0.46 versus 0.24, 0.36, 0.43 and 0.47 respectively. Whereas the ramjet thermal efficiencies are: 0.19, 0.35, 0.5 and 0.66 versus 0.21, 0.38, 0.56 and 0.73 at 10 km and 20 km respectively. In terms of overall efficiency, the turbojet achieves 0.16, 0.23, 0.27 and 0.3 versus 0.16, 0.24, 0.28 and 0.31 at 10 km and 20 km respectively. Whereas the ramjet overall efficiencies are: 0.19, 0.33, 0.46 and 0.6 versus 0.23, 0.39, 0.55 and 0.7 at 10 km and 20 km respectively. Note however, that the maximum overall efficiency (same as previous values) for the ramjet at 10 km are achievable at slightly lower Mach numbers: 4.35, 4.26, 4.2 and 4.17 for increases of inlet air mass flow split. Similarly, at 20 km the maximum overall efficiency for the ramjet are attained at: 5.07, 4.95, 4.88 and 4.82 Mach numbers for increasing mass

flow split; in addition, for 50% to 75% air flow split the overall efficiency increases by 1% and at a 100% air flow split the overall efficiency increases by 3%.

On the other hand Figure 5.8 indicates a better propulsive efficiency for the turbojet over the ramjet at all inlet air mass flow splits up to Mach 2. Beyond a Mach number of 2 the ramjet takes over and has a dominating effect on system performance. However, unlike the thermal and propulsive efficiency, the propulsive efficiency decreases as the inlet air mass flow to either system increases. This is due to the kinetic energy added to the air mass flow through the engine being higher than the propulsive power generated by the fully expanded exhaust jet. For the turbojet, the attainable propulsive efficiencies are: 0.69, 0.67, 0.67 and 0.66 versus 0.68, 0.66, 0.66 and 0.65 7 at 10 km and 20 km respectively. Whereas the ramjet propulsive efficiencies are: 1, 0.94, 0.92 and 0.91 versus 1, 1, 0.99 and 0.97 at 10 km and 20 km respectively; however, at 20 km and for 25% and 50% inlet air mass flow split the maximum propulsive efficiency is reached at 4.77 and 5.18 Mach respectively. What is also interesting to note from Figure 5.6 to Figure 5.8 is that the variations on thermal overall and propulsive efficiency for the turbojet show slight variations from 10 km to 20 km, whereas for the ramjet the changes are more pronounced. This effect is a direct result of the much higher attainable Mach numbers for the ramjet vs. the turbojet.

From Figure 5.9 and Figure 5.10 it is seen that the both the *f* and TSFC of either system decreases as the inlet air mass flow is increased. For a constant input of fuel this is an expected result. However, what is interesting to see is that the ramjet is not competitive enough with the turbojet until 75% inlet air mass flow is reached; below 75% (25% and 50%) the turbojet experiences lower *f* and *TSFC*. In addition, notwithstanding the changes of inlet air mass flow, the small change in temperature from 10 km 223 K to 20 km 216K has very little impact on the variation of *f*, which is completely independent of the free stream pressure and strongly dependent on the maximum temperature of the cycle; this effect is also observed on *TSFC*. For the turbojet the attainable *f* are: 0.103, 0.067, 0.056 and 0.05 versus 0.01, 0.066, 0.055 and 0.049 at 10 km and 20 km respectively. Whereas the ramjet *f* are: 0.1, 0.05, 0.033 and 0.025 versus 0.064, 0.032, 0.021 and 0.016 at 10 km and 20 km respectively. Here, we also see that the difference in altitude for the turbojet has very little impact on the *f*, whereas the ramjet experiences a significant decrease on *f* for an increase in altitude from 10 km to 20 km. When examining TSFC, the turbojet attains values of: 1.11e-04, 7.64e-05,

6.45e-05 and 5.85e-05 versus 1.06e-04, 7.34e-05, 6.23e-05 and 5.67e-05 at altitudes of 10 km and 20 km respectively. Whereas the ramjet TSFC values are:1.76e-04, 1.04e-04, 7.36e-05 and 5.70e-05 versus 1.74e-04, 1.03e-04, 7.33e-05 and 5.69e-05 at 10 km and 20 km respectively. Interestingly, it is observed that for the turbojet the TSFC slightly decreases for an increase in altitude from 10 km to 20 km and therefore more fuel efficient, however, the ramjet values of TSFC are extremely close to each other. Therefore, with just an increase in altitude the ramjet remains static in terms of fuel efficiency to thrust output however has an advantage of a higher Mach number.

Figure 5.11 also shows that as the inlet air mass flow to either system is increased the $I_a\ (s)$ decreases. This occurs as a consequence of the specific thrust; whereas the air mass flow increases the specific thrust decreases and therefore, so does the I_a. In general, the ramjet indicates higher attainable I_a at Mach 2 than the turbojet. In addition, the variations of I_a for the turbojet are modest between 10 km and 20 km, whereas the ramjet variations are slightly more pronounced. The turbojet attains specific impulse values of: 95, 90, 88 and 87 versus 96, 91, 90 and 89 at altitudes of 10 km and 20 km respectively. Whereas the ramjet specific impulse values are: 58, 49, 46 and 45 versus 38, 32, 30 and 29 at 10 km and 20 km respectively. However, for a value of 45s and at an altitude of 20 km the ramjet achieves Mach numbers of: 5.07, 4.87, 4.79 and 4.75. Therefore, for the same value of specific impulse, the ramjet is able to reach higher Mach numbers as the altitude increases.

In general, Figure 5.12 and Figure 5.13 illustrate that as the inlet air mass flow is increased to either system, the thrust and power also increases. At a Mach number of 2 the ramjet indicates improved thrust over the turbojet for an inlet mass flow above 25%. However, it is also clearly seen that as the altitude increases from 10 km to 20 km the thrust output decreases from both systems. The turbojet achieves maximum thrust values of: 35, 65, 95 and 126 versus 7, 14, 20 and 27 kN at 10 km and 20 km respectively; a decrease of approximately 4 to 5 fold for an increase in altitude. Whereas the ramjet attains thrust values of: 39, 66, 93 and 120 versus 6, 11, 15 and 19 kN at 10 km and 20 km respectively; a decrease of approximately 6 fold for an increase of altitude. However, the maximum attainable thrust for the ramjet at 10 km are: 50, 88, 126 and 165 at Mach numbers of 3.05, 2.96, 2.99 and 2.92 respectively. Whereas at 20 km the maximum thrust values for the ramjet are: 12, 21, 30 and 39 for Mach number of 3.29, 3.18, 3.16 and 3.12 respectively.

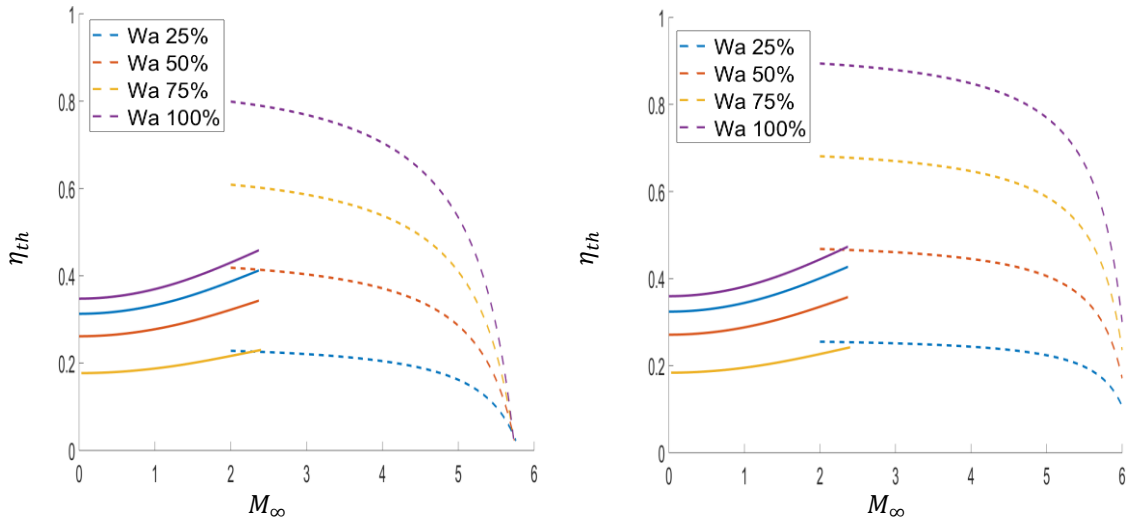

Figure 5.6: $\boldsymbol{\eta_{th}}$ for variations of inlet air mass flow at 10 km (a) and 20 km (b) for turboramjet engine as a function of $\boldsymbol{M_\infty}$.

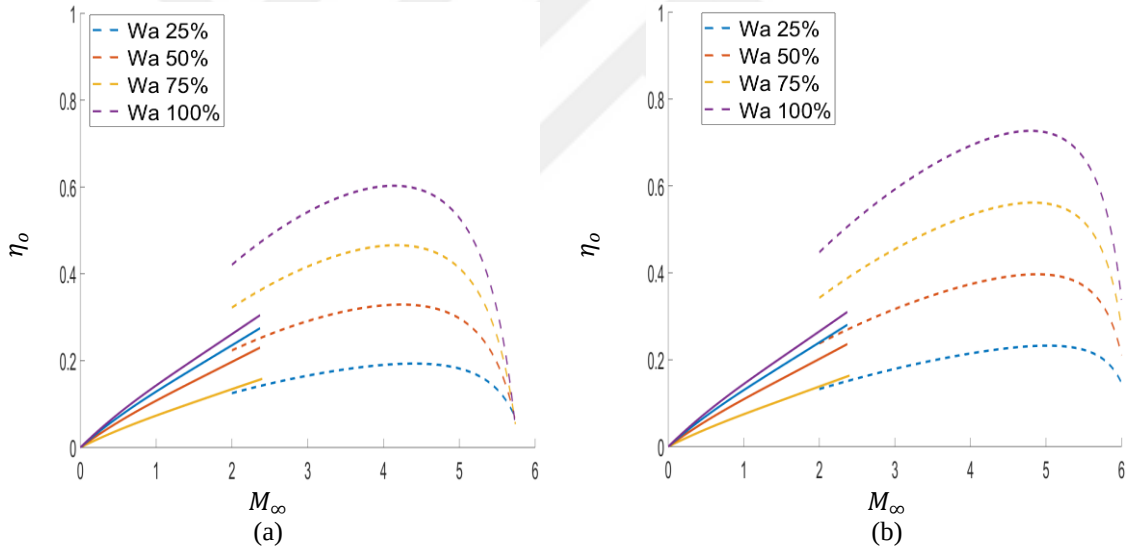

Figure 5.7: $\boldsymbol{\eta_0}$ for variations of inlet air mass flow at 10 km (a) and 20 km (b) for turboramjet engine as a function of $\boldsymbol{M_\infty}$.

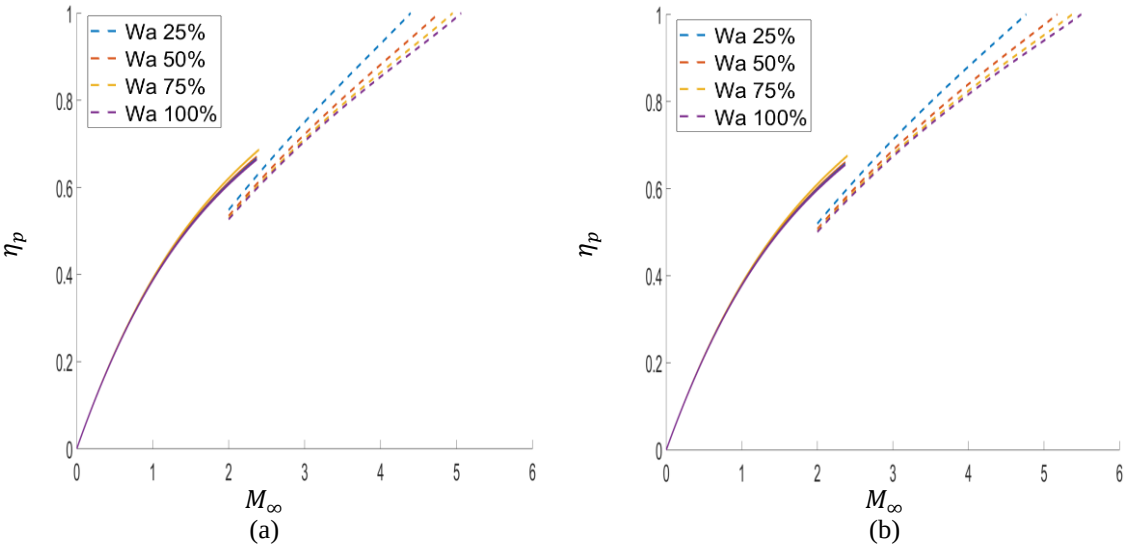

Figure 5.8: $\boldsymbol{\eta_p}$ for variations of inlet air mass at 10 km (a) and 20 km (b) flow for turboramjet engine as a function of $\boldsymbol{M_\infty}$.

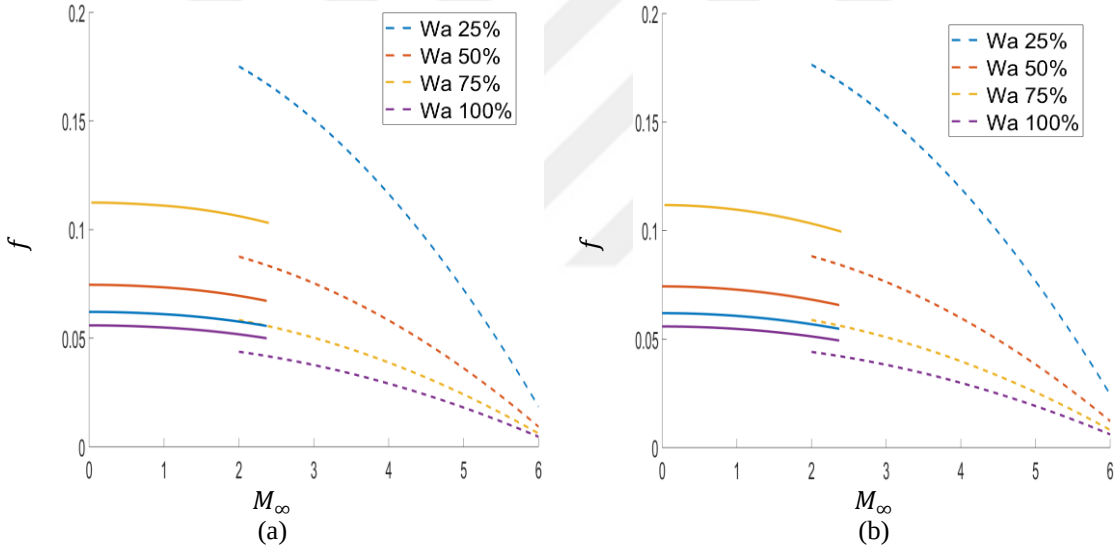

Figure 5.9: f for variations of inlet air mass flow at 10 km (a) and 20 km (b) for turboramjet engine as a function of $\boldsymbol{M_\infty}$.

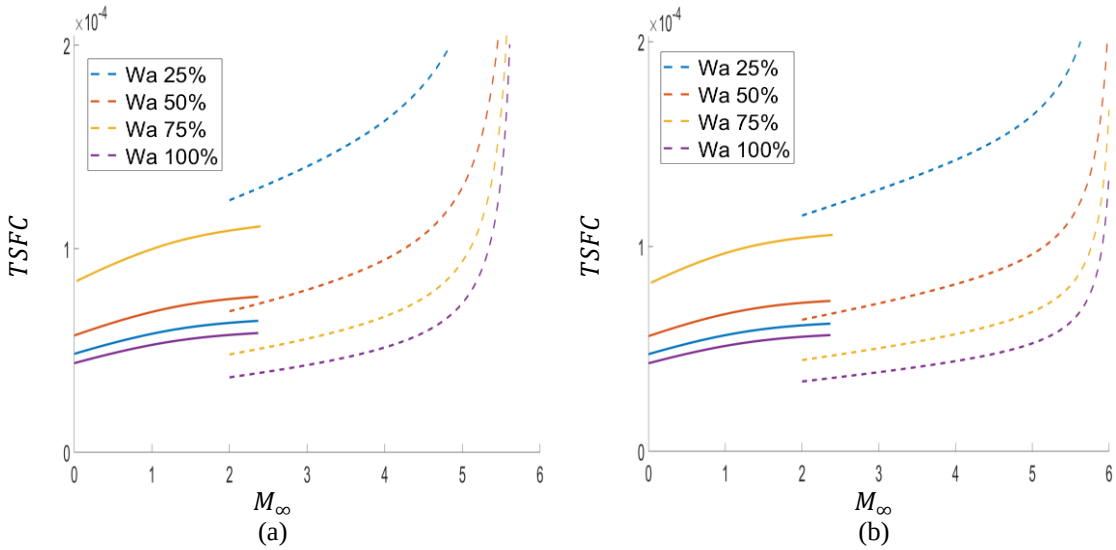

Figure 5.10: *TSFC* for variations of inlet air mass flow at 10 km (a) and 20 km (b) for turboramjet engine as a function of $\boldsymbol{M_\infty}$.

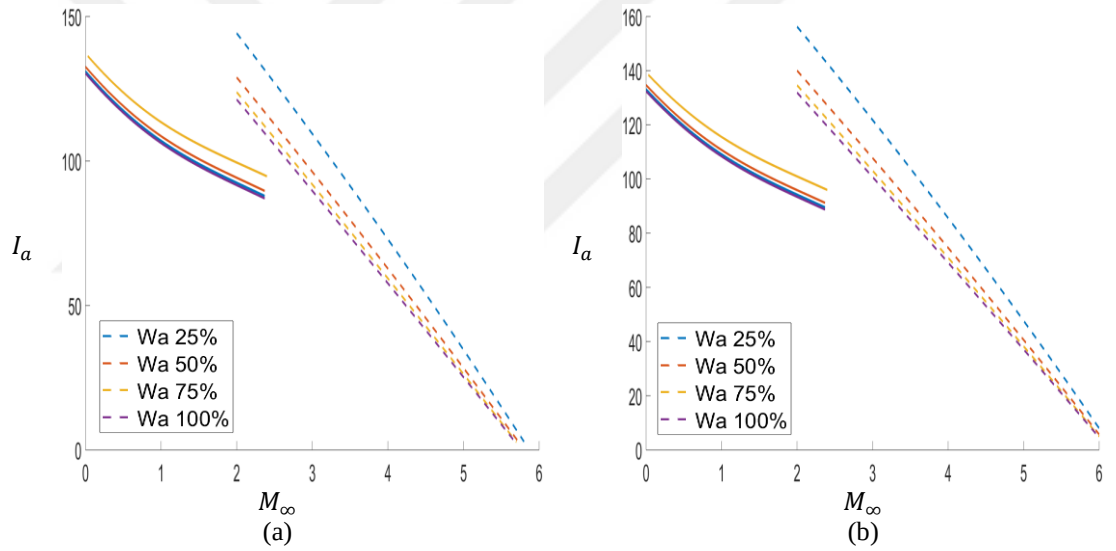

Figure 5.11: $\boldsymbol{I_a}$ for variations of inlet air mass flow at 10 km (a) and 20 km (b) for turboramjet engine as a function of $\boldsymbol{M_\infty}$.

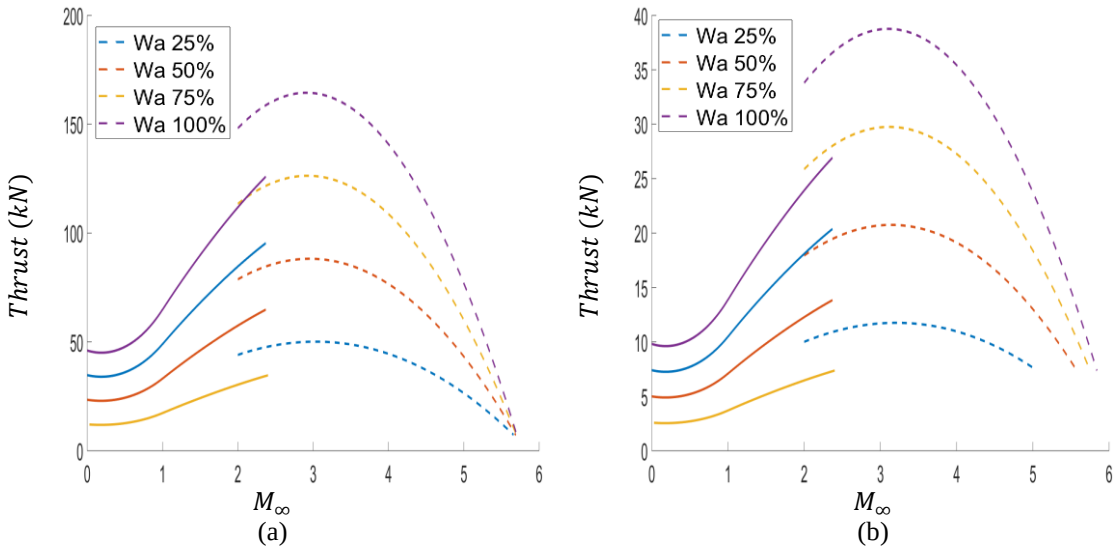

Figure 5.12: *Thrust* for variations of inlet air mass flow at 10 km (a) and 20 km (b) for turboramjet engine as a function of $\boldsymbol{M_\infty}$.

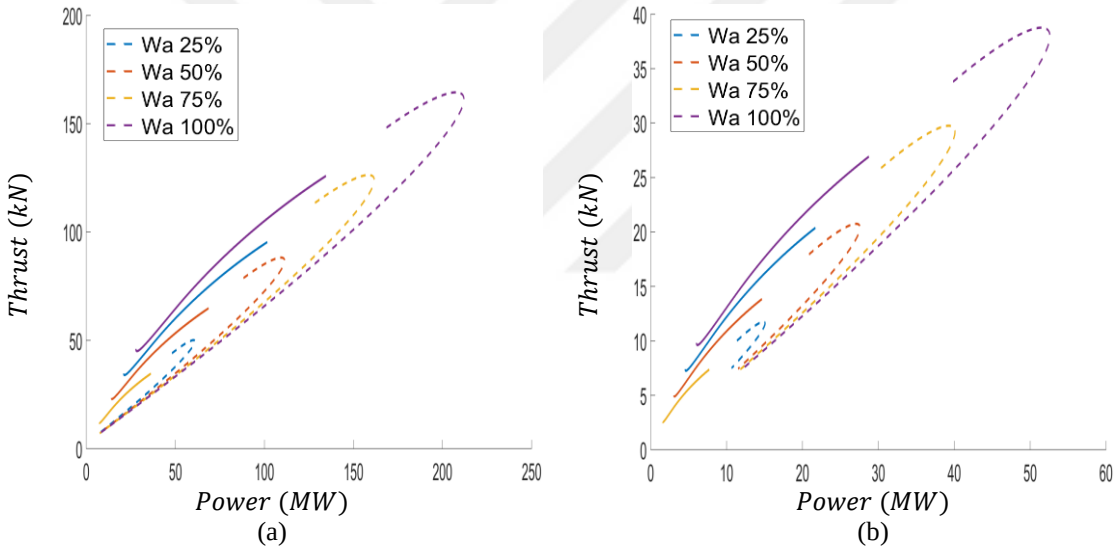

Figure 5.13: *Thrust* for variations of inlet air mass flow at 10 km (a) and 20 km (b) for turboramjet engine as a function of ***Power***.

From Figure 5.14 it can clearly be seen that at all Mach numbers the ramjet is far more advantageous than the turbojet and especially at 20 km. The specific volume of the turbojet at 10 km and 20 km is 10 and 48 (m^3/kg) respectively; whereas the ramjet values at 10 km and 20 km are 6 and 20 (m^3/kg) respectively. Therefore, the specific volume is 1.7 and 2.4 times larger than that of the ramjet at each altitude respectively; therefore, the trade off in weight is unequivocal. In addition, due to a weak dependency, the variation of inlet air mass flow has very little impact on the specific volume of the exhaust nozzle for both the turbojet and ramjet.

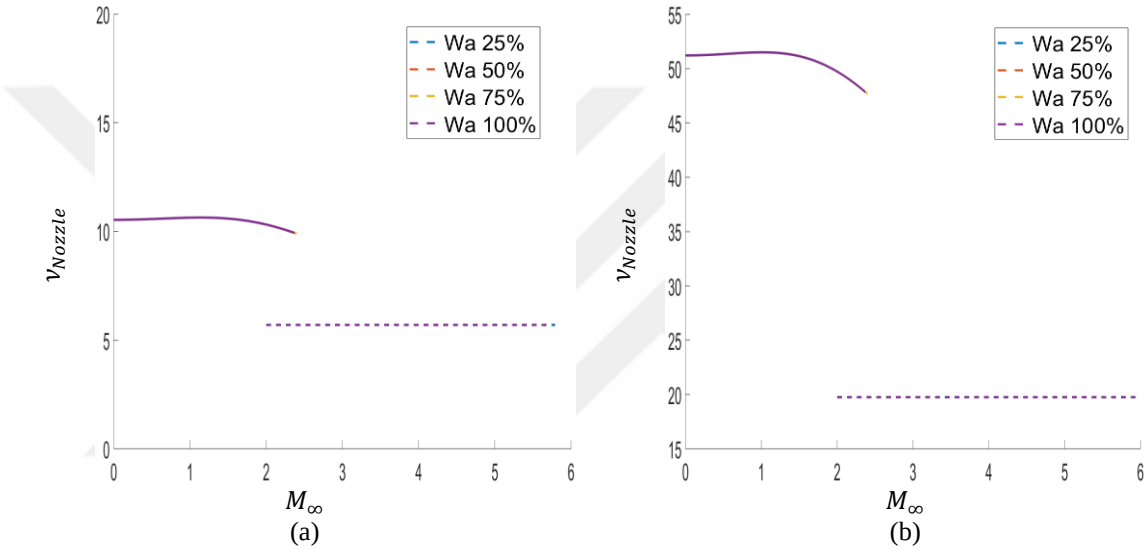

Figure 5.14: $\boldsymbol{v_{Nozzle}}$ for variations of inlet air mass flow at 10 km (a) and 20 km (b) for turboramjet engine as a function of $\boldsymbol{M_\infty}$.

5.3 Prospects of Turboramjets

The performace of the turboramjet engine under a maximum power objective function in dual mode operation for variation of altitude and inlet air mass flow split as a function of Mach number. Under dual mode operation the turbojet engine AB were taken to be in the operative state. The results show that the turbojet operation exhibits a Mach number limitation of 2.51 beyond an altitude of 12 km, whereas the ramjet limitation is in terms of TSFC where beyond a value of 5.694 e-05 at a Mach number of 5.26 and altitude of 20 km operation becomes unrealistic. Moreover, as the split of inlet air mass flow to the ramjet was increased beyond 50% the advantage in terms of η_{th}, η_o, f, TSFC, I_a, thrust and v_{NOZZLE} far supersede that of the turbojet with an AB.

The ramjet experiences a significant decrease on f for an increase in altitude from 10 km to 20 km and becomes more fuel efficient than the turbojet with an AB at inlet air mass flow splits above 75%. Furthermore, the ramjet is more economical at 20 km than at 10 km operation where for the same value of TSFC a higher Mach number can be attained 5.26 vs. 4.4 however at the expense of lower than maximum thrust. Where maximum thrust for the ramjet occurs at lower Mach number values: 165 kN at 2.92 Mach vs. 39 kN at 3.12 Mach at 10 km and 20 km respectively. Likewise, for the same value of specific impulse (45 s), the ramjet is able to reach higher Mach numbers (4.4 vs. 4.75 at 100% inlet air mass flow split) as the altitude increases, whereas for the turbojet the I_a exhibits minimal change. In addition, the specific volume of the turbojet with an AB is 1.7 and 2.4 times larger than that of the ramjet for an increase in altitude from 10 km to 20 km; therefore, the trade off in weight is indisputable. Moreover, it is seen that the ramjet can commence operation at a Mach number of 2 and begin diverting the inlet mass flow rate from the turbojet with an AB to the ramjet while still remaining competitive with the turbojet with an AB.

6. CONCLUDING REMARKS AND FUTURE WORKS

6.1 Conclusion: Turbojet without and with an AB, Ramjet and Turboramjet Engines

An irreversible Brayton cycle, which included the diffuser and exit nozzle, was assessed for various engine configurations: Turbojet without and with an AB, Ramjet and finally the TBCC Turboramjet. Where for all the engine configurations the exit nozzle was assumed to be fully expanded.

The turbojet without an AB was examined using newly defined performance parameters (PLOS, EPLOS and CBSF) and combined with the available objective functions of maximum power, maximum power density, ECOP and ECOL. In addition, the variable effects on the optimal operating conditions of MP, MPD, MECOP and MECOL for these parameters were shown and thier impact on engine performance. An advantage in the design of a turbojet engine without an AB is observed for efficiencies of $\eta_c \geq 85\%$ with respect to PLOS, Power, NG and shaft force; and for varying M_∞, an optimum range of $\theta_c = 2 \pm 0.4$ is obtained. In addition for a specified θ_c design point, an operational Mach number preference range of 1.4 < M_∞ <1.6 attaines higher thrust outputs while satisfing environmental responsibilities. Under MECOL and MECOP higher compression and temperature ratios as high as 30 ($\theta_c \approx 2.64$) and $\alpha = 7$ respectively become favorable, and leads to a reduction of burner, turbine and nozzle size and lower TSCF for a compromise in a larger compressor.

The turbojet with and AB was evaluated on a maximum power (MP), PLOS and EPLOS basis and compared to the turbojet without an AB. Although the turbojet with an AB showed a significant advantage of increased thrust at all altitudes and Mach numbers, it is only beyond a Mach number of unity does the thermal efficiency of the engine configuration portray higher relevance. It was also seen, that at a given altitude, the turbojet with an AB attained the same power and thrust output as the turbojet without an AB but at a much lower Mach number.

The ramjet was only investigated on a maximum power (MP) basis and compared to the turbojet without and with and AB. The performance of the ramjet was only realized at Mach numbers between 4-5, especially in terms of propulsive efficiency and exhibits a disadvantage due to a much higher fuel consumption in comparison to the turbojet with and without an AB.

Similar to the ramjet, the performace of the turboramjet engine was assessed using the maximum power (MP) objective function in dual mode operation for variations in altitude and inlet air mass flow as a function of Mach number. The operation of the turbojet with an AB and ramjet exhibit limitations due to the restraints of thermal efficiency and TSFC respectively. The turbojet engine operation with an AB is favorable upto to an altitude of 8 km with a maximum attainable Mach number of 2.31. Beyond 8 km the turbojet exhaust nozzle specific volume cannot compete with that of the ramjet. On the other hand, the ramjet becomes much more efficient and beneficial when the split of inlet air mass flow is 50% and higher. In addition, the ramjet is more economical at 20 km operation especially in terms of TSFC and can commence operation at a Mach number of 2 while still being competitive to the turbojet with an AB.

6.2 Towards the Future

As all the engine configurations were evaluated for a fully expanded exit nozzle, the next step would be to evaluate the engine configurations under a chocked or unchoked exit nozzle condition.

The engine configurations were strictly evaluated based on their thermodynamic propulsion cycles and equations. Unfortunately, using this type of assessment, the interconnectivity and interdependency between engine components is lost. As previously mentioned, the effect of the LHV on the maximum temperature (T_{MAX}) of the cycle is not known. In most cases a fixed inlet air mass flow is assumed and T_{MAX} is calculated. However, the engine models consider a variable inlet air mass flow due to the change of free stream Mach number and the *f* equation shows no connectivity to such a change unless forced. In addition, the f has no impact on the gas generator speed (NG), where in reality the two are very much strogly interdependent.

The driving factor of any engine is the change in fuel flow. An increase in fuel raises pressures, temperatures, NG and air flow; the opposite is also true. Therefore, for a true engine performance evaluation the interdependency of: ambient conditions (free stream pressure, temperature and Mach number); inlet air mass flow; compressor, combustion chamber, turbine and exit nozzle inlet and exit pressures and temperatures; fuel flow; and gas generator speed must influence each other. However, due to the limitation of the propulsion equations, this form of interconnectivity cannot be seen; unless updated. On the other hand, a manner in which such an effect can be observed is to include engine performance tables where all the above mentioned interdependencies are evaluated by the engine manufacturer.

Nevertheless, the propulsion equations and the objective functions are tools that can be used by the aviation industry as a guide for the design of ‘a new generation of intelligent engines’ with adaptive engine components and cycles which are economically and ecologically favourable; an engine that can assess its current operating state and morph its internal physical components to work under the most efficient regime.

REFERENCES

[1] **Url-1** <*https://en.wikipedia.org/wiki/Brayton_cycle#Early_gas_turbine_history*>, date retrieved 01.08.2022.

[2] **El-Sayed, A. F.** (2017). Aircraft Propulsion and Gas Turbine Engines, Boca Raton, FL, CRC Press.

[3] **Url-2** <*http://ffden-2.phys.uaf.edu/webproj/212_spring_2014/Joseph_Ofeldt/Joseph%20_ofeldt(2)/basic_thoery.html*>, date retrieved 01.08.2022.

[4] **Starr, F.** (2019). A Comentary on Future Developments in Aircraft Design, *Journal of Aeronautical History*, Paper No. 2019/01.

[5] **Whittle, F.** (1928). Future Developments in Aircraft Design (Thesis), Royal Air Foce, Cranwell, United Kingdom. Retrieved from Royal Aeronautical Society: *https://www.aerosociety.com/media/11404/paper-2019-01-starr-whittle-thesis.pdf*, date retrieved: 01.08.2022.

[6] **Whittle, F.** (1930). British Patent No. 347,206 Newport, South Wales, United Kingdom Intellectual Property Office.

[7] **Çengel, Y.A. and Boles, M.A.** (2015). Thermodynamics: An Engineering Approach, Eighth Edition, New York, NY, McGraw-Hill Education.

[8] **European Commission** (2019). Energy, Climate change, Environment, Climate Action, EU Action, Transport emissions. *https://ec.europa.eu/clima/policies/transport/aviation_en#tab-0-0*, date retrieved: 01.08.2019.

[9] **Federal Aviation Administration** (2005). Office of Environment and Energy, Aviation and Emissions a Primer.

[10] **Lee D.S., Fahey D.W., Forster P.M., Newton P.J., Wit R.C.N., Lim L.L., et al.** (2009). Aviation and global climate change in the 21st century. Atmos Environ;43:3520–37.

[11] **Angulo-Brown F.** (1991). An ecological optimization criterion for finite-time heat engines. J Appl Phys; 69:7465–69.

[12] **Şöhret Y.** (2017). Defining the Ecological Coefficient of Performance for an Aircraft Propulsion System, International *Journal Turbo Jet Engines*.

[13] **Cheng C. and Chen C.** (1997). The ecological optimization of an irreversible Carnot heat engine, *Journal of Physics* D: Applied Physics, 30 1602–1609.

[14] **Cheng C. and Chen C.** (1999). Ecological optimization of an irreversible Brayton heat engine, *Journal of Physics* D: Applied Physics, 32 350–357.

[15] **Blank D.** (1999). Analysis of a combined law power-optimized open Joule–Brayton heat-engine cycle with a finite interactive heat source, *Journal of Physics* D: Applied Physics 32 769–776.

[16] **Üst Y., Sahin B., and Kodal A.** (2005). Ecological coefficient of performance (ECOP) optimization for generalized irreversible Carnot heat engines, *Journal of the Energy Institute*, VOL 78 NO 3 145.

[17] **Üst Y., Sahin B., Kodal A. and Akçay I.** (2006). Ecological coefficient of performance analysis and optimization of an irreversible Regenerative-Brayton heat engine, Applied Energy, 83 558–572.

[18] **Üst Y., Sahin B., and Kodal A.** (2006). Performance analysis of an irreversible Brayton heat engine based on ecological coefficient of performance criterion, International *Journal of Thermal Sciences*, 45 (2006) 94–101.

[19] **Oliveira S., Scalon V., and Repinaldo V.** (2015). Ecological optimization of an irreversible Brayton cycle with regeneration, inter-cooling and reheating, Applied Mathematical Modeling, 39 6830–6844.

[20] **Haseli Y.** (2016). Efficiency of irreversible Brayton cycles at minimum entropy generation, Applied Mathematical Modelling, 40 8366–8376.

[21] **Gonca G.** (2017). Exergetic and ecological performance analyses of a gas turbine system with two intercoolers and two re-heaters, Energy 124 579e588.

[22] **Balli O.** (2017). Exergy modeling for evaluating sustainability level of a high by-pass turbofan engine used on commercial aircrafts, Applied Thermal Engineering 123 138–155.

[23] **Durmusoglu Y. and Üst Y.** (2014). Thermodynamic optimization of an irreversible regenerative closed Brayton cycle based on thermoeconomic performance criterion, Applied Mathematical Modelling 38 5174–5186.

[24] **Sadatsakkak S. A., Ahmadi M. H. and Ahmadi M. A.** (2015). Thermodynamic and thermo-economic analysis and optimization of an irreversible regenerative closed Brayton cycle, Energy Conversion and Management 94 124–129.

[25] **Açıkkalp E.** (2017). Performance analysis of irreversible solid oxide fuel cell – Brayton heat engine with ecological based thermo-environmental criterion, Energy Conversion and Management 148 279–286.

[26] **Gonca G.** (2018). The effects of turbine design parameters on the thermo-ecologic performance of a regenerated gas turbine running with different fuel kinds, Applied Thermal Engineering 137 419–429.

[27] **Saravanamutto H.I.H., Rogers G.F.C. and Cohen H.** (2009). Gas Turbine Theory, 5th ed., Pearson Prentice Hall.

[28] **Çengel Y.A. and Boles M.A.** (2012). Thermodynamics: An Engineering Approach, 7th ed., McGraw-Hill Education, New York,.NY.

[29] **Pasquale M. S.** (2017). Theory of Aerospace Propulsion, 2nd Edition, Butterworth Heinemann, Elsevier Aerospace Engineering Series.

[30] **Airbus** (2002). Flight Operations Support & Line Assistance - Getting to Grips with Aircraft Performance, Customer Services, France..

[31] **Rau S. S.** (2009). Engineering Optimization: Theory and Practice, Fourth Edition, John Wiley and Sons Inc..

[32] **Guest Editors: Tsai J-F, Carlsson J. G., Ge D., Hu Y-C, and Shi J.** (2012). Mathematical Problems in Engineering: Optimization Theory, Methods and Applications in Engineering, Hindawi Publishing Corporation.

[33] **Farokhi S.** (2014). Aircraft Propulsion, Second Edition, Aerospace Engineering Department, University of Kansas, USA, Wiley.

[34] **Najjar Y.S.H., Balawneh I.A.I.** (2015). Optimization of Gas Turbines for Sustainable Turbojet Propulsion. Propulsion and Power Research, 4:114–21.

[35] **Najjar Y.S.H. and Abu Eisheh H.** (2016). Exergy Analysis and Greening Performance Carpets for Turbojet Engines, *Journal of Engineering Thermophysics*, Vol. 25, No. 2, pp. 262–274.

[36] **Najjar Y.S.H. And Al-Sharif S.F.** (2006). Thermodynamic Optimization of the Turbofan Cycle, *Journal of Aircraft Engineering and Aerospace Technology*, *An International Journal*, Vol.78, No. 6, pp. 467-480..

[37] **Najjar Y.S.H. And Balawneh I.A.A.** (2015). Optimization of Gas Turbines for Sustainable Turbojet Propulsion, Propulsion and Power Research, 4(2): 114-121.

[38] **De Sa A. and Al Zubaidy S.** (2011). Gas turbine performance at varying ambient temperature. Applied Thermal Engineering, 31:2735-39.

[39] **Badami M., Nuccio P. and Signoretto A.** (2013). Experimental and numerical analysis of a small-scale turbojet engine. Energy Conversion and Management, 76:225–33.

[40] **Salpingidou C., Vlahostergios Z., Misirlis D., Donnerhack S., Flouros M., Goulas A. And Yakinthos K.** (2017). Thermodynamic analysis of recuperative gas turbines and aero engines. Applied Thermal Engineering, 124:250–60.

[41] **Wang H., Li X-S., Ren X., Gu C-W. and Ji X-X.** (2017). A thermodynamic-cycle performance analysis method and application on a three-shaft gas turbine. Applied Thermal Engineering, 127:465–72.

[42] **Guha A.** (2001). Optimization of aero gas turbine engines, *The Aeronautical Journal*, July.

[43] **Guha A.** (2001). Optimum Fan Pressure Ratio for Bypass Engines with Separate or Mixed Exhaust Streams, *Journal of Propulsion and Power*, Vol. 17, No. 5, September–October.

[44] **Patel V., Savsani V. and Mudgal A.** (2018). Efficiency, thrust, and fuel consumption optimization of a subsonic/sonic turbojet engine. Energy, 144:992-1002.

[45] **Kodal A.** (1999). Maximum Power Density Analysis for Irreversible Combined Carnot Cycle. *Journal of Physics D*: Applied Physics, 32:2958-63.

[46] **Chen L., Wang J. and Sun F.** (2011). Performance Comparison of an Endoreversible Closed Variable-Temperature Heat Reservoir Intercooled Regenerated Brayton Cycle Under Maximum Power and Maximum Power Density Conditions. International *Journal of Sustainable Energy*, 30:149–68.

[47] **Chen L., Lin J., Sun F. and Wu, C.** (1998). Efficiency of Atkinson Engine at Maximum Power Density. Energy Conversion and Management 1998, 39:337-41.

[48] **Gonca G., Şahin B., Üst Y. and Parlak A.** (2015). Comprehensive Performance Analyses and Optimization of the Irreversible Thermodynamic Cycle Engines (TCE) Under Maximum Power (MP) and Maximum Power Density (MPD) Conditions. Applied Thermal Engineering, 85:9-20.

[49] **Gonca G.** (2016). Performance Analysis and Optimization of İrreversible Dual–Atkinson Cycle Engine (DACE) with Heat Transfer Effects Under Maximum Power and Maximum Power Density Conditions. Applied Mathematical Modelling, 40:6725–36.

[50] **Al-Sarkhi A., Akash B.A., Jaber J.O., Mohsen M.S. and Abu-Nada E.** (2002). Efficiency of Miller engine at Maximum Power Density. Int. Comm. Heat Mass Transfer, 29:1158-67.

[51] **Cheng K., Qin J.,' Sun H., Dang C., Zhang S., Liu X. And Bao W.** (2019). Performance assessment of a closed-recuperative-Brayton-cycle based integrated system for power generation and engine cooling of hypersonic vehicle, Aerospace Science and Technology, Volume 87, April, Pages 278-288.

[52] **Fawal S. and Kodal A.** (2019) "Comparative performance analysis of various optimization functions for an irreversible Brayton cycle applicable to turbojet engines", Energy Conversion and Management, 199 111976.

[53] **Angulo-Brown F.** (1991). An ecological optimization criterion for finite-time heat engines. J Appl Phys; 69:7465–69.

[54] **Şöhret Y.** (2017). Defining the Ecological Coefficient of Performance for an Aircraft Propulsion System, *International Journal Turbo Jet Engines*.

[55] **Cheng C. and Chen C.** (1997). The ecological optimization of an irreversible Carnot heat engine, *Journal of Physics* D: Applied Physics, 30 1602–1609.

[56] **Cheng C. and Chen C.** (1999). Ecological optimization of an irreversible Brayton heat engine, *Journal of Physics* D: Applied Physics, 32 350–357.

[57] **Blank D.** (1999). Analysis of a combined law power-optimized open Joule–Brayton heat-engine cycle with a finite interactive heat source, *Journal of Physics* D: Applied Physics 32 769–776.

[58] **Üst Y., Şahin B. and Kodal A.** (2005). Ecological coefficient of performance (ECOP) optimization for generalized irreversible Carnot heat engines, *Journal of the Energy Institute*, VOL 78 NO 3 145.

[59] **Üst Y., Şahin B., Kodal A. and Akçay I.** (2006). Ecological coefficient of performance analysis and optimization of an irreversible Regenerative-Brayton heat engine, Applied Energy, 83 558–572.

[60] **Üst Y., Şahin B. and Kodal A.** (2006). Performance analysis of an irreversible Brayton heat engine based on ecological coefficient of performance criterion, *International Journal of Thermal Sciences*, 45 94–101.

[61] **Oliveira S., Scalon V. and Repinaldo V.** (2015). Ecological optimization of an irreversible Brayton cycle with regeneration, inter-cooling and reheating, Applied Mathematical Modeling, 39 6830–6844.

[62] **Haseli Y.** (2016). Efficiency of irreversible Brayton cycles at minimum entropy generation, Applied Mathematical Modelling, 40 8366–8376.

[63] **Gonca G.** (2017). Exergetic and ecological performance analyses of a gas turbine system with two intercoolers and two re-heaters, Energy 124 579e588.

[64] **Balli O.** (2017). Exergy modeling for evaluating sustainability level of a high by-pass turbofan engine used on commercial aircrafts, Applied Thermal Engineering 123 138–155.

[65] **Sadatsakkak S. A., Ahmadi M. H. and Ahmadi M. A.** (2015). Thermodynamic and thermo-economic analysis and optimization of an irreversible regenerative closed Brayton cycle, Energy Conversion and Management 94 124–129.

[66] **Açıkkalp E.** (2017). Performance analysis of irreversible solid oxide fuel cell – Brayton heat engine with ecological based thermo-environmental criterion, Energy Conversion and Management 148 279–286.

[67] **Gonca G.** (2018). The effects of turbine design parameters on the thermo-ecologic performance of a regenerated gas turbine running with different fuel kinds, Applied Thermal Engineering 137 419–429.

[68] **Zenkner S., Trost M., Beceker R. and Voß C.** (2019). Preliminary engine design and inlet optimization of the MULDICON concept, Aerospace Science and Technology, Volume 93, October, 105318.

[69] **Otter J.J., Stańkowski T., Robinson M. and MacManus D.G.** (2019) Installation aerodynamics of civil aero-engine exhaust systems, Aerospace Science and Technology, Volume 89, June, Pages 345-355.

[70] **Chen M., Zhang J. and Tang H.** (2018). Interval analysis of the standard of adaptive cycle engine component performance deviation, Aerospace Science and Technology, Volume 81, October, Pages 179-191.

[71] **El-Sayed A.F.** (2017). Aircraft Propulsion and Gas Turbine Engines, Second Edition, CRC Press.

[72] **El-Sayed A.F.** (2016). Fundamentals of Aircraft and Rocket propulsion, Department of Mechanical Engineering, Zagazig University, Zagazig, Egypt, Springer-Verlag London.

[73] **Mattingly J. D.** (1996). Elements of Gas Turbine Propulsion, TATA McGraw-Hill Edition.

[74] **Farokhi S.** (2014). Aircraft Propulsion, 2nd Edition, Wiley.

[75] **Şöhret Y., Ekici S. and Karakoç T. H.** (2017). Using Exergy for Performance Evaluation of a conceptual Ramjet Engine Burning Hydrgen Fuel, International *Journal of Hydrogen Energy*, XXX I-6.

[76] **Latypov A. F.** (2009). Exergy Analysis of Ramjet, Thermophysics and Aeromechanics, Vol. 16, No. 2.

[77] **Latypov A. F.** (2013). Mehtod for Estimating the Ramjet Specific Impulse, Thermophysics and Aeromechanics, 2013, Vol. 20, No. 5.

[78] **Ayaz S. K. and Altuntaş Ö.** (2017). Assessment of Ramjet Engine for Different Mach Numbers, International Jurnal of Sustainable Aviation, Vol. 3, No. 4.

[79] **Moorhouse D. J.** (2003). Proposed System-Level Multidisciplinary Analysis Technique Based on Exergy Methods, *Journal of Aircraft*, Vol. 40, No. 1, January – February.

[80] **Moorhouse D. J. and Suchomel C. F.** (2001). Exergy Method Applied to the Hypersonic ehicle Challenge, AIAA paper # 2001 – 3063.

[81] **Moorhouse D. J., Hoke C. M. and Prendergast J. P.** (2002). Thermal Analysis of Hypersonic Inlet Flow with Exergy-Based Design Methods, International *Journal of Applied Thermpdynamics*, vol. 5 (No. 4), pp. 161-168, December.

[82] **Marley C. D. and Riggins D. W.** (2011). The Thermodynamics of Exergy Losses and Thrust Production in Gas Turbine Engines, AIAA, 2011-6130.

[83] **Ispir A. C., Gonçalves P., Kurban E. And Saraçoğlu B. H.** (2020). Thermodynamic Efficency Analysis and Investigation of Exergic Efficiencies of STRATOFLY MR3 Aircraft Propulsion Plant, AIAA SciTech Forum, 6-10 January.

[84] **Ehyaei M. A., Anjiridezfuli A. And Rosen M. A.** (2013) Exergic Analysis of an Aircraft Turbojet Engine with an Afterburner, Thermal Science, Vol. 17, No. 4, pp 1181-1194.

[85] **Roth B. and Marvis D.** (2000). A Method for Propulsion Technology Impact Evaluation via Thermodynamic Work Potential, AIAA 2000-4854.

[86] **Camberos J. A. And Moorhouse D. J.** (2011) Exergy Analysis and Design Optimization for Aerospace Vehicles and Systems, AIAA, Vol. 238, Progress in Astronautics and Aeronautics.

[87] **Hayes D., Lone M., Whidborne J. F., Camberos J. and Coetzee E.** (2017). Adopting exergy analysis for use in aerospace, Progress in Aerospace Sciences xxx 1–22.

[88] **Riggins D. W. and Taylor T.** (2006). Methodology for Performance Analysis of Aerospace Vehicles Using the Laws of Thermodynamics, *JOURNAL OF AIRCRAFT*, Vol. 43, No. 4, July–August.

[89] **Balli Ö.** (2017). Advanced exergy analyses to evaluate the performance of a military aircraft turbojet engine (TJE) with afterburner system: Splitting exergy destruction into unavoidable/avoidable and endogenous/exogenous, Applied Thermal Engineering 111 152–169.

[90] **Balli Ö.** (2017). Exergetic, Exergoeconomic, Sustainability and Environmental Damage Cost Analyses of J85 Turbojet Engine with Afterburner, International *Journal of Turbo & Jet Engines*.

[91] **Balli Ö.** (2014). Afterburning effect on the energetic and exergetic performance of an experimental turbojet engine (TJE), *International Journal of Exergy*, January.

[92] **Akkaya A.V., Şahin B. and Erdem H.H.** (2007). Exergetic performance coefficient analysis of a simple fuel cell system, International *Journal of Hydrogen Energy* 32 4600 – 4609.

[93] **Yüksel B., Balli Ö., Günerhan H. and Hepbaslı A.** (2020). Comparative Performance Metric Assessment of a Military Turbojet Engine Utilizing Hydrogen and Kerosene Fuels Through Advanced Exergy Analysis Method, Energies, 13, 1205.

[94] **Balli Ö., Adak İ. and Güneş S.** (2017). Afterburner Effect on the Energetic and Exergetic Performance of J79-GE-17 Engine with Afterburner System used on F-4 Phantom II Aircrafts, International Symposium on Sustainable Aviation (ISSA-2017), Kiev, Ukraine, 10 – 13 September.

[95] **Akkaya A.V., Şahin B., Erdem H.H.** (2008). An analysis of SOFC/GT CHP system based on exergetic performance criteria, International *Journal of Hydrogen Energy* 33 2566 – 2577.

[96] **Bastani M., Jafari R. and Ghasemi H.** (2015). Exergy Analysis of an Aircraft Turbojet Engine, International *Journal of Engineering Sciences & Research Technology*, ISSN: 2277-9655, April.

[97] **Yüksel B., Balli Ö., Günerhan H. and Hepbaslı A.** (2020). Assessing Exergy-Based Economic and Sustainability Analyses of a Military Gas Turbine Engine Fueled with Various Fuels, Energies, 13, 3823.

[98] **Niknamian S.** (2020). The optimization of a jet turbojet engine by PSO and searching algorithms, Social Science Research Network, https://ssrn.com/abstract=3503740, January.

[99] **Sürer M.G. and Arat H.T.** (2018). A Critical Review of Exergy Studies on Jet Engines, 16th International Conference on Clean Energy (ICCE-2018), May.

[100] **Dong Z., Li D., Wang Z. and Sun M.** (2018). A Review on Exergy Analysis of Aerospace Power Systems, Acta Astronautica, AA 7090, S0094-5765(18)31012-9, September.

[101] **Noori F., Gorji M., Kazemi A. and Nemati H.** (2015). Thermodynamic optimization of ideal turbojet with afterburner engines using non-dominated sorting genetic algorithm II, *Journal of. Aerospace Engineering*, Proc. IMechE Vol. 224 Part G, February.

[102] **Nasab M.R.A. and Ehyaei M.A.** (2019). Optimization of turbojet engine cycle with dual-purpose PSO algorithm, Mechanics & Industry 20, 604, March.

[103] **MIL-E-5007D** (1973) General Specification for Engines, Aircraft, Turbojet and Turbofan, Military Specification, Department of the Air Force, Wright-Paterson AFB, OH, September.

[104] **Keith T.G. and John J.E.** (2006).Gas Dynamics, Third Edition, Pearson, Prentice Hall, Upper Saddle River, NJ.

APPENDICES

APPENDIX A: Turbojet Engine Formulation Without AB

APPENDIX B: Turbojet Engine Formulation With AB

APPENDIX C: Ramjet Engine Formulation

APPENDIX D: Sample of Matlab Code

APPENDIX E: Frank Whittle 1931 Patent

APPENDIX A: Turbojet Engine Formulation Without AB

Given Inputs:	
$\Delta P_b = 0.96$	Pressure loss in combustion chamber
$\xi = 0.01$	Heat leak factor
$T_L = 200\ K$	Sink Temperature
$T_H = 2200\ K$	Source Temperature
$T_{03} = 1200$	Turbine Inlet Temperature (TIT)
$\eta_i = 0.93$	Intake Efficiency
$\eta_n = 0.95$	Nozzle Efficiency
$\eta_m = 0.99$	Transmission/Mechanical Efficiency
$\eta_b = 0.98$	Combustion Efficiency
$\eta_c = 0.87$	Compressor Efficiency
$\eta_t = 0.9$	Turbine Efficiency
$C_{pa} = 1.005\ KJ/kg - K$	Specific Heat of Air at Constant pressure
$C_{pg} = 1.148\ KJ/kg - K$	Specific Heat of Gases at Constant pressure
$\gamma_a = 1.005\ KJ/kg - K$	Specific Heat Ratio of Air
$\gamma_g = 1.005\ KJ/kg - K$	Specific Heat Ratio of Gases
$R_a = 287\ J/kg - K$	Gas Constant of Air
$D_{A1} = 0.8\ m$	Upstream Capture Diameter
$A_1 = \pi D_{A1}/4$	Upstream Capture Area
$Q_{LHV} = 43\ 000\ KJ$	Lower Heating Value of Fuel
$M = 0.5$	Mach Number
$g = 9.81\ m/s^2$	Acceleration due to Gravity
$\theta_c = \left(\frac{P_{02}}{P_{01}}\right)^{\frac{\gamma_c - 1}{\gamma_c}}$	Compressor Ratio Parameter
$\alpha = \frac{T_{t3}}{T_{t2}} = \theta_c^{\frac{\gamma_c - 1}{\gamma_c e_c}} = \frac{T_{02}}{T_a}$	Temperature Ratio Parameter
$L = \frac{c(P_{t2})^{-r}}{\sqrt{T_{t2}}} = \frac{c(PR)^{-r}}{\alpha} = \frac{c(\theta_c)^{-r}}{\alpha}$	Length of Combustion Chamber: $r = n - \frac{\gamma - 1}{\gamma}\ ; n = 1.8$ $r = 1.514285714$ $P_{t2} = 2.5$ $T_{t2} = 6$ $c = 165.6216832$
$a = \sqrt{\gamma T_a R_a}$ m/s	Inlet Speed of Sound
$C_a = Ma$ m/s	Inlet Velocity
$P_a\ (kPa)$	Inlet Air Pressure
$T_a\ (K)$	Inlet Air Temperature
$\rho_a = \frac{P_a}{R_a T_a}\ kg/m^3$	Inlet Air Density
$v_a = \frac{R_a T_a}{P_a} = \frac{1}{\rho_a}\ m^3/kg$	Inlet Air Specific Volume

$A_0A_1 = \frac{1}{M}\left[\frac{2(1+o.5(\gamma-1)M^2)}{\gamma+1}\right]^{\frac{\gamma+1}{2(\gamma-1)}}$	
$\dot{m}_a = \rho_a A_0 A_1 C_a \ \ kg/s$	Inlet Mass Flow Rate of Air
Cycle Analysis:	
$T_{01} = T_a + \frac{C_a^2}{2C_p}$	Total Inlet Temperature
$P_{01} = P_a\left[1+\eta_i\left(\frac{T_{01}}{T_a}\right)^{\gamma/\gamma-1}\right]$	Total Inlet Pressure
$\nu_{01} = \frac{R_a T_{01}}{P_{01}}$	
$DIFF = \nu_a - \nu_{01}$	
$P_{02} = P_{01}\left(\theta_c^{\gamma/\gamma-1}\right)$	
$T_{02} = T_{01}\left(1+\frac{\theta_c-1}{\eta_c}\right)$	
$\nu_{02} = \frac{R_a T_{02}}{P_{02}}$	
$COMP = \nu_{01} - \nu_{02}$	
$\Delta P_{COMP} = \frac{P_{02} - P_{01}}{P_a}$	
$T_{04} = T_{03} - \frac{C_{pa}(T_{02}-T_{01})}{C_{pg}\eta_m}$	
$Q_{LK} = \xi \dot{m}_a C_{pa}(T_H - T_L)$	
$Q_{actual} = \eta_b Q_{LHV} - Q_{LK}$	
$f = \frac{C_{pg}T_{03} - C_{pa}T_{02}}{\eta_b Q_{LHV} - C_{pg}T_{03}} = \frac{C_{pg}T_{03} - C_{pa}T_{02}}{(\eta_b Q_{LHV} - Q_{LK}) - C_{pg}T_{03}}$	Fuel to Air Ratio
$P_{03} = \Delta P_b P_{02}$	
$\nu_{03} = \frac{R_a T_{03}}{P_{03}}$	
$COMB = \nu_{02} - \nu_{03}$	
$\Delta P_{b\ COMB} = {(T_{03}-T_{02})}/{T_a}$	
$PR = (\theta_c)^{\gamma/\gamma-1}$	
$L = \frac{c(PR^{-r})}{\alpha}$	
$T_{04s} = T_{03} - \frac{(T_{03}-T_{04})}{\eta_t}$	
$P_{04} = P_{03}\left(\frac{T_{04s}}{T_{03}}\right)^{\gamma/\gamma-1}$	
$\nu_{04} = \frac{R_a T_{04}}{P_{04}}$	
$TURB = \nu_{04} - \nu_{03}$	

$\Delta P_{b\,TURB} = {(P_{03} - P_{04})}/{P_a}$	
$P_5 = P_a$	
$T_{5s} = \left(\frac{P_5}{P_{04}}\right)^{\gamma-1/\gamma}$	
$T_5 = T_{04} - \eta_n(T_{04} - T_{5s})$	
$C_5 = \sqrt{2C_{pg}(T_{04} - T_5)}$	
$\nu_5 = \frac{R_a T_5}{P_5}$	
$NOZZ = \nu_5 - \nu_{04}$	
$NG = \frac{60\sqrt{\gamma R_a T_{04}}}{\pi D_{A1}}$	Gas Generator Speed
$\dot{W}_{turb} = \dot{m}_a(1+f)C_{pg}(T_{03} - T_{04})$	
$FSHAFT = \frac{\dot{W}_{turb}}{NG}$	Shaft Force
$FS = \frac{T}{\dot{m}_a} = (1+f)C_5 - C_a$	Specific Thrust
$TSFC = f/FS$	Thrust Specific Fuel Consumption
$F = \dot{m}_a FS$	Thrust
$I = FS/g$	Impulse
$\dot{W} = 0.5(1+f)C_5^2 - 0.5C_a^2$	Power
$\eta_p = \frac{(FS)C_a}{\dot{W}}$	Propulsive Efficiency
$\eta_{th} = \frac{\dot{W}}{f Q_{LHV} \eta_b}$	Thermal Efficiency
$\eta_o = \eta_p \eta_{th}$	Overall Efficiency
$W = \dot{W}\dot{m}_a$	Work
$\nu_{5A} = \frac{T_5}{T_a}$	
$W_d = W/\nu_{5A}$	
$\eta_c = 1 - \frac{T_L}{T_H}$	Carnot Efficiency
$\dot{m}_f = \dot{m}_a f$	Fuel Flow
$\dot{W}_{rev} = \dot{m}_f \eta_c Q_{LHV}$	
$T_0 S_{gen} = \dot{W}_{rev} - \dot{W}$	
$Q_{HT} = \dot{m}_f \eta_b Q_{LHV}$	
$\dot{W}_{Bray} = Q_{HT}\left[1 - \left(1/\left(\frac{P_{02}}{P_a}\right)^{\gamma-1/\gamma}\right)\right]$	
$Q_{LT} = Q_{HT} - W$	
$Q_H = \dot{m}_a\left[(1+f)C_{pg}T_{03} - C_{pa}T_{02}\right]$	
$X_{Destroyed} = \dot{W}_{rev} - \dot{W}$	Destroyed Exergy
$ECOL = \dot{W} - T_0 S_{gen}$	Ecological Coefficient

$ECOP = \frac{\dot{W}}{T_0 S_{gen}}$	Ecological Coefficient of Performance
$PLOS = \frac{X_{Destroyed}}{\dot{W}_{rev}} = \frac{\dot{W}_{rev} - \dot{W}}{\dot{W}_{rev}}$	Power Loss Parameter
$EPLOS = \frac{\dot{W}_{Bray} - \dot{W}}{\dot{W}}$	Effective Power Loss Parameter
$CBSF = PLOS - EPLOS = \frac{\dot{W}_{rev} - \dot{W}_{Bray}}{\dot{W}_{rev}}$	Carnot Brayton Shape Factor

APPENDIX B: Turbojet Engine Formulation With AB

The turbojet engine without an AB are applied in addition to the formulations below:

Afterburner	
$P_{05} = (1 - \Delta P_b)P_{04}$	
$T_{05} = T_{max}$ $f_{ab} = \dfrac{(1+f)C_{pg}(T_{05} - T_{04})}{\eta_{ab}Q_{LHV} - C_{pg}T_{05}}$	Operative Afterburner
Nozzle	
$P_{06} = P_a$	
$T_6 = T_{05}\left[1 - \eta_n\left\{1 - \left(\dfrac{P_6}{P_{05}}\right)^{\gamma_g - 1/\gamma_g}\right\}\right]$	
$V_6 = \sqrt{2C_{pg}(T_{05} - T_6)}$	
$TSFC = \dfrac{\dot{m}_f + \dot{m}_{f\,ab}}{F} = \dfrac{f + f_{ab}}{T/\dot{m}_a}$	
$T = \dot{m}_a[(1 + f + f_{ab})V_6 - V_a]$	
$\eta_p = \dfrac{TV_a}{TV_a + 0.5\dot{m}_a(1 + f + f_{ab})(V_6 - V_a)^2}$	
$\eta_{th} = \dfrac{TV_a + 0.5\dot{m}_a(1 + f + f_{ab})(V_6 - V_a)^2}{\dot{m}_a(f + f_{ab})Q_{LHV}}$	
$\eta_o = \dfrac{TV_a}{\dot{m}_a(f + f_{ab})Q_{LHV}}$	

APPENDIX C: Ramjet Engine Formulation

General Ramjet Formulations	
$r_d = \frac{P_{02}}{P_{0a}}$	Diffuser performance characterized by stagnation pressure ratio.
Cycle Analysis:	
$\frac{T_{0a}}{T_a} = \left(1 + \frac{\gamma - 1}{2} M_a^2\right)$	
$T_{0a} = T_{01} = T'_{01} = T_{02}$	
$\frac{P_{0a}}{P_a} = \left(1 + \frac{\gamma - 1}{2} M_a^2\right)^{\gamma/\gamma-1}$ $\left(\frac{P_{0a}}{P_a}\right)^{\gamma-1/\gamma} \left(1 + \frac{\gamma - 1}{2} M_a^2\right) = 1$	Stagnation pressure of free stream
$V_a = M_a\sqrt{\gamma R_a T_a}$	
$\boldsymbol{r_d = 1 \quad For\ Mach\ Number < 1}$ $\boldsymbol{r_d = 1 - 0.075(M_\infty - 1)^{1.35} \quad From\ 1\ to\ 5\ Mach\ Number}$ $\boldsymbol{r_d = 800/(M^4 + 938) \quad For\ Mach\ Number > 5}$	
It is assumed that the Mach number to combustion chamber does not exceed 0.25 $\boldsymbol{M_2 = 0.25}$ $\frac{T_{02}}{T_0^*} = \frac{(2(\gamma+1)M_2^2)}{(1+\gamma M_2^2)^2(1+0.5(\gamma-1)M_2^2)}$ $T_0^* = \left(1/\frac{T_{02}}{T_0^*}\right) T_{02}$ $\frac{T_{03}}{T_0^*} = T_{max}/T_0^*$	
Given $\frac{\boldsymbol{T_{02}}}{\boldsymbol{T_0^*}}$ from Rayleigh Tables we obtain: $\frac{P_{02}}{P_0^*}$ Then: $P_{03} = \left(1/\frac{P_{02}}{P_0^*}\right) \boldsymbol{r_d} \frac{P_{0a}}{P_a} P_a$ $\frac{P_{03}}{P_a} = \left(1/\frac{P_{02}}{P_0^*}\right) \boldsymbol{r_d} \frac{P_{0a}}{P_a}$	
$f = \frac{C_p(T_{max} - T_{0a})}{\eta_b Q_{LHV} - C_p T_{ax}}$	
$T_5 = T_{max}\left(1 - \eta_n \left(\frac{1}{P_{03}/P_a}\right)^{(\gamma-1/\gamma)}\right)$ $\frac{T_5}{T_{05}} = \frac{T_5}{T_{max}}$	

$$M_5 = \sqrt{\left(\left(\frac{1}{T_5/T_{05}}\right) - 1\right)\left(\frac{2}{\gamma - 1}\right)}$$

$$V_5 = M_5\sqrt{\gamma R_a T_5}$$

$$\frac{P_{05}}{P_5} = (T_{max}/T_5)^{(\gamma/\gamma-1)}$$

$$P_5 = P_a$$

$$P_{05} = \frac{P_{05}}{P_5} P_a$$

$$T = \dot{m}_a[(1+f)V_5 - V_a]$$

$$TSFC = \frac{\dot{m}_f}{F} = \frac{f}{T/\dot{m}_a}$$

$$\eta_p = \frac{2V_a[(1+f)V_5 - V_a]}{(1+f)V_5^2 - V_a^2}$$

$$\eta_{th} = \frac{(1+f)V_5^2 - V_a^2}{2fQ_{LHV}}$$

$$\eta_o = \frac{V_a[(1+f)V_5 - V_a]}{fQ_{LHV}}$$

APPENDIX D: Sample of Matlab Code

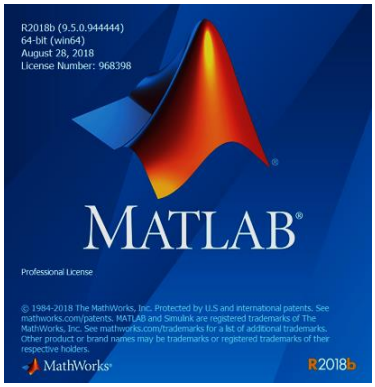


```
%%%% The following code for the Turbojet engine thermodynamic, power
%%%% density and exergy cycle analysis was developed using the 'Gas Turbine
%%%% Theory' fifth edition written by HIH. SARAVANAMUTOO, H. Cohen and
GFC.
%%%% Rogers.

%%%% Inputs for the Turbojet Thermodynamic Cycle Analysis are:

clear
clc

PRLS=0.96;      % press loss combust chamber
RKSI=0.01;      % heat Leak
TL=200;         % Sink Temperature
TH=2200;        % Source Temperature
TA=223.3;       % inlet temp (K)
T03=1200;       % turbine inlet temp
ALFA=T03/TA;    % max min temp ratio
PA=26.5;        % inlet press (kPa)
ETAI=0.93;      % intake efficiency
ETAJ=0.95;      % nozzle efficiency
ETAM=0.99;      % transmission eff
ETAB=0.98;      % combust eff
CPA=1.005;      % const press heat coeff air
CPG=1.148;      % const press heat coeff burned gases
GAMA=1.4;       % spec heat ratio air
GAMG=4/3;       % spec heat ratio burned gases
RAIR=287;       % gas const air
PI=4*atan(1);   % The value of pi
DIA1=0.8;       % Upstream capture diameter (m)
A1=PI*DIA1^2/4; % Upstream capture area
A=sqrt(GAMA*RAIR*TA);       % inlet speed of sound
RMA=0.5;        % flight Mach number
CA=RMA*A;       % inlet velocity
RGAMA=3.5;      % gama/(gama-1)  air
RGAMG=4;        % gama/(gama-1)   gases
QR=43000;       % Lower heating value (kJ)
```

```
G=9.81;        % Acceleration due to gravity

THETAC1=1:0.001:6;
THETAC=THETAC1';

ETAC=0.87;      % comp efficiency
ETAT=0.9;      % turbine efficiency

RHO=1000*PA/(RAIR*TA);
TEMP1=1+0.5*(GAMA-1)*RMA^2;
TEMP2=2*TEMP1/(GAMA+1);
UST=(GAMA+1)/(2*(GAMA-1));
TEMP3=TEMP2^UST;
A0A1=TEMP3/RMA;
RMASS=RHO*A1*A0A1*CA;

TEM=(CA^2)/(2.*CPA*1000.);
T01=TA+TEM;
P01=PA*((1.+ETAI*TEM/TA)^RGAMA);
P02=P01*(THETAC.^RGAMA);
T02=T01*(1+(THETAC-1)/ETAC);
T04=T03-CPA*(T02-T01)/(CPG*ETAM);

TEMP4=CPG*T03-CPA*T02;
QLK=RKSI*RMASS*CPA*(TH-TL);
QACT=ETAB*QR-QLK;
TEMP5=QACT-CPG*T03;
F=TEMP4/TEMP5;

P03=PRLS*P02;
T04S=T03-(T03-T04)/ETAT;
P04=P03.*((T04S/T03).^RGAMG);
P5=PA;
THETAN=(P5./P04).^(1/RGAMG);
T5S=THETAN.*T04;
T5=T04-ETAJ*(T04-T5S);
C5=sqrt(2.*CPG*1000.*(T04-T5));

ASOU4=sqrt(GAMG*RAIR*T04);
UTAN=ASOU4;
DIA4=DIA1;
RN=60*UTAN/(PI*DIA4);
WTURB=RMASS*(1.+F).*CPG.*(T03-T04);
FSHAF=WTURB./UTAN;

FS=((1.+F).*C5)-CA;
TSFC=F./FS;
RIA=FS/G;   % Impulse

W=((1+F).*(C5.^2/2))-(CA^2/2); % Joules
```

```
ETAP=FS.*CA./W;
W=W/1000.; %KJ
ETA=W./(F.*QR*ETAB);
ETAO=ETAP.*ETA;
W=RMASS*W;
V5A=T5/TA;
WD=W./V5A;

ETACAR=1-TL/TH;
FMASS=RMASS*F;
THEAT=FMASS.*QR;
WREV=FMASS*ETACAR*QR;
TSG=WREV-W;
QHT=FMASS*QR*ETAB;
QLKWREV=ETACAR*(QHT-QLK);
QLT=QHT-W;
QH=QHT-QLK;
THETA=(P02/PA).^(1/RGAMA);
WBRAY=QHT.*(1-1./THETA);
WUSE=RMASS*FS*CA/1000;
% QH=RMASS*((1+F)*CPG*T03-CPA*T02);

PLOS=TSG./WREV;
EPLOS=(WBRAY-W)./WREV;
ECOP=W./TSG;
ECOL=(W-TSG)/(RMASS*CPA*TA);
CBSF=PLOS-EPLOS;
BBSF=(WBRAY-W)./WBRAY;

WDMAX=max(WD(1:4000));
WD1=WD./WDMAX; % Normalized Power Density
WMAX=max(W);
WN=W./WMAX; % Normalized Power
VR=V5A-1;
VRMAX=max(VR(1:4000));
VRN=VR/VRMAX;

S1 = find(ECOP < 0, 1);
if isempty(S1)
   S1=5001;
end

[ECOPMAX,I3]=max(ECOP(1:S1));
ECOPN=ECOP./ECOPMAX;

S6 = find(ECOL < -6, 1);
if isempty(S6)
   S6=5001;
end
```

```
[ECOLMAX,I4]=max(ECOL(1:S6));
ECOLN=ECOL./ECOLMAX;



save('W_PLOS_THETA.mat',
'THETAC','THEAT','WREV','QLKWREV','WBRAY','W',...
   'WUSE','PLOS','EPLOS','CBSF','BBSF','WD1','WN','VRN','ECOPN','ECOLN',...
   'ETA','EPLOS');


figure(1)
yyaxis left
plot(THETAC,ETA,'Color',[0.47,0.67,0.19],'LineStyle','--')
hold all
plot(THETAC,WD1,'Color',[0.85,0.33,0.10],'LineStyle','-')
hold all
plot(THETAC,WN,'Color',[0.93,0.69,0.13],'LineStyle','-')
hold all
plot(THETAC,ECOPN,'Color',[0.49,0.18,0.56],'LineStyle','-')
hold all
plot(THETAC,VRN,'Color',[0.30,0.75,0.93],'LineStyle','-')
ylim([0,1])
yyaxis right
plot(THETAC,ECOL,'Color',[1.00,0.07,0.65],'LineStyle','-')
ylim([-3.3,-0.3])
xlim([1,4.5])
legend({'ETA','WDN','WN','ECOPN','VRN','ECOL'},'Location','northeast')
set(findall(gca, 'Type', 'Line'),'LineWidth',2);
set(findall(gcf,'-property','FontSize'),'FontSize',20)
saveas(gcf,'ETA_WDN_WN_EPN_EPL','fig')

% figure(2)
% plot(THETAC,THEAT)
% hold all
% plot(THETAC,WREV)
% hold all
% plot(THETAC,QLKWREV)
% hold all
% plot(THETAC,WBRAY)
% hold all
% plot(THETAC,W)
% ylim([0,55000])
% hold all
% plot(THETAC,WUSE)
% hold all
% yyaxis right
% plot(THETAC,PLOS)
% hold all
% plot(THETAC,EPLOS)
```

```
% hold all
% plot(THETAC,CBSF)
% hold all
% plot(THETAC,BBSF)
% ylim([0,1])
% xlim([1,4])
% legend({'THEAT','WREV','QLKWREV','WBRAY IDEAL','WBRAY
REAL','WUSE','PLOS',...
%     'EPLOS','CBSF','BBSF'},'Location','northeast')
% set(findall(gca, 'Type', 'Line'),'LineWidth',2);
% set(findall(gcf,'-property','FontSize'),'FontSize',20)
% saveas(gcf,'EPLOS_PLOS_ACT','fig')
%
%
% figure(3)
% plot(THETAC,THEAT./WREV)
% hold all
% plot(THETAC,WREV./WREV)
% hold all
% plot(THETAC,QLKWREV./WREV)
% hold all
% plot(THETAC,WBRAY./WREV)
% hold all
% plot(THETAC,W./WREV)
% hold all
% plot(THETAC,WUSE./WREV)
% hold all
% plot(THETAC,PLOS)
% hold all
% plot(THETAC,EPLOS)
% hold all
% plot(THETAC,CBSF)
% hold all
% plot(THETAC,BBSF)
% xlim([1,4])
% ylim([0,1.2])
% legend({'THEAT','WREV','QLKWREV','WBRAY IDEAL','WBRAY
REAL','WUSE',...
%     'PLOS','EPLOS','CBSF','BBSF'},'Location','northeast')
% set(findall(gca, 'Type', 'Line'),'LineWidth',2);
% set(findall(gcf,'-property','FontSize'),'FontSize',20)
% saveas(gcf,'EPLOS_PLOS_NORM','fig')
```

APPENDIX E: Frank Whittle 1931 Patent

PATENT SPECIFICATION

Application Date: Jan. 16, 1930. No. 1521/30. **347,206**

Complete Left: Oct 16, 1930.

Complete Accepted: April 16, 1931.

PROVISIONAL SPECIFICATION.

Improvements relating to the Propulsion of Aircraft and other Vehicles.

I, FRANK WHITTLE, of Glenhaven, Regent St., Coventry, British Subject, do hereby declare the nature of this invention to be as follows:—

This invention concerns improvements relating to propulsion and whilst at present it is deemed to be particularly adapted to the propulsion of aircraft, it is not necessarily limited to this use and may be adapted for the propulsion of other vehicles.

The main object of this invention is to provide means whereby the principle of obtaining propulsive force in the one sense of direction by the reaction caused by expelling fluid in the opposite sense of direction, may be applied efficiently to aircraft or other vehicles.

It is believed that an embodiment of this invention will provide a large thrust in proportion to its weight, that it will perform at greater altitudes than are at present obtainable, that it makes possible higher speeds than have up to the present been obtained, that it will operate with any fuel now in use, and that it will have a reasonably low fuel consumption. Further that simplicity and convenient external form is achieved.

According to the invention, a heat cycle is employed, consisting of one, or more stages of compression, one or more stages of expansion and a heat addition between the end of compression and the beginning of expansion, part of the work done in expansion being employed to do the work of compression, and the remainder to provide the fluid reaction.

Describing the invention in a simple form as applied to aircraft, there is a compression apparatus, consisting of a compressor, which may be a blower type compressor, a cylinder compressor, or a combination of the two, by means of which air as the working fluid is compressed into a heating chamber where heat is added by the combustion of fuel. The air then expanding through apparatus designed to absorb sufficient of the work of expansion to drive the compressor, and which may consist of a turbine rotor, or cylinder expander or a combination of the two, and which is on the same shaft as, or connected with the compressing mechanism. The air then passes through a suitably designed tunnel to the atmosphere, either having velocity as a result of its passage through expansion apparatus, of being capable of further expansion through suitably designed nozzles at the rear, or both.

In another form, a portion of the air only may expand through the expansion apparatus which drives the compression apparatus, and the remainder expands to the atmosphere providing fluid reaction.

In more particularly describing the invention in an aircraft adaption, I propose to use a centrifugal rotary vane blower or turbo-compressor as a compressor. The air intake is a tunnel situated in the nose of the aircraft and leading in an axial direction to the inlet orifice of blower. The gas is passed circumferentially through suitably designed passages or diffusers into the heating chamber, which is of suitable material, and probably lagged externally to conserve heat. Into this chamber are directed burners for oil fuel and any further necessary details of construction such as pilot burners, cleaning devices etc. At the rear of the heating chamber the gas passes through suitable nozzles to impinge on the buckets or blades of a De Laval or Curtis type turbine wheel, the latter being mounted on the same shaft as the compressor. The gas passes into a tunnel after leaving the turbine and is led to the rear, where the final stage of expansion to the atmosphere takes place through suitably designed nozzles.

The invention is not limited to the mechanism detailed above. For instance, instead of the air passing through apparatus for driving compressor after heating, it may pass through and give up some of its heat to the water in a steam boiler, the steam so generated being utilised to drive the compression mechanism by means of a steam turbine or other steam engine. This would then be a substitute for the gas turbine above specified.

Controlling means may include fuel control, gas flow control, or mechanical control of the speed of the blower and/or

its mover. The final emission of gas may perhaps be directionally controlled for manœuvring purposes. One or a plurality of the complete power units may be provided in a single vehicle or aircraft and they may to some extent be interdependent, e.g. a single turbine may operate subsidiary blowers etc.

It may be necessary to provide auxiliary apparatus for starting, fuel injections, lubrication or like purposes.

It will be clear that the invention gives scope for wide modification without departing from its principle as herein outlined.

Dated this 14th day of January, 1930.

F. WHITTLE.

COMPLETE SPECIFICATION.

Improvements relating to the Propulsion of Aircraft and other Vehicles.

I, FRANK WHITTLE, late of "Glenhaven", Regent Street, Coventry, and now of "Hill Crest" Dorrington, Lincoln, British Subject, do hereby declare the nature of this invention and in what manner the same is to be performed, to be particularly described and ascertained in and by the following statement:—

This invention relates to apparatus for propulsion of the type in which air is taken in, compressed, heated, and expelled with high velocity on re-expansion in order to provide a propulsive thrust.

The main object of this invention is to provide improved apparatus of the above mentioned type, and in particular improved means for driving the compressor.

According to the invention I provide means for propulsion of the above mentioned type characterised by the feature that the compressor is driven by a turbine, and that the pressure drop on expansion takes place in two stages, the first pressure drop taking place through the nozzles of the turbine, and the second pressure drop taking place through the propelling nozzles.

Describing the invention in a simple form as applied to aircraft, there is a compressor, preferably of the turbo-centrifugal type, by means of which air as the working fluid is compressed into a heating chamber where heat is added by the combustion of fuel. The air is then expanded through apparatus designed to absorb sufficient of the work of expansion to drive the compressor, and which consists of a turbine rotor, and which is on the same shaft as or connected with the compressing mechanism. The air then passes through a suitably designed tunnel or nozzles to the atmosphere, either having velocity as a result of its expansion through the expansion apparatus, or being capable of further expansion through suitably designed nozzles at the rear, or both.

The invention will now be described with aid of the accompanying drawing and diagram in which:—

Fig. 1 is a diagram showing the cycle of energy or thermal cycle on which the invention relies fundamentally.

Fig. 2 is a part-section showing diagrammatically a preferred form of the invention, applicable to the propulsion of aircraft.

The thermal cycle employed which is shown in Fig. 1 is a pressure-volume diagram in which:

AG represents the atmospheric line.

DC represents compression.

CE represents heating at constant pressure.

EF represents that portion of expansion which is utilised to do the work of compression.

FG represents the expansion to the atmosphere providing thrust by fluid reaction.

The device consists of a compressor having casing "1" intake passages 2, a rotor "3", with bucket rings "4" working in conjunction with stator bucket or nozzle rings "5" inside the casing "1" and centrifugal radial blading "7" and diffusers "8" through which the output is delivered under pressure through header or collector ring "9" into combustion or heating chambers "10" in which fuel is burnt. This may be heavy oil or other fuel burning at jets "11". The chambers "10" are preferably lagged or otherwise heat insulated to conserve heat energy, and perhaps lined with refractory material. The heated gases pass into a collector or header "12" from chambers "10" which are of any suitable number and disposition. From header "12" the gases expand through a turbine "13" with buckets "14" and stator "15", the turbine rotor "13" being fast on the spindle "16", which is also the driving spindle of the compressor rotor "3",

" 7 ". From the turbine the gases further expand through nozzles " 17 " to the atmosphere in an axial direction.

Any suitable type of turbine may be used, but in order that the relatively high temperature proposed to be employed may be withstood, the buckets may be of some suitable refractory material.

The turbine drives the compressor direct as shown, but direct drive is not essential, any gearing or the like may of course be employed.

The air entering at " 2 " is first of all compressed by the bucket system " 4 " " 5 ", and by blades " 7 ". In the chambers " 10 " the air is heated at constant pressure and expands through the turbine " 13 " losing energy by driving the turbine and compressor. Its remaining pressure and velocity energy is then converted into velocity out of the nozzles " 17 ", whereby reaction in the nature of axial thrust is set up according to the usual laws.

It can be demonstrated that the efficiency of this device conceived as a propulsive engine. will not be reduced by reduction of the density of the atmosphere, and owing to the low temperature of the upper atmosphere may actually be enhanced.

Controlling means may include fuel control, gas flow control, or mechanical control of the speed of the blower and/or its mover. The final emission of gas may perhaps be directionally controlled for manœuvering purposes.

It may be necessary to provide auxiliary apparatus for starting, fuel injections, lubrication or like purposes.

Having now particularly described and ascertained the nature of my said invention and in what manner the same is to be performed, I declare that what I claim is:—

1. Means for propulsion of the type described, characterised by the feature that the compressor is driven by a turbine, and that the pressure drop on expansion takes place in two stages, the first pressure drop taking place through the nozzles of the turbine, and the second pressure drop taking place through the propelling nozzles.

2. Means for propulsion according to Claim 1, in which a multi-stage turbine is employed.

3. A propulsion device in which a centrifugal turbo-compressor supplies compressed air to a heating chamber whence the air passes to drive a turbine which mechanically drives the compressor, and whence in turn the air and products of combustion escape to the atmosphere through passages which cause them to produce propulsive thrust.

4. A device according to claims 1 and 3, constructed and operating substantially as described with reference to Fig. 2 of the accompanying drawings.

Dated this 14th day of October, 1930.

F. WHITTLE.

Redhill: Printed for His Majesty's Stationery Office, by Love & Malcomson, Ltd.—1931.

Fig 1.

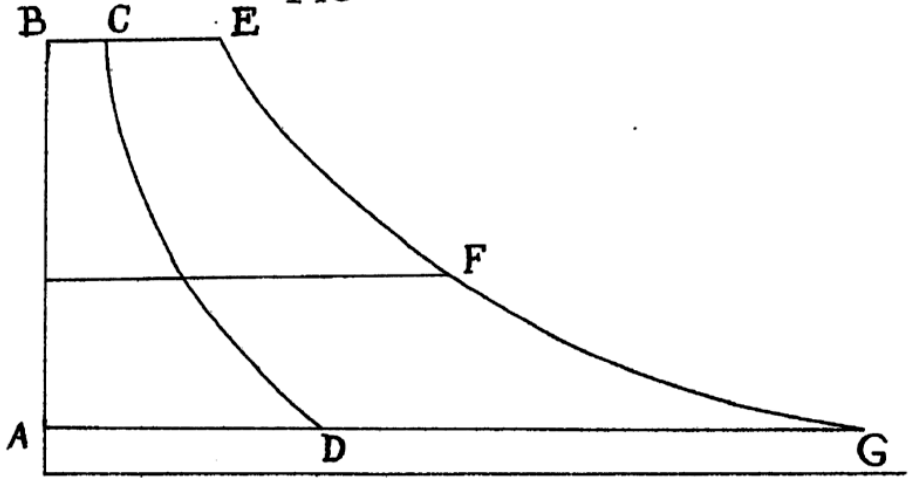

Fig. 2

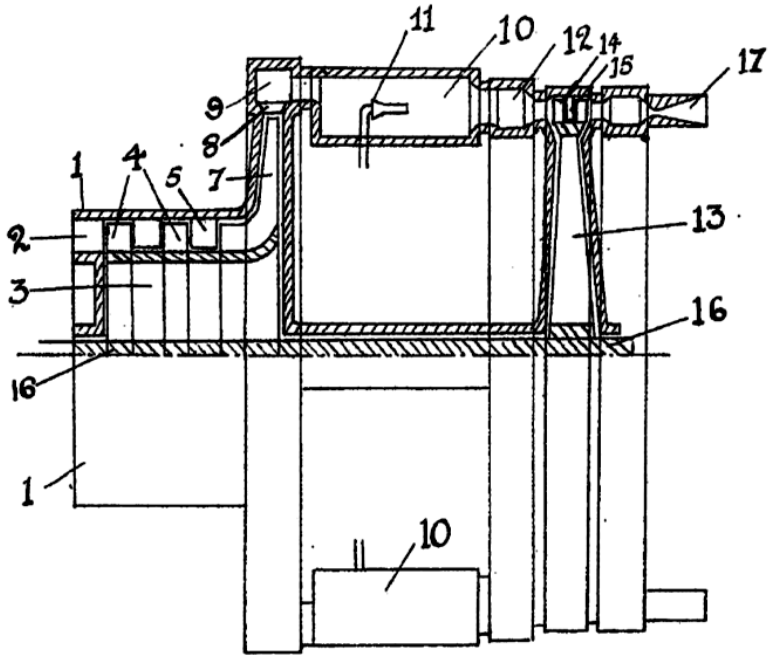

Charles & Read Ltd. Photo Litho.

CURRICULUM VITAE

Name Surname : Sara FAWAL

EDUCATION:

- **B.Sc.** **:** 2004, University of Watrloo, Faculty of Science, Honors Science
- **B.Sc.** **:** 2011, Concordia University, Faculty of Engineering, Mechanical Engineering
- **M.Sc.** **:** 2015, Concordia University, Faculty of Engineering, Mechanical Engineering

PROFESSIONAL EXPERIENCE AND REWARDS:

- 2010, Richard Cheng Design Award in Mechanical Engineering
- 2008, 2009 and 2010 NSERC
- 2009 CRIAQ
- 2013-2017, Aviya Aerospace Systems: Operability, Simulation and Integrtion
- 2011, Concordia University: Wind Turbines and Applications
- 2011, Rolls Royce: LCGO
- 2010, Dessau: HVAC

PUBLICATIONS, PRESENTATIONS AND PATENTS ON THE THESIS:

- **Fawal S.** and Kodal A. (2019) Comparative performance analysis of various optimization functions for an irreversible Brayton cycle applicable to turbojet engines, Energy Conversion and Management, 199 111976. (Article Instance)
- **Fawal S.** and Kodal A. (2021) Overall and Component Basis Performance Evaluations for Turbojet Engines Under Various Optimal Operating Conditions, Aerospace Science and Technology 117 106943. (Article Instance)